Ciblage de MYC par étude de l'axe LIN28B/let-7 et de l'initiation de la traduction dans le myélome multiple

Salomon Manier

UNIVERSITE DROIT ET SANTÉ DE LILLE 2

Ecole Doctorale Biologie-Santé

THÈSE

Présentée pour l'obtention du grade de

DOCTEUR DE L'UNIVERSITÉ Discipline : Hématologie

Salomon Manier

CIBLAGE DE MYC PAR ETUDE DE L'AXE LIN28B/LET-7 ET DE L'INITIATION DE LA TRADUCTION DANS LE MYELOME MULTIPLE

Soutenue publiquement le 4 Juillet 2017 devant le jury composé de :

Professeur Bruno Quesnel	**Président**
Professeur Martine Amiot	**Rapporteur**
Professeur Bertrand Arnulf	**Rapporteur**
Professeur Irene Ghobrial	**Examinateur**
Professeur Hervé Avet-Loiseau	**Examinateur**
Professeur Catherine Roche-Lestienne	**Directeur de thèse**
Professeur Xavier Leleu	**Directeur de thèse**

REMERCIEMENTS

Ce travail est dédié au Dr Irene Ghobrial, qui m'a accueilli pendant quatre ans dans son laboratoire au Dana-Faber Cancer Institute. Son dynamisme et sa curiosité scientifique ont permis de mener ces travaux à terme. Il est aussi dédié à tous mes collègues rencontrés au Dana-Farber, au contact desquels j'ai beaucoup appris : Aldo Roccaro, Antonio Sacco, Siobhan Glavey, Michaela Reagan, Patricia Maiso, Kareem et Feda Azab, Yong Zhang, Yosra Aljawai, Ilyas Sahin, Daisy Huynh, Michele Moschetta, Yuji Mishima, Andrea Kolligian, Ranjit Banwait, Yawara Kawano.

Je souhaite remercier mes directeurs de thèse, les Drs Catherine Roche-Lestienne et Xavier Leleu, pour leur soutien tout au long de cette thèse et leur aide pour mes projets à venir.

Je remercie aussi particulièrement le Dr Bruno Quesnel de m'avoir accueilli au sein de l'équipe 4 de l'UMR-S 1172 à mon retour et d'avoir tout mis en oeuvre pour faciliter mon insertion.

Je remercie les Drs Martine Amiot, Bertrand Arnulf et Hervé Avet-Loiseau d'avoir accepté de participer au jury de cette thèse. Tous trois portent la recherche sur le Myélome Multiple en France.

ABREVIATIONS

ADN : Acide Désoxyribonucléique

ARN : Acide Ribonucléique

ARNm : Acide Ribonucléique messager

BCL2 : B-cell lymphoma 2

CCND1 : Cycline D1

CRISPR : Clustered regularly interspaced short palindromic repeats

GEP : Gene Expression Profiling

H3K27ac : Acétylation de la Lysine 27 de l'Histone H3

H3K4me : Tri-méthylation de la Lysine 4 de l'Histone H3

HSF1 : Heat shock factor 1

IC50 : Half Maximal Inhibitory Concentration

IGH : Immunoglobulin heavy chain

IMiDs : Immunomodulatory Drugs

IRF4 : Interferon regulatory factor 4

ISS : international staging system

KD : Knockdown

KO : Knockout

KRAS : Kirsten rat sarcoma viral oncogene homolog

LIN28B : Lin-28 Homolog B

LNA : Locked Nucleic Acid

MAPK : Mitogen-activated protein kinases

MAX : Myc-associated Factor X

MAF : V-Maf Avian Musculoaponeurotic Fibrosarcoma

MCL1 : Myeloid Cell Leukemia Sequence 1

MDM2 : Mouse double minute 2 homolog

MGUS : Monoclonal Gammopathy of Undertermined significance

miARN : Micro Acide Ribonucléique

MM : Multiple Myeloma

MYC : Avian Myelocytomatosis Viral Oncogene Homolog

NRAS : Neuroblastoma RAS Viral Oncogene Homolog

PKM : pyruvate kinase muscle isozyme

POL I, II, III : ADN polymerase I, II et III

qRT-PCR : quantitative reverse transcription – polymerase chain reaction

RISC : RNA-induced silencing complex

R-ISS : Revised International Staging System

siARN : ARN silenceur

SMM : Smoldering Multiple Myeloma

WB : Western Blot

SOMMAIRE

RESUME

Le Myélome Multiple (MM) est une hémopathie maligne caractérisée par la prolifération de plasmocytes tumoraux médullaires. MYC occupe un rôle central dans l'oncogenèse du MM car son activation est responsable de la progression du stade précurseur de MGUS en MM symptomatique. Dans ce travail, nous rapportons que l'expression de LIN28B est corrélée à celle de MYC et est associée à un mauvais pronostic dans le MM. Nous montrons que l'axe LIN28B/let-7 module l'expression de l'ARNm de MYC, lui-même cible de let-7. De plus, la perturbation de l'axe LIN28B/let-7 induit une régulation la prolifération des lignées cellulaires de MM *in vitro* et *in vivo*. L'analyse par séquençage d'ARN de modèles de KO par utilisation de la technologie CRISPR a montré que l'axe LIN28B/let-7 régule les voies de signalisation de MYC et du cycle cellulaire dans MM. Nous avons de plus établi une preuve de principe thérapeutique de la possibilité de cibler MYC par l'emploi de LNA-GapmeR contenant une séquence analogue à let-7b. Dans un modèle de xénogreffe murin, nous montrons que des niveaux élevés d'expression de let-7, par administration de LNA-GapmeR let-7b, répriment la croissance tumorale en régulant l'expression de MYC. Ces résultats révèlent un nouveau mécanisme de ciblage thérapeutique de MYC *via* l'axe LIN28B/let-7 dans MM. Nous nous sommes ensuite intéressés à évaluer de nouvelles formes de biomarqueurs moléculaires dans le MM par étude des miARN contenus dans les exosomes circulants. Nous avons examiné le rôle pronostique des miARN exosomaux dans une cohorte de 156 échantillons de patients uniformément traités pour un MM au diagnostic. Après analyse du profil de miARN exosomaux par séquençage de nouvelle génération, nous avons utilisé technique de qRT-PCR pour étudier la corrélation entre

le niveau d'expression de 22 miARN et la survie sans progression (SSP) et la survie globale (SG). Deux miARN, à savoir let-7b et miR-18a, étaient significativement associés à la SSP et SG en analyse univariée, et étaient statistiquement significatifs après ajustement pour le système international de stratification du risque (ISS) et les marqueurs cytogénétique en analyse multivariée. Nos résultats confirment le niveau d'expression des miARN let-7b et miR-18a au sein des exosomes circulants permettent d'améliorer la stratification du risque chez les patients atteints de MM. Enfin, pour mieux comprendre le programme oncogénique piloté par MYC, nous avons étudié l'efficacité thérapeutique d'une librairie de petites sur des lignées cellulaires avec une forte expression de MYC, dans le MM. Les résultats ont permis d'identifier les rocaglates, une famille de composés inhibant l'initiation de la traduction, comme étant les plus actifs. L'étude du profil transcriptionnel par séquençage de l'ARN de lignées cellulaires de MM traitées par CMLD010509 ou DMSO a révélé l'activation d'un programme de transcription et l'inhibition d'un programme traductionnel, caractéristique de l'inactivation de HSF1 secondaire à l'inhibition de la traduction. Le profile traductionnel était étudié par spectrométrie de masse quantitative, permettant d'identifier un ensemble de protéines, tels que MYC, MDM2, CCND1, MAF et MCL-1, spécifiquement affectées par l'inhibition de la traduction liée au composé CMLD010509 dans le MM. Nous avons confirmé l'efficacité thérapeutique des rocaglates dans plusieurs modèles murins de MM. Ces résultats démontrent la possibilité de cibler le programme de traduction oncogénique lié à MYC dans MM.

Mots-clés : Myélome Multiple; MYC; LIN28B/let-7; microARN; Exosomes; Rocaglate ; Traduction

ABSTRACT

TARGETING MYC IN MULTIPLE MYELOMA BY INTERFERING WITH THE LIN28B/LET-7 AXIS AND INHIBITING TRANSLATION INITIATION

MYC is a major oncogenic driver of Multiple Myeloma (MM) and yet almost no therapeutic agents exist that target MYC in MM. Here we report that the let-7 biogenesis inhibitor LIN28B correlates with MYC expression in MM and is associated with adverse outcome. We also demonstrate that the LIN28B/let-7 axis modulates the expression of MYC, itself a let-7 target. Further, perturbation of the axis regulates the proliferation of MM cells in vivo in a xenograft tumor model. RNA-sequencing and gene set enrichment analyses of CRISPR-engineered cells suggested that the LIN28/let-7 axis regulates MYC and cell cycle pathways in MM. We provide proof of principle for therapeutic regulation of MYC through let-7 with an LNA-GapmeR (locked nucleic acid-GapmeR) containing a let-7b mimic in vivo, demonstrating that high levels of let-7 expression repress tumor growth by regulating MYC expression. These findings reveal a novel mechanism of therapeutic targeting of MYC through the LIN28B/let-7 axis in MM. We next sought to establish new biomarkers in MM, enable to capture the molecular alterations of the disease. For this purpose, we examined the prognostic significance of circulating exosomal microRNAs (miRNAs) in a cohort of 156 patients with newly diagnosed MM, uniformly treated and followed. Circulating exosomal miRNAs were isolated and used to perform small RNA sequencing analysis on 10 samples and a qRT-PCR array on 156 samples. We studied the relationship between miRNA levels

and patient outcomes including progression-free survival (PFS) and overall survival (OS). We identified miRNAs as the most predominant small RNAs present in exosomes isolated from the serum of MM patients and healthy controls by small RNA sequencing of circulating exosomes and used a qRT-PCR assay to measure the expression of 22 exosomal miRNAs. Two of them, namely let-7b and miR-18a, were significantly associated with both PFS and OS in the univariate analysis, and were still statistically significant after adjusting for the International Staging System (ISS), and adverse cytogenetics in the multivariate analysis. Our findings support the use of circulating exosomal let-7b and miR-18a improves the identification of patients with newly diagnosed MM with poor outcomes. Finally, to better understand the oncogenic program driven by MYC and investigate its potential as a therapeutic target, we screened a chemically diverse small molecule library for anti-MM activity in cell lines with high expression of MYC. The most potent hits identified were rocaglate-scaffold inhibitors of translation initiation. Expression profiling of MM cells revealed reversion of the oncogenic MYC-driven transcriptional program by CMLD010509, the most promising rocaglate. Proteome-wide, reversion correlated with selective depletion of short-lived proteins that are key to MM growth and survival, most notably MYC, MDM2, CCND1, MAF, and MCL-1. The efficacy of CMLD010509 in several mouse models of MM confirmed the therapeutic relevance of these findings in vivo and supports the feasibility of targeting the oncogenic MYC-driven translation program in MM with rocaglates.

Key Words: Multiple Myeloma; MYC; LIN28B/let-7; microRNA; Exosomes; Rocaglates; Translation

GENERALITES

I. Aspects cliniques du Myélome Multiple

1. Epidémiologie

Le myélome multiple (MM) est une hémopathie maligne caractérisée par une prolifération clonale de plasmocytes tumoraux au niveau la moelle osseuse [1]. Il représente environ 10 % des cancers hématologiques, ce qui le situe au deuxième rang par ordre de fréquence après les lymphomes. En France, l'incidence annuelle est de 6 à 7 cas pour 100 000 habitants par an, ce qui correspond à environ 4 000 nouveaux cas diagnostiqués chaque année [2]. La survie médiane est de 5 à 7 ans, mais le pronostic varie selon les patients : certains décèdent en quelques mois, d'autres, au contraire, ont une survie pouvant se prolonger au-delà de 10 ans [3]. La médiane d'âge au diagnostic est de 69 ans [4].

2. Sémiologie du myélome multiple

Les principales manifestations du myélome résultent de l'accumulation de plasmocytes tumoraux au niveau de la moelle osseuse, pouvant entraîner :

- la production et la sécrétion d'une protéine monoclonale dans le sang et/ou les urines;
- des lésions osseuses;
- une insuffisance médullaire avec anémie et/ou leucopénie et thrombopénie;

- une immunodépression avec inhibition de la production des immunoglobulines normales et sensibilité accrue aux infections

Certains patients n'ont aucune symptomatologie clinique au moment du diagnostic et la maladie est alors découverte de manière fortuite, à l'occasion, par exemple, de la détection d'un pic sur une électrophorèse des protéines sériques pratiquée lors du bilan d'une autre pathologie.

L'altération de l'état général représente un des signes les plus fréquents au diagnostic.

Les cytopénies sont avant tout marquées par un syndrome anémique. Il s'agit d'une anémie normochrome normocytaire arégénérative. Les causes en sont multiples, parmi lesquelles la prolifération plasmocytaire médullaire, une suppression de l'érythropoïèse induite par les cytokines, un phénomène d'hémodilution lié à l'hyperprotidémie et la diminution de sécrétion d'érythropoïétine (EPO) en cas d'insuffisance rénale. L'expression à la surface des cellules myélomateuses des récepteurs Fas-ligand et TRAIL (*tumor necrosis factor-related apoptosis-inducing ligand*) intervient dans l'apoptose des progéniteurs érythroïdes. Il existe aussi, à un degré moindre, des thrombopénies et des neutropénies.

L'atteinte osseuse est liée à l'infiltration plasmocytaire qui s'accompagne d'une activation des ostéoclastes et d'une inhibition ostéoblastes, notamment par sécretion de DKK-1. Les douleurs osseuses sont présentes chez 70 % des patients au diagnostic et intéressent surtout le squelette axial. Les douleurs osseuses nécessitent souvent le recours aux antalgiques de palier III, et retentissent sur les capacités fonctionnelles des patients. L'atteinte osseuse peut se compliquer de fractures pathologiques,

compressions neurologiques, médullaires, radiculaires ou tronculaires, secondaires à un tassement vertébral, une épidurite ou un plasmocytome. L'IRM en urgence est nécessaire dans ces situations.

L'insuffisance rénale est présente chez 50% des patients au diagnostic. Le recours à l'hémodialyse est requis dans 5 à 10% des cas. La cause la plus fréquente est la tubulopathie myélomateuse (environ 75% des atteintes rénales), qui est caractérisée par la précipitation de cylindres, formés de chaînes légères d'immunoglobulines et de protéines de Tamm-Horsfall, dans les tubules distaux. L'atteinte pré-rénale est aussi fréquente et souvent liée à une hypercalcémie. Les atteintes glomérulaires sont plus rares et secondaire à une complication du myélome comme le développement d'une Amylose AL ou d'une cryoglobulinémie. Les atteintes rénales des gammapathies monoclonales sont résumées dans le Tableau 1.

Tableau 1. Atteinte rénale dans les gammapathies monoclonales.

Pré-rénale (insuffisance rénale fonctionnelle)		- Par déshydratation extra cellulaire dans un contexte : - d'hypercalcémie - de pertes digestives (vomissements)
Rénale	**Tubulaire**	- Tubulopathie myélomateuse (tubes distaux) - Nécrose tubulaire aiguë (notamment après utilisation de produits de contraste iodés) - Syndrome de Fanconi : traduction clinique d'une atteinte tubulaire proximale (tubulopathie « microcristalline » proximale)

	Glomérulaire	- Amylose AL - Maladie à dépôts monotypiques (de chaînes légères et/ou de chaînes lourdes) non organisés = syndrome de Randall - Dépôts organisés non amyloïdes : ces dépôts glomérulaires ont une organisation microtubulaire (glomérulonéphrite immunotactoïde) - Atteintes glomérulaires au décours des cryoglobulinémies (de type I ou II)

L'hypercalcémie est retrouvée dans 20% des cas au diagnostic. Elle représente une urgence thérapeutique et se complique souvent d'insuffisance rénale aiguë fonctionnelle ou par atteinte tubulo-interstitielle. Plusieurs mécanismes en expliquent la survenue. L'activation ostéoclastique par les plasmocytes tumoraux induite localement par les cellules myélomateuses, provoquant une lyse osseuse. A moindre mesure, la baisse du débit de filtration glomérulaire et l'augmentation de la résorption tubulaire du calcium participe aussi à la survenue d'une hypercalcémie.

Un syndrome infectieux est présent au diagnostic dans environ 10% des cas. Le MM induit un déficit de l'immunité humorale en lien avec une hypogammaglobulinémie, dont la conséquence est l'augmentation du risque d'infections à germes encapsulés, telles que le pneumocoque et *Haemophilus influenzae.* Les infections sont aussi favorisées par les différents traitements du MM, dont la Dexaméthasone et demeurent la première cause de décès chez les patients atteints de myélome, en cause dans 20% à 50% des cas. Les vaccinations anti-pneumococcique et anti-haemophilus sont recommandées car elles diminuent significativement l'incidence des événements

infectieux. Dans les cas d'hypogammaglobulinémie profonde, certains recommandent une antibioprophylaxie par Oracilline ou une supplémentation par immunoglobulines polyvalentes après un premier épisode infectieux.

Le risque thrombo-embolique est élevé chez les patients atteints de MM et ce en raison de la sécrétion de cytokines pro-inflammatoires, de la présence d'un composant monoclonal élevé, de l'âge souvent avancé des patients, d'une mobilité réduite liée aux complications osseuses et neurologiques, voire de la présence d'un syndrome néphrotique chez certains patients. Une cause majeure de maladie thrombo-embolique veineuse ou artérielle dans le myélome reste l'utilisation de chimiothérapies telles que les anthracyclines, de la dexaméthasone à hautes doses et des IMiDs (thalidomide et lénalinomide). Une prévention du risque thrombo-embolique, par aspirine ou héparine de bas poids moléculaire selon le risque estimé de thrombose, est nécessaire en cas d'utilisation de ces agents thérapeutiques [5].

Le syndrome d'hyperviscosité est peu fréquent dans le MM à l'inverse de la maladie de Waldenstöm. Ceci s'explique par le fait que l'IgG (monomérique) et l'IgA (dimérique) ont un poids moléculaire plus faible que l'IgM (pentamérique). Un syndrome d'hyperviscosité peut s'observer lorsque le taux du composant monoclonal sérique (IgA ou IgG) est très élevé. Ses signes cliniques sont marqués par un syndrome confusionnel, des céphalées, des vertiges, voire des convulsions ou un coma. En cas de suspicion clinique, le diagnostic est facilement confirmé par la réalisation en urgence d'un fond d'œil, retrouvant des lésions telles que dilatations veineuses, hémorragie rétinienne, micro-anévrismes, exsudats et œdème papillaire. Un traitement par

plasmaphérèse en urgence est alors indiqué en complément de la mise en place du traitement spécifique du MM.

Les atteintes neurologiques survenant dans le MM sont souvent liées à une atteinte médullaire par compression secondaire à une fracture vertébrale ou à une épidurite tumorale. Des localisations plasmocytaires de la voûte crânienne compliquées de syndrome de masse peuvent aussi se voir. L'IRM médullaire constitue l'examen de choix pour confirmer le diagnostic, établir l'étiologie et aider à la décision thérapeutique (radiothérapie ou neurochirurgie). Les atteintes périphériques à type de polyneuropathies sensitives sont fréquentes et invalidantes [6]. Elles peuvent être iatrogènes, induites par le thalidomide ou le bortezomib et imposent des réductions de doses, voire l'arrêt du traitement incriminé. D'autres causes de neuropathies périphériques sont notamment liées à une amylose AL, une activité cryoglobulinémique ou anticorps anti-MAG de l'immunoglobuline monoclonale.

3. Diagnostic positif

Le diagnostic de MM repose sur la présence d'une plasmocytose médullaire > 10%, à la différence de la gammapathie monoclonale de signification indéterminée (MGUS). Les critères diagnostiques distinguent les MM symptomatiques (présence d'au moins un des critères CRAB ou d'une plasmocytose >60% ou d'un rapport de chaînes légères libres sériques > 100) des MM asymptomatiques (smoldering MM - SMM) [7], (Tableau 2).

Tableau 2. Critères diagnostiques différenciant le MM symptomatique, le SMM et la MGUS.

Myélome multiple symptomatique	Plasmocytose médullaire ≥ 10 %, **ET** présence d'au moins un critère CRAB. **ET/OU** un des biomarqueur de malignité: - Plasmocytose médullaire ≥ 60 % - Rapport chaîne légère libre affectée/non affectée > 100 - Plus d'une lésion osseuse focale à l'IRM
Myélome multiple asymptomatique	Prolifération plasmocytaire ≥ 10 % et < 60% **ET/OU** Présence d'une protéine sérique monoclonale (IgG ou IgA) ≥ 30 g/l **ET/OU** protéinurie de Bence Jonce ≥ 500mg/24h **ET** absence de critère CRAB ou de signe d'amylose
MGUS	Plasmocytose médullaire < 10 % **ET** protéine monoclonale < 30 g/l **ET** absence de critères CRAB

Les critères CRAB définissent les atteintes d'organes dues à la maladie. [8]

• C pour hyper**C**alcémie > 0.25 mmol/L au-dessus de la limite supérieure ou > 2.75mmol/L;

• R pour insuffisance **R**énale avec créatininémie > 177 µmol/l ou > 20 mg/l ou clairance de la créatinine < 40mL/min ;

• A pour **A**némie avec un taux d'hémoglobine < 10 g/dl ou plus de 2 g/dl en dessous de la limite inférieure de la normale;

• B pour lésions osseuses (**B**one lesions) caractérisées par une ou plusieurs lésions osseuses par radiographie, scanner ou TEP-scanner.

4. Pronostic

L'International Myeloma Work Group a récemment révisé l'index pronostic international (Revised-International Staging System) [9]. L'évaluation du pronostic comporte le dosage de la β2m et le taux d'albuminémie pour définir l'International Staging System (ISS), le dosage de la lactate déshydrogénase (LDH) et une analyse cytogénétique des plasmocytes par FISH à la recherche de translocation (4 ;14), translocation (14 ;16) et délétion 17p. La combinaison de ces marqueurs pronostiques permet de stratifier les patients en 3 groupes (Tableau 3). Les médianes de survie globale à 5 ans sont de 82% pour le R-ISS I, 62% pour le R-ISS II et 40% pour le R-ISS III ; les médianes de survie sans progression à 5 ans sont de 55%, 36% et 24%, respectivement.

Tableau 3. Définition des stades du R-ISS et impact sur la survie [4].

Facteur Pronostic	Stade	Définition
ISS	I	β2m < 3,5 mg/l et Albumine ≥ 35 g/l
	II	Ni stade I, ni stade III
	III	β2m ≥ 5,5 mg/l
FISH	Risque standard	Pas de haut-risque
	Haut risque	Présence d'une del17p et/ou t(4 ;14) et/ou t(14 ;16)

LDH	Normales	< limite supérieure de la normale
	Hautes	> limite supérieure de la normale
R-ISS	I	ISS I et Risque cytogénétique standard et LDH normales
	II	Pas R-ISS I ni III
	III	ISS III et soit haut-risque cytogénétique soit LDH augmentées

5. Prise en charge thérapeutique du MM

Bien que le MM reste une maladie incurable, l'avènement des nouveaux agents thérapeutiques (inhibiteurs du protéasome, immunomodulateurs et plus récemment les anticorps-monoclonaux) depuis ces 15 dernières années ont significativement amélioré le pronostic des patients.

a. Myélome multiple asymptomatique

Pour l'heure, aucun traitement n'est recommandé pour les myélomes asymptomatiques en dehors d'essais thérapeutiques et seule une surveillance est préconisée. Les recommandations de l'IMWG préconisent de répéter le bilan 2 à 3 mois après le diagnostic puis tous les 4 à 6 mois pendant un an puis tous les 6 à 12 mois [10]. Cependant des essais cliniques ont montré le possible intérêt d'une intervention thérapeutique précoce pour les MM asymptomatiques [11].

b. Myélome Multiple symptomatique

Deux groupes de patients sont distingués, ceux éligibles à un traitement intensif (moins de 65 ans, voire 70 ans et absence de comorbidité importante) de ceux non éligibles à une autogreffe de cellules souches hématopoïétiques (de façon générale, les patients de plus de 65 à 70 ans et/ou présentant une comorbidité importante).

Chez les sujets éligibles à une intensification thérapeutique, le principe du traitement de première ligne repose sur la succession de phases d'induction, d'intensification, de consolidation et de maintenance. La phase d'induction est constituée par une combinaison d'une triplette thérapeutique associant un inhibiteur de protéasome, un immunomodulateur et de la dexaméthasone [12]. Quatre cycles sont habituellement réalisés, au cours desquels un recueil de cellules souches hématopoïétique est réalisé après mobilisation par endoxan. L'intensification thérapeutique est réalisée par une autogreffe de cellules souches hématopoïétiques après conditionnement par du melphalan à haute dose [13,14]. Un traitement de consolidation et de maintenance peut permettre d'améliorer la réponse et notamment la maladie résiduelle [15]. Le traitement de consolidation comprend classiquement la combinaison utilisée dans la phase d'induction. Enfin, un traitement de maintenance est administré pendant une période d'un an, souvent par un immunomodulateur. Le Lénalidomide a reçu l'AMM dans cette indication début Mars 2017. De nombreuses études ont montré une corrélation entre la qualité de la réponse au traitement et les taux de survie sans progression et survie globale dans le MM chez les sujets éligibles à un traitement intensif, d'où l'importance d'obtenir une réponse complète [16].

Traitement de première ligne des patients non éligibles à une intensification thérapeutique. Les patients âgés de plus de 65 ans représentent plus de 60% des nouveaux patients diagnostiqués avec un MM. L'intensification thérapeutique par autogreffe de cellules souches périphériques n'est pas accessible aux patients âgés en raison de morbidités associées trop importantes.

VMP (Bortezomib, Melphalan, Dexamethasone) : la combinaison VMP s'est avérée supérieure au MP pour la survie sans progression, la survie globale, la survie sans traitement et les taux de RC dans l'essai international de phase 3 VISTA (Velcade as Initial Standard Therapy) [17].

RD (Revlimid et Dexamethasone) : un récent essai de phase 3 dirigé par l'IFM a montré la supériorité d'une combinaison par RD pendant 18 mois ou jusqu'à la rechute en comparaison d'un traitement associant MPT (melphalan, prednisone, thalidomide) [18].

c. Perspectives

De nouvelles approches thérapeutiques sont à l'étude en première ligne ou à la rechute dans le MM. Il s'agit notamment d'immunothérapies et de thérapies ciblées. Concernant l'immunothérapie, deux anticorps monoclonaux, l'un anti-CD38 (daratumumab) [19] et l'autre anti-SLAMF7 (elotuzumab) [20], ont été développés et ont démontré une efficacité prometteuse. Ces anticorps monoclonaux ciblent des marqueurs de surface des plasmocytes (CD38 et SLAMF7) et induisent une réaction de type ADCC (*Antibody-dependent cell-mediated cytotoxicity*) permettant l'activation des cellules NK contre les cellules tumorales. Une nouvelle génération d'immunothérapies dans la prise en charge

des cancers est représentée par les inhibiteurs de checkpoint PD-1 et PD-L1. Ces approches sont actuellement à l'étude, ce qui permettra d'en définir la place dans l'arsenal thérapeutique du MM. D'autres thérapies ciblées tels que le Venetoclax (inhibiteur de Bcl-2), S63845 (inhibiteur de Mcl-1) et Selinexor (inhibiteur de XPO-1) pourraient présenter un intérêt, notamment dans des sous-groupes moléculaires spécifiques de tumeurs. En effet, le Venetoclax semble avoir une efficacité notable dans les MM avec t(11 ;14) qui présentent un ratio Bcl-2/Bcl-X_L élevé. Il sera intéressant d'étudier le nouvel inhibiteur de Mcl-1 dans les MM avec gain de 1q – siège du gène *MCL-1*. Par ailleurs, il a été rapporté une efficacité particulière du Selinexor dans les cancers du poumon présentant une mutation de KRAS. De plus, les nouvelles générations d'inhibiteurs du protéasome et d'immunomodulateurs pourront vraisemblablement améliorer la prise en charge thérapeutique des patients atteints de MM.

d. Evaluation de la réponse au traitement

L'évaluation de la réponse au traitement du myélome repose essentiellement sur le suivi du composant monoclonal. L'examen de la moelle osseuse est indiqué afin de définir la réponse complète stringente par cytométrie en flux et d'évaluer la maladie résiduelle (par technique de cytométrie en flux et de *next generation sequencing*).

II. Rôle de MYC dans le Myélome Multiple

1. Dérégulation de MYC dans le MM

a. MYC est un oncogène central dans le MM

Tout MM est précédé du stade précurseur MGUS [21,22], qui a un taux de progression de 1% par an [23]. L'identification des marqueurs moléculaires responsables de la progression de MGUS à MM représente une étape importante dans la perspective d'une médecine de précision et du traitement de la maladie.

L'activation de MYC est l'un des événements centraux induisant la progression de la maladie [24]. L'analyse de *gene expression profiling* (GEP) a montré que la signature de l'activation MYC n'était pas présente au niveau de plasmocytes normaux ou de MGUS, mais exprimée dans environ 67% des cas de MM, (Tableau 4).

Tableau 4. Dérégulation de MYC dans le myélome multiple

	MGUS	MM
MYC translocations	3%	15-20%
Gain of MYC	< 5%	15-20%
MAPK mutations	7%	40%
DIS3 mutations	-	10%
MYC activation signature	0%	67%

Le rôle prépondérant de MYC dans la progression de MGUS à MM a aussi été démontré par un modèle de souris transgéniques, appelé Vk*MYC [25]. Dans ce modèle,

MYC est sous le contrôle des éléments de régulation du gène de la chaîne légère kappa (Vk). Cependant, le troisième codon de Vk a été muté pour, à la fois, générer un codon stop et créer un motif DGYW, cible préférentielle de l'enzyme AID (*activation induced cytidine deaminase*) au cours de l'hypermutation somatique (SHM). Par voie de conséquence, l'activation MYC ne se produit que dans les plasmocytes subissant une SHM, lorsque le codon stop est muté de façon aléatoire, permettant ainsi une surexpression de MYC. Dans ce modèle, les souris C57BL/6 contrôles développent une MGUS à l'âge adulte, tandis que les souris Vk*MYC développent un MM [25].

Ces travaux indiquent le rôle central de l'activation de l'oncogène MYC dans la progression de MGUS à MM. En outre, les données clinico-biologiques de cohortes de patients ont informé sur l'existence de réarrangements et des gains impliquant le locus MYC, ainsi que sur la surexpression de l'ARNm de MYC et la stabilisation de la protéine MYC (Figure 1).

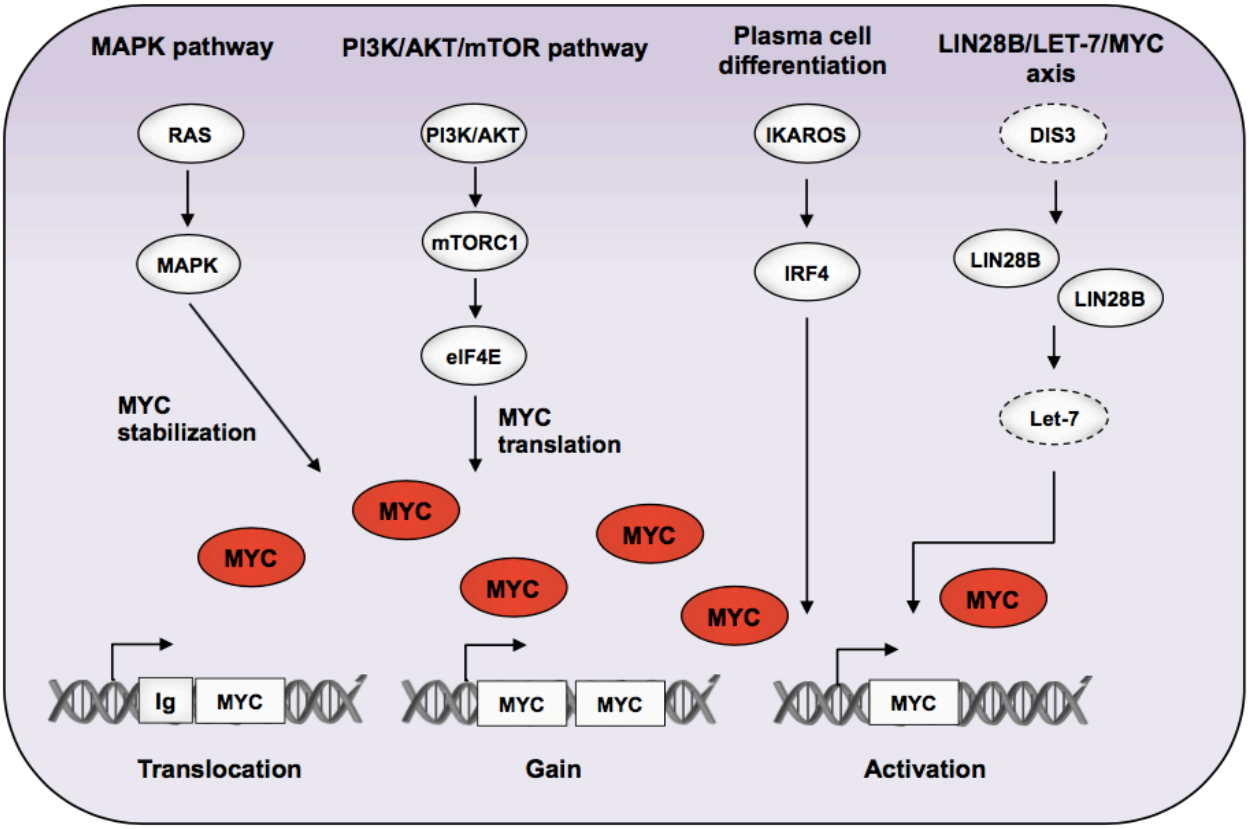

Figure 1. Régulation de MYC dans le myélome multiple

b. Translocations impliquant le locus MYC

Environ 15 à 20% des patients ayant un nouveau diagnostic de MM ont une translocation impliquant MYC [26,27]. Ces translocations concernent les loci d'immunoglobuline (Ig) (IgH > IgL > IgK) et certains partenaires non-Ig tels que FAM46C, FOXO3 et BMP6. Dans tous les cas, MYC est sous le contrôle d'amplificateurs des loci partenaires, ce qui entraîne une surexpression de l'oncogène [26,28,29]. Les patients présentant une translocation impliquant MYC ont une survie sans progression (SSP) et une survie globale (SG) diminuées [26]. Une signature de kataegis, correspondant à des sites focaux d'hypermutations somatiques associées à la

dérégulation de protéines APOBEC, est fréquemment retrouvée au niveau des sites de translocation, suggérant son rôle mécanistique dans les translocations de MYC dans le MM [26]. De façon notable, **l**es translocations de MYC sont rarement détectées chez les patients atteints de MGUS et de SMM (3% et 4% respectivement) [27].

c. Gain du 8q24.21

Les gains et les amplifications de MYC au locus 8q24.21 sont présents dans environ 15% des patients MM nouvellement diagnostiqués et est associé à une survie plus courte dans l'analyse univariée [30,31]. Les données d'anomalies du nombre de copies par analyses de séquençage exomique complet retrouvaient des gains de MYC dans 19% des cas au diagnostic. Parmi eux, 38% avaient un gain de MYC associé à une translocation MYC [26]. Il est à noter que le gain de MYC est rarement observé dans les cas de MGUS [32].

d. RAS stabilise la protéine MYC

NRAS et KRAS sont les deux gènes les plus fréquemment mutés dans le MM. Les mutations de la famille RAS sont présentes dans environ 40% des MM nouvellement diagnostiqués [33,34]. L'activation de la voie RAS induit une stabilisation de la protéine MYC, la protéine MAPK phosphoryle MYC au niveau de la Ser62, prolongeant ainsi sa demi-vie en empêchant sa dégradation protéolytique [35,36]. De plus, l'analyse de GEP a démontré que presque tous les MM mutés pour RAS expriment la signature d'activation de MYC [24], sans que des translocations MYC ne soient retrouvées, suggérant le rôle de RAS dans l'activation de MYC.

f. IRF4 dépendance et MYC

IRF4 appartient à la famille du facteur régulateur de l'interféron (IRF), qui se compose d'un ensemble de facteurs de transcription en aval de la voie de signalisation de l'interféron. L'expression d'IRF4 est limitée au système immunitaire, et a un rôle critique dans le développement des cellules lymphoïdes [37]. Des études d'ARN interférence ont révélé qu'IRF4 est un gène essentiel dans le MM [38]. En effet, le knockdown (KD) d'IRF4 entraîne la mort cellulaire dans les lignées de MM, indépendamment d'autres anomalies génétiques présentées dans chaque ligne. Le profil d'expression génique ainsi que l'analyse de l'immunoprécipitation de l'ADN des sites de liaison d'IRF4 ont établi que MYC est un gène directement cible d'IRF4 [38]. IRF4 se fixe au promoteur de MYC et active ainsi son expression. MYC active aussi l'expression d'IRF4, créant une boucle de rétrocontrôle positif. De plus, il existe une corrélation positive entre les expressions d'IRF4 et de MYC sur des échantillons primaires de patients atteints de MM [38].

2. Fonction de MYC dans le cancer

a. MYC active la réplication de l'ADN

MYC a un rôle direct dans le contrôle de la réplication de l'ADN par son interaction avec les protéines du complexe pré-réplicatif telles que MCM2, MCM7, ORC2, Cdc6 et Cdt1. MYC se localise au niveau des sites de synthèse de l'ADN et module l'activité de réplication de l'ADN. Il a été constaté que la surexpression de MYC induit une augmentation du nombre de fourches réplicatives de l'ADN dans la phase S [39]. Cette

activation de réplication induite par MYC est associée à des dommages de l'ADN, pouvant expliquer la présence de modifications génomiques associées à la dérégulation de MYC, telles que l'aneuploïdie et les cassures chromosomiques [39,40], (Figure 2).

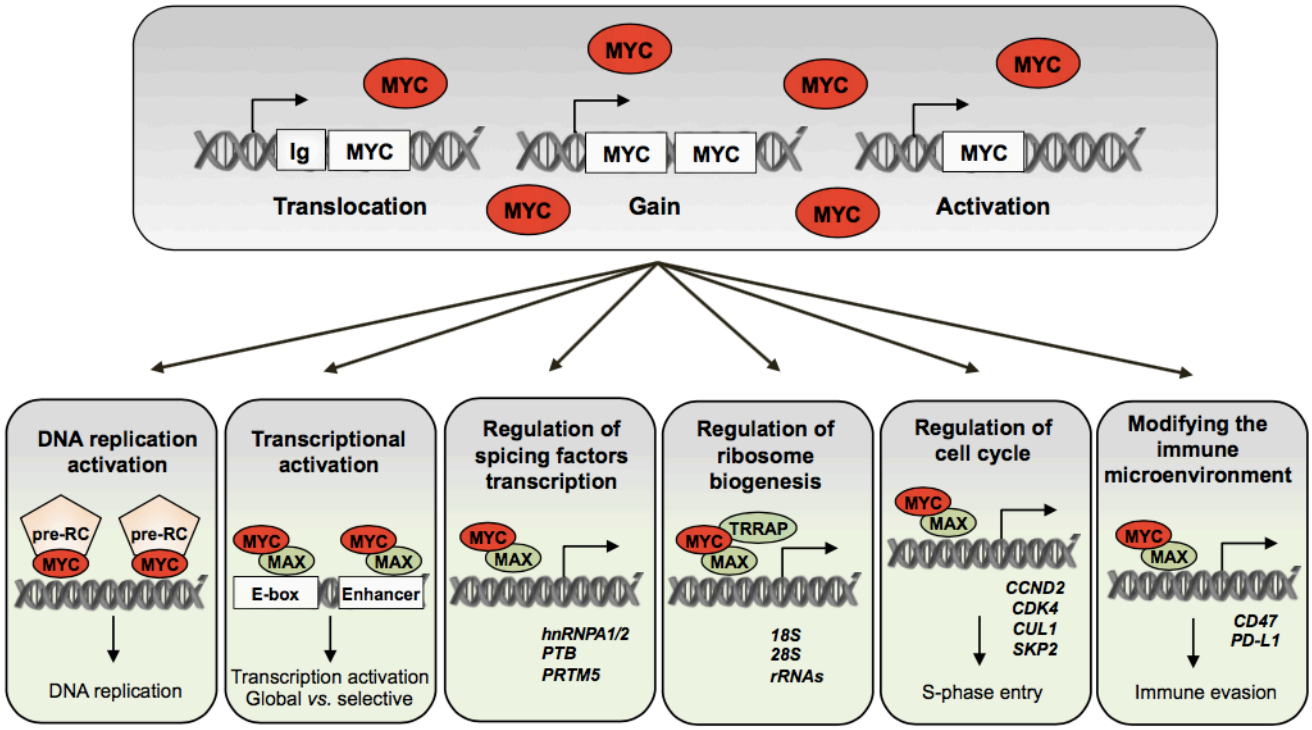

Figure 2. Function de MYC dans le cancer

b. MYC régule la transcription selon deux modèles opposés

On estime que MYC régule environ 10 à 15% du génome [41]. À de faibles niveaux d'expression, MYC se lie aux séquences E-box de promoteurs aux niveaux d'histones H3K4me3 et induit la transcription par l'ARN polymérase II (Pol II). Cependant, en cas de surexpression, MYC se fixe à un plus grand nombre de promoteurs, caractérisés par la présence d'histones H3K4me1, H3K4me3 et H3K27ac et active la transcription de gènes par les trois ARN polymérases (Pol I, II et III) [42]. MYC agit comme un activateur

de la transcription lorsqu'il est hétérodimérisé à MAX et comme un répresseur lorsqu'il se lie aux facteurs de transcription de la famille MXD.

Malgré une recherche intensive, la définition des gènes cibles MYC n'est pas claire et deux modèles différents existent: l'un global ou l'autre sélectif. Le premier modèle est soutenu par deux publications en 2012, suggérant que MYC agit comme un amplificateur général de la transcription, étant présent au niveau de tous les promoteurs actifs de la cellule ; un phénomène appelé « invasion de la chromatine » [43,44]. Dans ce cas, la surexpression de MYC n'induirait pas la transcription d'un pool de gènes spécifiques, mais amplifierait le programme transcriptionnel existant de la cellule. Cependant, une publication en 2014 a proposé un scénario différent où MYC régule directement un ensemble de gènes sélectif, activant ou réprimant leur transcription [45]. Ces données sont fondées sur des résultats d'immunoprécipitation de la chromatine à l'échelle du génome et de profils d'expression d'ARN pendant la lymphomagenèse des lymphocytes B, ayant permis de distinguer les effets directs et indirects de MYC sur la transcription [45]. Ces travaux ont conduit à la conclusion que l'amplification de l'ARN au niveau des cellules surexprimant MYC est indépendante de l'invasion de la chromatine par MYC, qui régule un nombre sélectif de gènes eux-mêmes pouvant être responsables d'activation transcriptionnelle (Figure 2).

c. MYC régule les facteurs d'épissage

MYC régule directement la transcription d'un certain nombre de gènes impliqués dans la machinerie du spliceosome, tels les petits gènes d'assemblage de la ribonucléoprotéine nucléaire (snRNP) hnRNPA1 et hnRNPA2, PTB et PRTM5.

Plusieurs exemples illustrent que la dérégulation de l'épissage des ARN par une surexpression de MYC, participe à l'oncogenèse.

L'épissage alternatif de la pyruvate kinase (PKM) génère deux variantes possibles d'épissage - PKM1, qui favorise la phosphorylation oxydante (isoforme adulte) et PKM2, qui favorise la glycolyse aérobie (isoforme embryonnaire / tumorale) [46,47]. MYC induit l'augmentation de la transcription de PTB, hnRNPA1 et hnRNPA2, assurant un ratio PKM2/PKM1 élevé, responsable de la progression tumorale.

Au cours de la lymphomagenèse, MYC active la transcription du gène d'assemblage de particules de ribonucléoprotéines nucléaires, PRMT5, qui est essentiel pour l'épissage, la survie et la prolifération des cellules tumorales [48]. Ces résultats suggèrent que les cellules surexprimant MYC sont en général plus sensibles à l'inhibition de l'épissage (Figure 2).

d. MYC active la traduction des protéines

MYC induit la transcription de l'ARN ribosomique (ARNr) en se liant aux motifs E-box dans leurs promoteurs et en stimulant leur transcription par l'ARN polymérase I [49,50].

Les expériences effectuées sur les souris transgéniques Eμ-Myc (surexpression de MYC au niveau des lymphocytes B) ont montré que la capacité de MYC à augmenter et à activer la traduction est nécessaire à son potentiel oncogène. Chez les souris transgéniques Eμ-Myc, la perte d'un allèle des gènes RPL24 ou RPL38 codant pour des protéines ribosomales entraîne une suppression de la lymphomagenèse. Ces résultats suggèrent que le ciblage de composants de la biogenèse du ribosome pourrait être utilisé pour inhiber la tumorigenèse induite par MYC.

Les cancers liés à une surexpression de MYC sont également dépendant de l'activité traductionnelle. La protéine 1 de liaison à eIF4E (EIF4EBP1) réprime l'initiation de la traduction en se liant au facteur de l'initiation de la traduction eIF4E, empêchant ainsi le recrutement d'ARNm au niveau du ribosome. Dans le modèle de souris transgéniques Eμ-MYC, la surexpression de MYC induit l'hyper-phosphorylation de EIF4EBP1, ce qui bloque sa fixation à eIF4E et induit une activation de la traduction, nécessaire à la prolifération tumorale [51,52], (Figure 2).

e. Cycle cellulaire, métabolisme et apoptose

Cycle cellulaire. Dans les cellules normales, l'inhibition de MYC entraîne une interruption du cycle cellulaire aux phases G0/G1 et G1/S [53,54]. MYC favorise la transition vers la phase S du cycle cellulaire par divers mécanismes [55-58]. MYC active la transcription de la plupart des gènes impliqués dans la régulation du cycle cellulaire. Ces gènes cibles MYC comprennent les cyclines dépendantes des kinases (CDK), les cyclines et les facteurs de transcription E2F. En outre, MYC antagonise l'activité des inhibiteurs de CDK tels que p21 et p27, en bloquant la transcription CDKN1A (codant pour p21) ou en induisant Skp2, une protéine impliquée dans la dégradation p27 [59]. MYC induit également CUL1, qui est un composant du complexe d'ubiquitine ligase E3, requis pour l'ubiquitination et la dégradation de p27 [60], ce qui conduit à l'entrée des cellules en phase S [61], (Figure 2).

Métabolisme. Afin de maintenir un taux de prolifération élevé, les cellules cancéreuses subissent des changements métaboliques profonds. MYC régule la transcription de plusieurs gènes qui participent à la glycolyse et à la glutaminolyse, tels que les

transporteurs de membrane du glucose GLUT1 (SLC2A1) et le transporteur de glutamine ASCT2 (SLC1A5) [62,63]. En plus d'induire l'expression de ces gènes, MYC favorise également l'expression de variants d'épissage tels que PKM2, qui active la glycolyse [47]. A l'état physiologique, l'expression de MYC est inhibée en cas de faibles apports en métabolites à la cellule, ce qui induit une diminution de la prolifération cellulaire. Lorsque MYC est surexprimé, il n'y a pas de rétrocontrôles négatifs et les cellules cancéreuses sont dépendantes d'un apport nutritif élevé, ce qui pourrait représenter une vulnérabilité thérapeutique [64].

Apoptose. Outre son rôle important dans la progression du cycle cellulaire, MYC est impliqué dans le processus de mort cellulaire programmée (apoptose). Il peut paraître paradoxal que MYC ait la capacité d'induire l'apoptose. Cependant, à l'état physiologique, les cellules d'organismes multicellulaires possèdent des mécanismes de régulation induisant l'apoptose en cas de survenue de niveau d'expression oncogénique de MYC. La capacité de MYC à induire la mort cellulaire – ainsi que dans le cas d'autres oncoprotéines - a été appelée « activité suppresseur de tumeur latente ou intrinsèque » [65]. L'activation de la protéine anti-apoptotique Bcl-2 représente un mécanisme d'échappement à l'apoptose en cas de surexpression de MYC. Dans les tumeurs où MYC est surexprimé, divers réarrangements dans le locus Bcl-2 ont également été rapportés [66,67]. Des expériences de surexpression simultanée de MYC et BCL-2 dans des modèles de souris transgéniques ont permis de démontrer que la surexpression de la BCL-2 compense des niveaux élevés de MYC, qui normalement induisent l'apoptose [68-70].

f. MYC et le microenvironnement immunitaire

Les tumeurs doivent échapper à la surveillance immunitaire. La surexpression de molécules immunosuppressives telles que la PD-L1 (*Programmed death-ligand 1*) représente un mécanisme clé de l'évasion immune dans les cancers. MYC régule l'expression de deux gènes impliqués dans le contrôle immunologique et exprimés à la surface de la cellule tumorale: le régulateur de l'immunité inné CD47 et le régulateur de l'immunité adaptative PD-L1 [71], en se liant directement à leurs promoteurs. L'inactivation de MYC dans les modèles de souris induit une sous-expression de CD47 et PD-L1, induisant une réponse immunitaire anti-tumorale (Figure 2).

3. Ciblage de MYC

Les cellules de MM dépendent de l'activité de MYC, qui est une cible thérapeutique potentielle [72]. L'inhibition directe des facteurs de transcription tels que MYC reste un défi dans le domaine de la pharmacologie. Plusieurs approches ont été développées pour cibler directement ou indirectement MYC dans le MM (Figure 3), dont certaines sont évaluées dans les essais cliniques (Tableau 5).

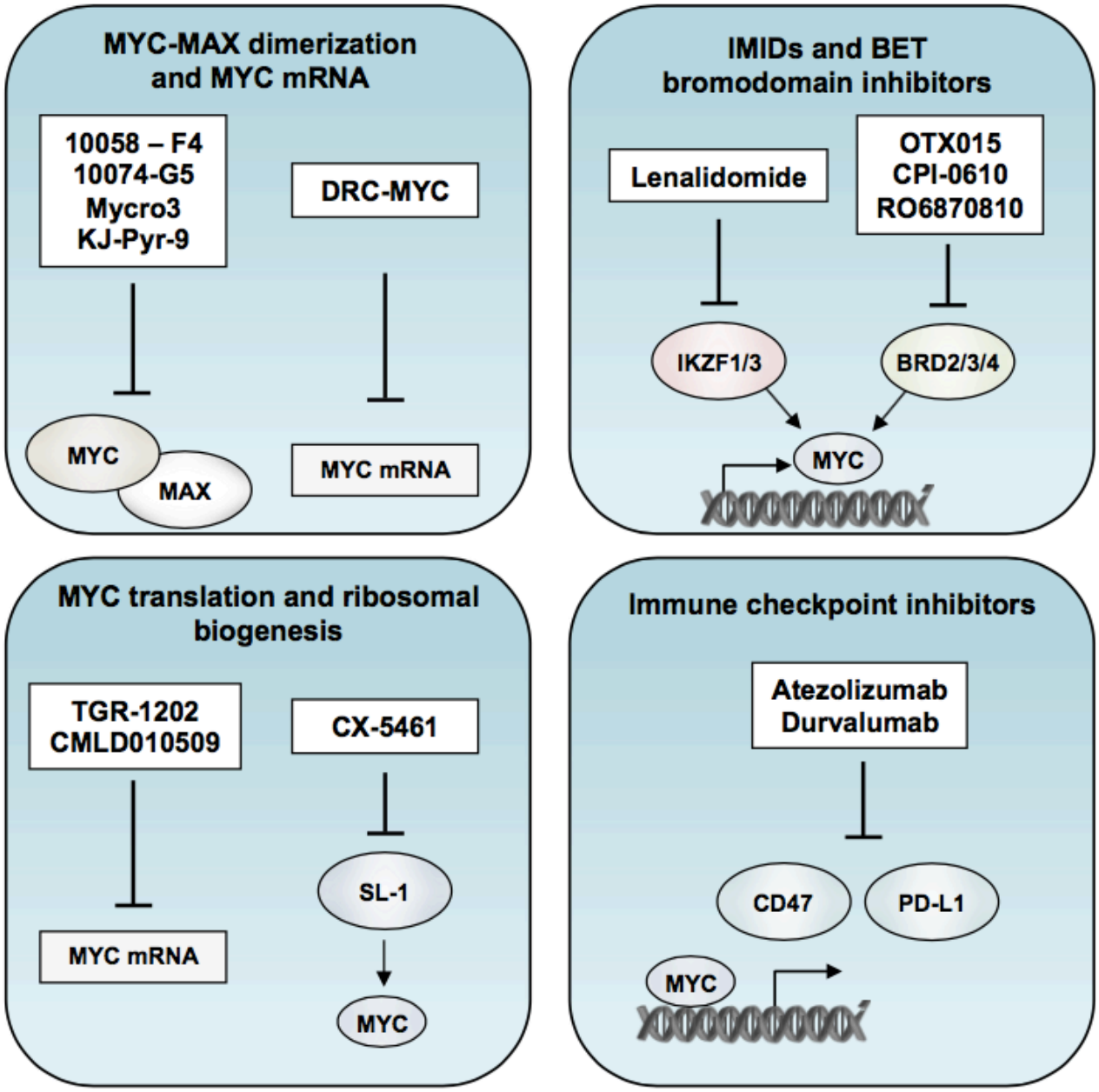

Figure 3. Ciblage de MYC dans le myelome multiple

a. Ciblage de MYC par des siARN

L'inhibition directe de MYC a été étudiée par emploi d'ARN interférence (siARN) ciblant l'ARNm de MYC, encapsulé dans des nanoparticules lipidiques, appelés DCR-MYC. Le

siRNA correspond à un DsiARN, conçu pour activer l'endoribonucléase DICER [73]. Le DsiARN se lie aux ARNm de MYC et induit sa dégradation par DICER, empêchant ainsi la traduction et l'expression de la protéine MYC. Un essai clinique de phase 1 (NCT02110563) évalue la sécurité et la tolérance de DCR-MYC chez les patients atteints de tumeurs solides, de MM ou de lymphomes.

b. Inhibition de l'interaction MYC-MAX

MYC s'hétérodimérise à MAX et se lie aux séquences E-box au niveau des promoteurs de ses gènes cibles. L'inhibition de la dimérisation MYC/MAX représente une option thérapeutique attrayante. Plusieurs molécules, telles que 10058-F4 76 ou 10074-G5 78, ont démontré une activité importante dans l'inhibition de la dimérisation MYC/MAX *in vitro*. Cependant, la dégradation rapide et la mauvaise répartition de ces molécules *in vivo* ont entravé leur développement ultérieur. Néanmoins, de nouvelles molécules inhibant MYC/MAX – telles que Mycro3 ou KJ-Pyr-9 - ont montré une biodisponibilité accrue et une efficacité dans différents modèles murins de xénogreffes [74,75].

c. inhibition des protéines à bromodomain

Les membres de la sous-famille BET (Bromo- and Extra-Terminal domain) de protéines à bromodomain, telles que BRD2, BRD3 et BRD4, reconnaissent les résidus de lysine acétylés N-terminaux des histones, conduisant ainsi à la modulation de la structure de la chromatine et à l'expression des gènes cibles. L'expression de MYC est directement régulée par les protéines BET. Le développement récent de JQ1, un inhibiteur sélectif des motifs protéiques de type bromodomaine, permet d'envisager le ciblage de MYC

par inhibition de sa transcription [76]. Ce thiéno-triazolo-1,4-diazépine se lie à la poche de fixation au bromométhane-acétyl-lysine, empêchant la fixation des protéines BET à la chromatine. L'inhibition BET par JQ1 régule la transcription MYC et, par conséquent, les gènes cibles dépendants de MYC. Cela a été associé à un effet antiprolifératif avec arrêt du cycle cellulaire et sénescence cellulaire [76].

Les inhibiteurs BRD sont évalués dans des essais cliniques en phase initiale. Le premier inhibiteur - OTX015 (MK-8628) - a été testé dans un essai de phase I pour établir la dose maximale tolérée chez les patients atteints de lymphomes et de MM (NCT01713582) [77]. D'autres molécules comme CPI-0610 ont montré une activité préclinique en inhibant IKZF1, IRF4 et MYC [78,79] et est aussi testée dans un essai de phase I incluant des patients atteints de MM (NCT02157636). Une autre étude de Phase Ib est conçue pour évaluer la sécurité et la tolérance de RO6870810, en monothérapie et en association avec le daratumumab, chez des patients présentant un MM réfractaire (NCT03068351).

d. Immunomodulateurs

Le développement de médicaments immunomodulateurs (IMiDs), dont le thalidomide, le lénalidomide et le pomalidomide, a considérablement amélioré la prise en charge des patients atteints de MM au cours des 20 dernières années. Les IMiDs ont démontré une efficacité thérapeutique remarquable dans le MM, avec des taux de réponse supérieurs à 70% pour le lenalidomide en association à la dexaméthasone en première ligne thérapeutique [80,81]. Cependant, le mécanisme d'action des IMiDs dans le MM n'a été découvert que récemment. Les protéines Ikaros (IKZF1 et IKZF3) sont des facteurs de

transcription qui régulent une différenciation lymphocytaire B. IKZF3 régule l'expression d'IRF4, régulant lui-même l'expression de MYC. Le lénalidomide exerce son activité anti-tumorale dans le MM par sa liaison d'une part, à l'ubiquitine ligase céréblon (CRBN) et, d'autre part, aux protéines IKZF1 et IKZF3. Ainsi, le lénalidomide induit l'ubiquitination et la dégradation d'IKZF1 et IKZF3, réprimant l'expression d'IRF4 et de MYC ce qui conduit à la mort cellulaire [82,83].

e. Inhibition du splicéosome

MYC participe à l'épissage des ARN en régulant l'expression de gènes impliqués dans la machinerie du splicéosome. Des études de dépendances géniques ont montré que les tumeurs surexprimant MYC sont dépendantes de l'expression de facteurs du splicéosomes tels que SF3B1, U2AF1, SNRPF, EFTUD2 et BUD31 [84]. Le knockdown de BUD31 ou SF3B1, ou l'inhibition pharmacologique de SF3B1 par la molécule SD6, retarde l'apparition de tumeurs primaires et la formation de métastases dans des modèles murins de xénogreffes de cancer du sein surexprimant MYC [84]. Ces résultats suggèrent que le ciblage du splicéosome offre une opportunité thérapeutique dans les cancers liés à MYC.

Tableau 5. Ciblage de MYC dans le myélome multiple

Strategy	Mechanism of action	Drug	Development phase
Direct inhibition of MYC	Prevent MYC/MAX dimerization	Mycro3	Effective in mouse models
		KJ-Pyr-9	Effective in mouse models
	MYC mRNA degradation	DCR-MYC	Phase I (NCT02110563)
Indirect inhibition of MYC	Inhibit MYC transcription	OTX015	Phase I (NCT01713582)
		CPI-0610	Phase I (NCT02157636)
		RO6870810	Phase I (NCT03068351)
		Lenalidomide	FDA approved
	Inhibit MYC translation	CMLD010509	Effective in mouse models
		TGR-1202	Phase I/II (NCT02867618)
	Inhibit ribosomal biogenesis	CX-5461	Effective in mouse models
Target adaptive immune checkpoint	Anti-PD-L1 agents	Atezolizumab	Phase I (NCT02784483, NCT02431208, NCT01375842)
		Durvalumab	Phase I (NCT02616640, NCT02685826, NCT02886065, NCT02716805) Phase II (NCT02807454, NCT03000452)

ARTICLE 1

The *LIN28B/let-7* axis is a novel therapeutic pathway in Multiple Myeloma

Résumé

Dans ce travail, nous rapportons que l'expression de LIN28B est corrélée à celle de MYC et est associée à un mauvais pronostic dans le MM par étude de bases de données de *Gene Expression Profiling*. Nous montrons que l'axe LIN28B/let-7 module l'expression de l'ARNm de MYC, lui-même cible de let-7. En effet, la protéine fixant des ARN Lin28B se fixent aux microARN let-7 et bloque leur maturation. A l'état physiologique, let-7 se fixe au 3'UTR de MYC dans les plasmocytes normaux et induit sa dégradation par activation du complexe RISC (*RNA-induced silencing complex*). Dans les plasmocytes tumoraux, la surexpression de LIN28B induit la dégradation de let-7 et par conséquent une surexpression de MYC. De plus, la perturbation de l'axe LIN28B/let-7 régule la prolifération des lignées cellulaires de MM *in vitro* et *in vivo*. L'analyse par séquençage d'ARN de modèles de lignées KO pour LIN28B, par utilisation de CRISPR, a montré que l'axe LIN28B/let-7 régule les voies de signalisation de MYC et du cycle cellulaire dans MM. Nous avons ensuite utilisé la technologie LNA-GapmeR (*locked nucleic acid*) pour étudier la possibilité de cibler MYC par emploi de séquences d'acides nucléiques contenant une séquence analogue à let-7b. Dans un modèle murin de xénogreffe de MM, nous montrons que des niveaux élevés d'expression de let-7, par administration de LNA-GapmeR let-7b par voie intra-

péritonéale, répriment la croissance tumorale en régulant l'expression de MYC, *in vivo*. Ces résultats montre l'existence d'un nouveau mécanisme de régulation de MYC dans le MM par l'axe LIN28B/let-7 et la possibilité ciblage thérapeutique de MYC par emploi d'acides nucléiques mimant let-7.

Contribution de l'auteur

Salomon Manier a participé à l'ensemble du design et à la réalisation de toutes les expériences *in vitro* et *in vivo* : qRT-PCR des miARN et ARNm, Western Blot, confection et infection de lignées cellulaires avec des lentivirus contenant des shRNA ou sgRNA associés à la protéine Cas9, prolifération cellulaire par thymidine uptake, transfection de miARN par lipofectamine, préparation des librairies d'ARN pour séquençage à haut débit, injection des souris, suivi des souris. Il a aussi réalisé l'ensemble des analyses bioinformatiques par analyse de base de données et GSEA (Gene Set Enrichment Analysis). Salomon Manier a interprété les résultats, généré les figures et écrit le manuscrit.

The *LIN28B/let-7* axis is a novel therapeutic pathway in Multiple Myeloma

Salomon Manier[1-3], John T. Powers[4], Antonio Sacco[1], Siobhan V. Glavey[1], Daisy Huynh[1], Michaela R. Reagan[1], Karma Z. Salem[1], Michele Moschetta[1], Jiantao Shi[1], Yuji Mishima[1], Catherine Roche-Lestienne[3], Xavier Leleu[2], Aldo M. Roccaro[1], George Q. Daley[4], Irene M. Ghobrial[1]

[1]Department of Medical Oncology, Dana-Farber Cancer Institute, Harvard Medical School, Boston 02215 MA, USA; [2]Service des Maladies du Sang, CHRU Lille, 59000 Lille, France; [3]Jean-Pierre Aubert Research Centre, INSERM U1172, University Lille 2, 59000 Lille, France; [4]Division of Pediatric Hematology/Oncology, Children's Hospital, Harvard Medical School, Boston 02215 MA, USA;

Corresponding author:

Irene M. Ghobrial,

Medical Oncology, Dana-Farber Cancer Institute,

HIM 237, 77 Ave Louis Pasteur,

Boston, Massachusetts 02115, USA.

Phone: 617.632.4198; Fax: 617.632.4862;

E-mail: irene_ghobrial@dfci.harvard.edu.

Running title: *Lin28B*/*let-7*/*MYC* axis in MM

Abstract

MYC is a major oncogenic driver of Multiple Myeloma (MM) and yet almost no therapeutic agents exist that target *MYC* in MM. Here we report that the *let-7* biogenesis inhibitor *LIN28B* correlates with *MYC* expression in MM and is associated with adverse outcome. We also demonstrate that the *LIN28B/let-7* axis modulates the expression of *MYC*, itself a *let-7* target. Further, perturbation of the axis regulates the proliferation of MM cells *in vivo* in a xenograft tumor model. RNA sequencing and gene set enrichment analyses of CRISPR-engineered cells further suggest that the *LIN28*/*let-7* axis regulates *MYC* and cell cycle pathways in MM. We provide proof-of-principle for therapeutic regulation of *MYC* through *let-7* with an LNA-GapmeR containing a *let-7b* mimic *in vivo*, demonstrating that high levels of *let-7* expression repress tumor growth by regulating *MYC* expression. These findings reveal a novel mechanism of therapeutic targeting of *MYC* through the *LIN28B/let-7* axis in MM that may impact other *MYC* dependent cancers as well.

Introduction

Multiple myeloma (MM), a tumor originating from plasma cells in the bone marrow (BM), has an annual incidence of 6.3 new cases per 100,000 individuals [85]. Despite the major advances in therapy for MM, it remains incurable and there are no targeted therapies for MM, in part due to the lack of therapies that target specific oncogenes involved in the pathogenesis of the disease. Genomic events such as chromosomal translocations, copy number variation, somatic mutations, and epigenetic modifications all contribute to gene deregulation of specific oncogenes or tumor suppressors during MM tumorigenesis [86]. Among those, *MYC* plays a central role in the progression of the disease. Approximately two thirds of newly diagnosed patients harbor *MYC* activation, which correlates with adverse clinical outcome [24]. *MYC* activation is commonly driven by translocation or copy number gain of chromosome 8q24, which contains the *MYC* locus [26,29]. Despite the dominant role of *MYC* in MM, there are very few therapeutic options targeting *MYC*. Previous studies have attempted to target *MYC* by using a bromodomain inhibitor to target BET proteins, which regulate *MYC* [76,87].

The *let-7* miRNA was originally discovered in *C. elegans* as a regulator of developmental timing and cell proliferation [88]. *Let-7* expression increases as cells become more differentiated. In humans, *let-7* miRNAs comprise a family of 12 members distributed over 8 genomic loci [89] that are often repressed in cancer [90]. *Let-7* miRNAs function as a tumor suppressor through regulation of key oncogenes, including *MYC* and *RAS*, by binding specific sites in the mRNA 3'-UTRs and inhibiting translation of these targets [91, 92]. Low expression of *let-7* family members is associated with poor prognosis in several cancer types [93,94].

In humans, *let-7g* and *let-7i* are located individually on chromosomes 3 and 12 respectively. The remaining *let-7* family members are distributed among six miRNA clusters at genetically distinct loci. The *let-7a2* and *let-7c* clusters are involved in hematopoietic stem and progenitor cell (HSPC) homeostasis by regulating the balance between TGFβ and Wnt signaling[95], whereas the *let-7e* cluster is highly expressed in HSPC and confers hematopoietic phenotypes [96]. However, the exact role of the various *let-7* family members in mammalian development has not yet been fully elucidated [97,98], in large part because it is technically difficult to knock out multiple *let-7* family members in the same individual cell. Moreover, these multiple *let-7* family members are likely to have functionally similar roles.

LIN28B is an RNA-binding protein highly expressed in stem cells and developing tissues where it impairs the processing of *let-7* precursors into mature, functional miRNAs [99]. Over-expression of *LIN28B* has been reported in several cancers [100] and is associated with advanced disease and poor outcome in ovarian [94], breast [101], colon [102], hepatocellular carcinoma [103,104] and neuroblastoma [105,106]. Transgenic *LIN28B* has been shown to induce multiple tumors types in mice including liver, Wilms, colon, and neuroblastoma, all of which solidify its oncogenic role [104,105,107,108]. *LIN28B* has also been reported to act through a *let-7*-independent manner, especially via regulation of *IGF2* [104].

While the *LIN28B*/*let-7* axis has been implicated in the regulation of *MYC* in different tumor types [100], its potential as a therapeutic target has not yet been explored, specifically in blood cancers. In this study, we define the mechanistic activity of the *LIN28/let-7* axis in clonal plasma cells and establish a potential therapeutic role of this

pathway in targeting *MYC* in MM, which could lead to significant therapeutic advances in MM and other cancers.

Methods

Cell and primary cells. The MM cell lines MM.1S and RPMI8226 were purchased from ATCC; KMS12BM and MOLP-8 were purchased from DSMZ and KMM-1 was purchased from JCRB Cell Bank. The MM.1S GFP^+Luc^+ cell line was generated by retroviral transduction with the pGC-GFP/Luc vector (gift of A. Kung, Dana-Farber Cancer Institute). Cells were authenticated by short tandem repeat DNA profiling. Primary samples were obtained from bone marrow aspiration from both MM patients and healthy controls. Plasma cells were isolated using $CD138^+$ microbead selection (Miltenyi Biotec®, Auburn, CA). All patients were diagnosed with active MM at diagnosis or at relapse, based on criteria of the International Myeloma Working Group [109]. Informed consent was obtained from all patients and healthy volunteers in accordance with the Declaration of Helsinki protocol.

Lentivirus-mediated shRNA silencing. *LIN28B* shRNA in lentiviral plasmid (TRCN0000122191 and TRCN0000122599) and control shRNA (SHC216V) were purchased from Sigma-Aldrich. For viral production, 293T cells were transfected with lentiviral gag/pol, VSV-G, and the lentiviral plasmid, at a ratio of 1:0.4:1, using Lipofectamine 2000. Viral particles were harvested after 24hrs and 48hrs. Two milliliters of viral supernatant were used to infect 1,000,000 cells in the presence of Polybrene (8 ng/μL). Infected cells were selected on Puromycin antibiotic before subsequent analysis.

Lentivirus-mediated CRISPR silencing. LentiCRISPRv2 (Addgene plasmid #52961) and lentiCRISPR:EGFPsgRNA-1 (#51760) were gifts from Feng Zhang [110]. *LIN28B* sgRNA were designed using the MIT Optimized CRISPR design tool. Sequences of sgRNA

were: 5'-CATCGACTGGAATATCCAA G-3' for sg*LIN28B*#1 and 5'-CAGAGCAAACTATTCATGGA-3' for sg*LIN28B*#2. Human U6 (hU6) primer 5'-GAGGGCCTATTTCCCATGATT-3' was used for validation by Sanger sequencing after cloning. Lentivirus production was processed as above for shRNA lentiviral production.

miRNA mimic transfection. Cell lines were transfected with hsa-let-7b mimic or with a control probe (mirVana miRNA mimic, Life Technology) at final concentration of 40 nM, using Lipofectamine 2000 according to manufacturer's instructions (Invitrogen). Culture medium was changed to regular medium 24 hours after transfection and cells were used for functional assays at 48 hours. For the rescue experiment, MOLP-8 sgGFP or sg*LIN28B*#1 were transfected with a control probe or a mix of anti-*let-7a, b, d*, and *g* (mirVana anti-miRNA, Life Technology) at a final concentration of 40 nM, using X-tremeGENE 9 according to manufacturer's instructions (Roche, Life Science).

Quantitative reverse transcription PCR. Mature miRNA and mRNA expression were analyzed by qRT-PCR using SYBR green dye on an Applied Biosystems AB7500 Real Time PCR System. All PCR reactions were run in triplicate. Ct values were normalized on RNU6B and 18S, respectively, and relative changes were calculated using the 2-ΔΔCt. The following primer sequences were used: *LIN28B*-F: 5'-GCCCCTTGGATATTCCAGTC-3'; *LIN28B*-R: 5'-TGACTCAAGGCCTTTGGAAG-3'; *MYC*-F: 5'-TCGGTCCTCGGATTCTCTGCTCT-3'; *MYC*-R: 5'-GCCTCCAGCAGAAGGTGATCCA-3'; KRAS-F: 5'-TGTGTCTCATATCAGGTTGACGA-3'; KRAS-R: 5' -CAAGAGTCGAGTGTGGTCTCA- 3'; CCND1-F: 5'-TCTACACCGACAACTCCATCCG-3'; CCND1-R: 5'-TCTGGCATTTTGGAGAGGAAGTG-3'; DICER1-F: 5'-

CTCCTACCACTACAATACTATCACT-3'; DICER1-R: 5'-GGTCTTCATAAAGGTGCTTGGT-3'; E2F6-F: 5'-GCGGAGAGTGTATGACATCACC-3'; E2F6-R: 5'-GTCAGAAAGTTCCTCCTGTAGCT-3'; HMGA1-F: 5'-GAAGTGCCAACACCTAAGAGACC-3'; HMGA1-R: 5'-GGTTTCCTTCCTGGAGTTGTGG-3'; pri-let-7d-F: 5'-GCCAAGTAGAAGACCAGCAAG-3'; pri-let-7d-R: 5'-CAAGGAAACAGGTTATCGGTG-3'; pri-let-7g-F: 5'-GTTCCTCCAGCGCTCCGTT-3'; pri-let-7g-R: 5'-CCATTACCTGGTTTCCCAGAGA-3'. Sequences for full mature *let-7* miRNA were used to design *let-7* forward primers, in combination with universal 3' miRNA reverse primer.

Immunoblotting. Whole-cell lysates were subjected to SDS-PAGE, and transferred to polyvinyldene fluoride (PVDF) membrane (Bio-Rad Laboratories). For immunoblotting we used antibodies against *LIN28B* (Cell signaling #4196S), c-*MYC* (Cell signaling #9402S) and GAPDH (Cell signaling #2118S).

Proliferation assay. Proliferation rates were measured by DNA synthesis, using (3H)-thymidine uptake (Perkin Elmer, Boston, MA) as described [111].

RNA-sequencing. RNA was extracted using Qiagen RNeasy Kit. Whole RNA (500ng) was subject to library preparation with NEBNext Ultra RNA Library prep for Illumina kit (BioLabs). A single unique index was assigned to each sample. Quality control of the libraries was evaluated by Bioanalyzer analysis with High Sensitivity chips (Agilent). Libraries were quantified by qPCR (Kapa assay) and multiplex before sequencing on a HiSeq 2000 (2X50bp paired-end reads) at the Biopolymers Facility of Harvard Medical School. Cutadapt was used to trim adapters; trimmed reads were aligned to Human reference genome (GRCh37) with tophat2; and read counts for each gene was

calculated by HT-seq. RNA-seq data have been deposited to the Gene Expression Omnibus (http://www.ncbi.nlm.nih.gov/geo/) under accession numbers GSE71100.

In vivo studies. SCID/bg mice (n=5/group) used for xenograft experiments were injected subcutaneously with MOLP-8 cells that were infected with either a *LIN28B* shRNA, or a control shRNA. Tumor volume (measured by caliper) were calculated by the formula: length × width^2 × 0.52 [112]. To evaluate the effect of *let-7* LNA-GapmeR (containing the sequence 5'-AGGTAGTAGGTTGTGT-3'), SCID/bg mice (n=5/group) were i.v. injected with 5x10^6 MM.1S GFP$^+$Luc$^+$ cells on day 0; followed by i.p. injections of *let-7* (20 mg/kg) or control LNA-GapmeR 2 times a week starting on day 2. Tumor growth was evaluated by bioluminescence imaging (BLI) and mice were followed for survival.

Results

Deregulation of *LIN28B/Let-7* axis in MM.

We first sought to determine whether *LIN28B* is deregulated in MM**,** and therefore analyzed two independent publicly available gene expression profiling datasets containing plasma cells from patients with newly diagnosed MM and healthy control donors. These included GSE24080 and GSE2658, containing 22 normal donor plasma cell samples and 559 plasma cell samples from patients with newly diagnosed patients - both from UAMS - and GSE16558, with 5 normal donor plasma cells and 65 plasma cell samples from patients with newly diagnosed MM**.** We identified a significant overexpression of *LIN28B* in MM cells compared to normal plasma cells in both datasets (Fig. 1a). We next sought to determine the prognostic relevance of *LIN28B* in the survival of patients with MM. We performed Kaplan Meier analysis on a cohort of 542 patients treated with Total Therapy 2 (GSE2658), and observed that high expression of *LIN28B* was associated with significantly worse overall survival, (p=0.0075) (Fig. 1b).

Therefore, we explored whether targeting the *LIN28B/let-7 axis* would have a therapeutically relevant role in MM and silenced *LIN28B* using two lentiviral short hairpins (shRNA) constructs that target the mRNA coding sequence in several *LIN28B*-expressing MM cell lines: MOLP-8, KMS12BM, RPMI8226 and KMM-1. The shRNAs caused degradation of *LIN28B* mRNA in all cell lines (Fig. 1c). Moreover, pri-let-7 RNA was not modified as shown for pri-let-7g, consistent with the post-transcriptional regulation of *let-7* by *LIN28B* (Supplemental Fig. 1a).

***LIN28B* regulates *let-7* and *MYC* in MM.**

Consistent with the role of *LIN28B* in regulating *let-7* expression, we observed de-repression of *let-7* family members in cells with *LIN28B* knockdown compared to non-targeting control (Fig. 2a). We next analyzed the downstream targets of *LIN28B*/*let-7* and found a decreased protein expression of *MYC* in *LIN28B*-silenced cells in several MM cell lines (Fig. 2b). Moreover, knockdown of *LIN28B* significantly impaired the proliferation of these cell lines tested (Fig. 2c). Consistent with these observations, we identified, through gene set enrichment analysis (GSEA), an enrichment of *let-7* target genes in MM patient samples who displayed a high level of *LIN28B* expression in two independent datasets (GSE2658 and MMRC dataset), suggesting that *LIN28B* represses *let-7* and indirectly enriches *let-7* target expression (Fig. 3a).

In addition, among *let-7* target genes, *MYC* expression significantly correlated with *LIN28B* expression level in two independent datasets (GSE16558 and GSE2658). As shown in Supplemental Fig. 1b, a strong correlation existed between *LIN28B* and *MYC* in MM tumor cells from patient samples in GSE16558 and in total therapy 2 GSE2658, $p<0.028$ and $p<0.001$, respectively.

To validate whether MM cells are dependent on *LIN28B* for growth, we examined tumor growth of MOLP-8 cell line with a *LIN28B* specific hairpin or non-targeting control in a xenograft mouse model using SCID/bg mice. Tumor growth was significantly lower in mice injected subcutaneously with *LIN28B* knockdown compared to scrambled control (Fig. 3b), resulting in a significant prolongation of survival in the experimental group, $p = 0.0045$ (Fig. 3c). In addition, *MYC* expression was significantly reduced in cells obtained

ex-vivo from mice injected with *LIN28B* knockdown compared to scrambled control (Supplemental Fig. 1c).

Together, these data suggest a deregulation of *LIN28B/let-7* axis in a proportion of patients with MM and can function as a novel therapeutic target of *MYC* regulation in MM.

MYC* and cell cycle pathways are highly enriched in cells with high expression of *LIN28B.

To control for possible off-target effect of shRNAs and for incomplete *LIN28B* knockdown mitigating the observed phenotype, we next used CRISPR/Cas9 technology to knock-out (KO) *LIN28B* in the MOLP-8 cell line. Single guide RNAs (sgRNA) targeting exons 2 and 3 of *LIN28B* were used (Supplemental Fig. 2a). Significant decrease in *LIN28B* protein levels were observed, indicating high frequency *LIN28B* KO in the cell population. *MYC* protein level were similarly decreased (Fig. 4a). Moreover, *LIN28B* KO resulted in de-repression of *let-7*, which was consistent with the shRNA experiment (Fig. 4b). Moreover, *LIN28B* KO led to the reduced proliferation by thymidine uptake assay (Fig. 4c).

For further characterization of the *LIN28B/let-7* axis in MM, we performed RNA-sequencing of the *LIN28B* CRISPR-KO cells and *GFP* sgRNA control cells in triplicate. *LIN28B* was confirmed to be the most significantly down-regulated gene in *LIN28B*-silenced cells (Fig. 5a), confirming efficient knock-out. We then queried the top 150 down regulated genes in *LIN28B* KO cells against the MSigDB 'H' hallmark, 'c2' canonical pathways and 'c3' transcription factor target gene sets. The 10 most enriched

gene sets were present in *E2F* cell cycle pathway regulation (Fig. 5b). Of note, *E2F2*, a *let-7* target gene, was one of the most down-regulated genes in *LIN28B* KO cells. Moreover, we found a significant enrichment of *let-7* target genes in control compared to *LIN28B* KO cells (Fig. 6a). Using an unsupervised GSEA analysis of the whole data set against the MSigDB 'H' hallmark gene sets, we found that *MYC* pathway gene set was in the top 5 genes sets, which further suggests that the *LIN28B*/*let-7* axis regulates *MYC* in MM. Moreover, significant enrichment of *MYC* pathway in control cells was also validated using several *MYC* pathway gene sets (Fig. 6b). These results support a model where *LIN28B* represses *let-7*, thereby enriching *let-7* targets such as *E2F2* and *MYC* in MM.

Given that *LIN28B* has been reported to act both in a *let-7*-dependent and independent manner [113], we next asked whether the functional role of *LIN28B* is mediated via *let-7* in MM. We thus performed a rescue experiment by transfection of a *let-7* inhibitor into *LIN28B*-KO MOLP-8 cells. We observed a significant decrease of *let-7* family members in *LIN28B* KO cells plus the anti-*let-7* (Fig. 6c). *Let-7* inhibition also significantly rescued cell proliferation (Supplemental Fig. 2b), indicating that *let-7* is likely the main target of direct regulation by *LIN28B,* in *let-7* dependent manner in MM.

Deregulation of *let-7* in MM.

Given that we demonstrated that *LIN28B* regulates MM proliferation through *let-7*, we sought to define the direct role of *let-7* in MM. We first assessed the expression level of *let-7* family members in primary bone marrow MM $CD138^+$ cells compared to healthy control $CD138^+$ bone marrow plasma cells by qRT-PCR. *Let-7* miRNAs were lower in

plasma cells from six patients with relapsed MM and in four MM cell lines, as compared to plasma cells from three healthy donors (Fig. 7a). To determine whether *let-7* directly regulates *MYC* in MM, we transfected a *let-7b* mimic into MM.1S cells (Supplemental Fig. 3a) and observed a reduction of cell proliferation (Fig. 7b) as well as a decrease level of *MYC* protein (Supplemental Fig. 3b). To validate these findings in patient samples, we assessed the correlation between *let-7* and *MYC* expressions in publicly available gene expression profiling with matched miRNA array from MM patients (GSE16558). We found a significant inverse correlation between expression of *let-7b* and *g* and the expression level of *MYC* in a cohort of 60 patients (Fig. 7c). These data support the idea that *LIN28B* acts in a *let-7*-dependent manner in MM and suggest that low expression levels of *let-7* in MM patients contributes to *MYC* dysregulation and tumor proliferation.

***Let-7* as a potential therapeutic target that regulates *MYC* in MM.**

We next sought to confirm the importance of *let-7* in MM in vivo and to assess whether *let-7* could serve as a therapeutic strategy to directly target *MYC* in MM. We therefore developed a *let-7* Locked Nucleic Acid (LNA)-GapmeR mimic, which was designed based on the seed region of *let-7* miRNAs to efficiently mark *let-7* target genes for degradation by RNAse H. We first tested the ability of the *let-7* LNA-GapmeR to decrease *let-7* target genes *in vitro.* MM.1S cell line was cultured in presence of a control probe or three different concentrations of *let-7* LNA GapmeR (10nM, 100nM and 1uM). By qRT-PCR we observed a consistent decrease of *MYC*, *KRAS*, *CCND1*, *E2F6*, *DICER1* and *HMGA1* expression levels in parallel to increased concentration of the

GapmeR (Supplemental Fig. 4a). We next tested the *let-7* LNA-GapmeR *in vivo* in a xenograft mouse model. SCID/bg mice were injected with $5x10^6$ MM.1S GFP^+Luc^+cells intravenously, followed by intraperitoneal (i.p.) injections of *let-7* LNA-GapmeR two times a week. The treatment was well tolerated and did not induce obvious toxicity or weight loss. The tumor growth was evaluated by BLI, and was significantly reduced in the group of mice that received *let-7* LNA-GapmeR as compared to the control group, p=0.018 (Fig. 8a and Supplemental Fig. 4b). This was associated with consequent significant survival benefit, p=0.026 (Fig. 8b). *Ex-vivo*, MM cells were analyzed for *MYC* expression, confirming the repression of *MYC* in the *let-7* LNA-GapmeR group (Fig. 8c). This experiment provides proof of principle that *let-7* could represent a new therapeutic approach targeting *MYC* in MM.

Discussion

In this study, we describe the role of the *LIN28B/let-7* axis in MM and identify *let-7* as a potential new therapeutic approach for targeting *MYC.* High expression of *LIN28B* in MM is associated with both adverse outcomes and *MYC* overexpression. *LIN28B* represses *let-7* expression in MM cells, resulting in deregulation of MYC protein and cell proliferation *in vitro* and *in vivo*. A pathway enrichment analysis in *LIN28B* KO cells reveals the importance of the *MYC* and *E2F* cell cycle pathways within the *LIN28B/let-7* axis. Moreover, *LIN28B*-induced proliferation and *MYC* deregulation is *let-7* dependent. The tumor growth impairment *in vivo* by administration of a *let-7b* based LNA-GapmeR provides proof of principle for a new therapeutic option to target *MYC* in MM (Supplemental Fig. 5).

Let-7 miRNAs have been described as tumor suppressor in several cancers, by targeting major oncogenic pathways [89]. Copy number loss [114-116] or epigenetic silencing [117] of individual *let-7* family members has been reported in some cancers. In MM, several *let-7* genes are located in frequently deleted regions, such as *let-7g* at 3p21, *let-7i* at 12q14, or *let-7a-2* at 11q24. These copy number aberrations might participate in deregulation of the *LIN28B/let-7* axis in MM. Here, we have described a mechanism of regulation of *let-7* miRNAs in MM involving *LIN28B,* which inhibits *let-7* miRNAs, resulting in deregulation of the *MYC* and E2F cell cycle pathways. Although *LIN28B* has been reported in liver cancer to act through both *let-7*-dependent and *let-7*-independent manners [104], our findings suggest the predominance of a *let-7*-dependent mechanism in MM.

LIN28B is located in the 6q21 cytogenetic band, which is amplified in some cases of neuroblastoma, resulting in *LIN28B* overexpression [105]. In MM, previously published CGH array did not find amplification at 6q21 locus [30]. The increased expression of *LIN28B* might therefore result from epigenetic changes such as altered methylation or histone modification or deregulation of upstream processes. *MiR-125b* was reported to inhibit *LIN28B* in embryonic stem cells as well as in some case of cancers [105,118,119]. Interestingly, *miR-125b* is located in 11q23, which is frequently deleted in MM. Of note, *let-7* miRNAs themselves have also been reported to regulate *LIN28B* expression, in a feedback loop manner [120]. Moreover, a recent report suggests that inactivation of *DIS3* increases *LIN28B* expression in MM[121], by impairing its mRNA degradation. *DIS3* is an exosome endoribonuclease involved in the turnover and degradation of mRNA in the cytoplasm. Strikingly, *DIS3* is one of the most frequently mutated genes in MM [122,123], further suggesting a central role for *LIN28B/let-7* axis in MM.

Despite key roles for *MYC* in MM, there are very few therapeutic options targeting *MYC*. Previous studies attempted to target *MYC* by using a bromodomain inhibitor to target BET proteins, which regulate *MYC* [76,87]. The clinical impact of these inhibitors is being elucidated in early phase clinical trials with some potentially promising results in hematological malignancies. Our findings provide proof of principle that therapeutic use of *let-7* can allow the repression of multiple oncogenes concurrently in MM. We show that *in vivo* use of *let-7* effectively regulates *MYC*, which is an essential regulator of tumor progression in MM and other cancers. Our findings indicate the importance of *let-7* regulation in MM and suggest that *let-7* may be an effective therapeutic option that can directly target *MYC* in MM.

Authors' Contributions

S.M., J.T.P., G.Q.D., I.M.G designed research; S.M., A.S., S.V.G, D.H., M.R.R., Y.M. performed *in vitro* research; S.M., K.S., M.M. performed *in vivo* research; J.S. processed RNA-sequencing data; S.M., J.T.P., C.R-L., X.L, A.M.R., G.Q.D., I.M.G analyzed data; S.M., J.T.P., S.V.G, G.Q.D., I.M.G wrote the paper.

Acknowledgments

S.M. was supported by a grant from ARC Foundation. This work was supported by a grant from the National Cancer Institute (R01CA154648).

Conflicts of Interest Disclosure

We declare that we have no conflicts of interest.

Author Information

RNA-seq data have been deposited to the Gene Expression Omnibus (http://www.ncbi.nlm.nih.gov/geo/) under accession numbers GSE71100.

Figure legends

Figure 1. *LIN28B* expression level in MM. *LIN28B* expression level in MM patients, compared to healthy individuals, by analysis of **(a) Left panel:** GSE16558 (5 normal donor plasma cells and 65 plasma cell samples from patients with newly diagnosed MM) and **right panel:** GSE24080 – containing 22 normal donor plasma cell samples - and GSE2658 – 559 plasma cell samples from patients with newly diagnosed patients - both from UAMS, which were normalized using GeneSpring. **(b)** Kaplan-Meier analysis of 542 patients with MM of the Total Therapy 2 cohort (GSE2658). Patients were classified as high vs. low expression of *LIN28B* based on the mean expression level. *LIN28B* was associated with significantly worse overall survival, (p=0.0075). **(c)** MOLP-8, KMS12BM, RPMI 8226 and KMM-1 cells infected with control shRNA, or 2 different *LIN28B* shRNAs, were studied for relative expression of *LIN28B* mRNA as determined by qRT-PCR.

Figure 2. The *LIN28B*/let-7/*MYC* axis in Multiple Myeloma.

(a) relative expression of mature *let-7* miRNA species as determined by quantitative PCR in 4 MM cell lines infected with control shRNA or 2 different *LIN28B* shRNAs. **(b)** Protein blot analysis for *LIN28B* and *MYC* expression in MOLP-8, KMS12BM, RPMI 8226 and KMM-1 cells infected with control shRNA or 2 different *LIN28B* shRNAs, and **(c)** proliferation assay by thymidine uptake over a 48hr time in the same cell lines. P values were obtained by two-tailed Student t test (*$P < 0.05$)

Figure 3. The *LIN28B*/let-7 axis in data sets and in vivo.

(a) GSEA analysis showing an enrichment of *let-7* target genes in MM patients who display a high level of *LIN28B* expression in two independent datasets (GSE2658 and MMRC dataset). **(b)** Tumor volume and **(c)** survival of SCID/bg mice (5 per group) injected subcutaneously with 5.10^6 MOLP-8 cells expressing pLKO control shRNA or pLKO.LIN28BshRNA; average survival time was 26 days versus 33 days, respectively, $P = 0.0045$. Bars indicate mean ± SD (n = 3).

Figure 4. *LIN28B* KO with CRISPR/Cas9 leads to MYC regulation and *Let-7* upregulation.

MOLP-8 cell line was infected with a lentiCRISPR control (sgGFP) or 2 different sgLIN28B and studied for **(a)** Protein blot analysis, **(b)** relative expression of *let-7* miRNAs by qRT-PCR and **(c)** proliferation assay by thymidine uptake. Bars indicate mean ± SD (n = 3). P values were obtained by two-tailed Student t test (*$P < 0.01$).

Figure 5. RNA sequencing and differential expression of genes downstream of *LIN28B*

RNA sequencing was performed with MOLP-8 lentiCRISPR control and sgLIN28B#2. **(a)** Scatter plot showing differential expression of genes ranked by Z score (metric of fold change and –log10 of the p value) of control cells against *LIN28B*-silenced cells. **(b)** Heat map of the top 150 down-regulated and up-regulated genes in *LIN28B*-silenced cells. Bar plot representing the p value of the top 10 gene sets enriched in the high-*LIN28B* signature.

Figure 6. RNA sequencing and gene set enrichment analysis.

(a) Gene set enrichment analysis (GSEA) for the *let-7* target gene set and **(b)** GSEA analysis for several *MYC* gene sets in control vs. *LIN28B* KO cells. **(c)** MOLP-8 cells were infected with either lentiCRISPR control (sgGFP) or sgLIN28B#1, and transfected with a control probe or a mix of anti-*let-7 b* and *g*. Cells were studied for *let-7* expression level by qRT-PCR.

Figure 7. *Let-7* is down-regulated in MM and regulates *MYC*.

(a) qRT-PCR analysis of *let-7* family members in primary plasma cells from healthy donors and MM patients, as well as in 4 MM cell lines. **(b)** proliferation assay using thymidine uptake and 72 hours after transfection of a *let-7b* mimic or a control probe in MM.1S cells. Bars indicate mean ± SD (n = 3). P values were obtained by two-tailed Student t test (*$P < 0.05$). **(c)** Correlation between *let-7* and *MYC* expression in patients with MM. Scatter plot showing the correlation between *let-7b* and *g, respectively,* and *MYC* from GSE16558. A Pearson correlation coefficient and a two-tailed p value were computed for each of them.

Figure 8. Increased expression of *let-7 in vivo* decreases MM proliferation.

(a) Mice were followed by bioluminescence intensity (BLI), after injection of 5 million of MM.1S GFP^+Luc^+cells. SCID/bg mice (5 per group) were injected i.p. 2 times a week with 20mg/kg of LNA control or LNA *let-7* mimic. **(b)** Survival of the mice by Kaplan Meier analysis. Average survival time was 35 days in control group versus 42 days in LNA *let-7* mimic group, P = 0.0026. **(c)** qRT-PCR analysis of *MYC* in MM.1S cells *ex*

vivo. Bars indicate mean ± SD (n = 3). P values were obtained by two-tailed Student t test (*$P < 0.05$).

Figures

Figure 1

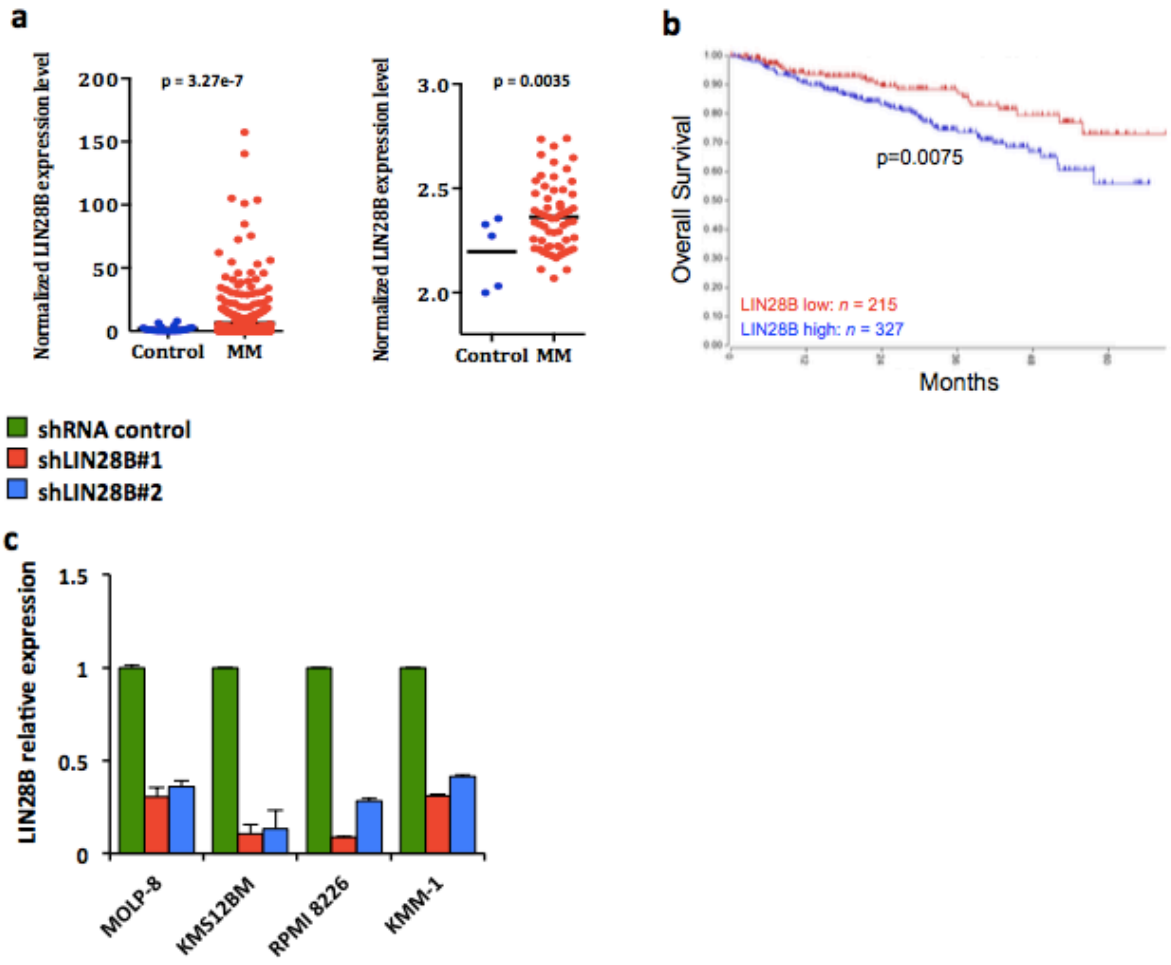

Figure 2

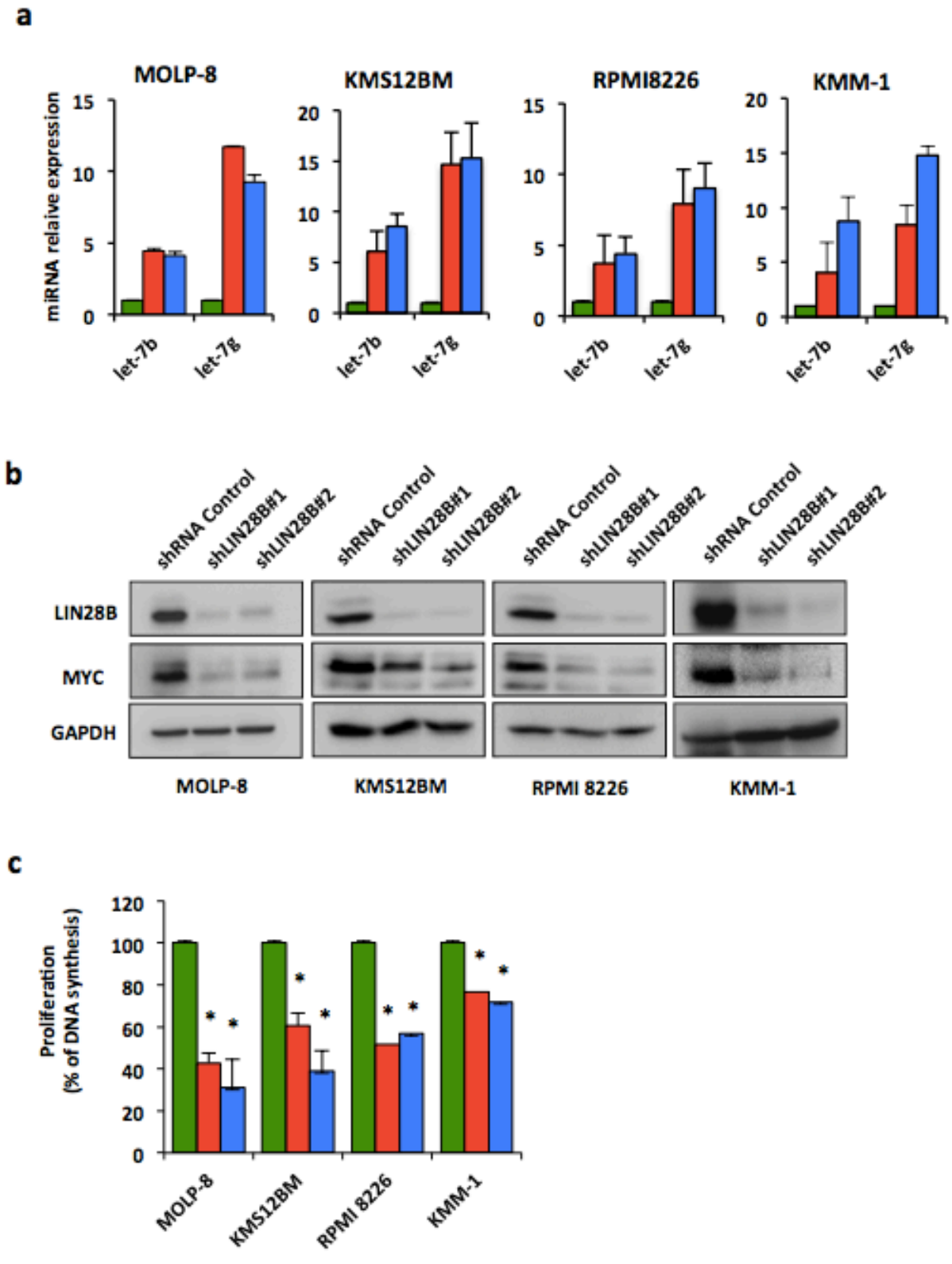
a
MOLP-8
KMS12BM
RPMI8226
KMM-1
miRNA relaive expression
let-7b
let-7g
b
shRNA Control
shLIN28B#1
shLIN28B#2
LIN28B
MYC
GAPDH
MOLP-8
KMS12BM
RPMI 8226
KMM-1
c
Proliferation (% of DNA synthesis)
MOLP-8
KMS12BM
RPMI 8226
KMM-1

Figure 3

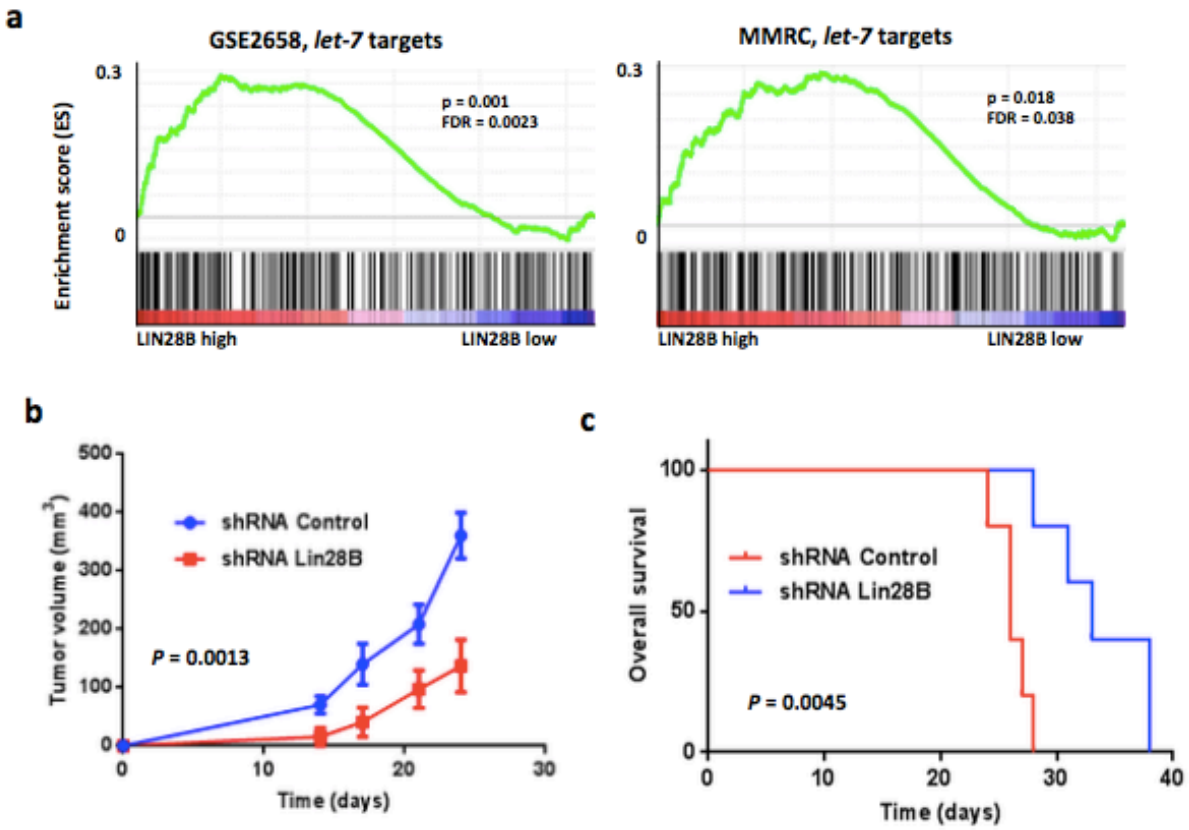
a
GSE2658, let-7 targets
Enrichment score (ES)
0.3
0
p = 0.001
FDR = 0.0023
LIN28B high
LIN28B low
MMRC, let-7 targets
0.3
0
p = 0.018
FDR = 0.038
LIN28B high
LIN28B low
b
Tumor volume (mm3)
500
400
300
200
100
0
shRNA Control
shRNA Lin28B
P = 0.0013
0
10
20
30
Time (days)
c
Overall survival
100
50
0
shRNA Control
shRNA Lin28B
P = 0.0045
0
10
20
30
40
Time (days)

Figure 4

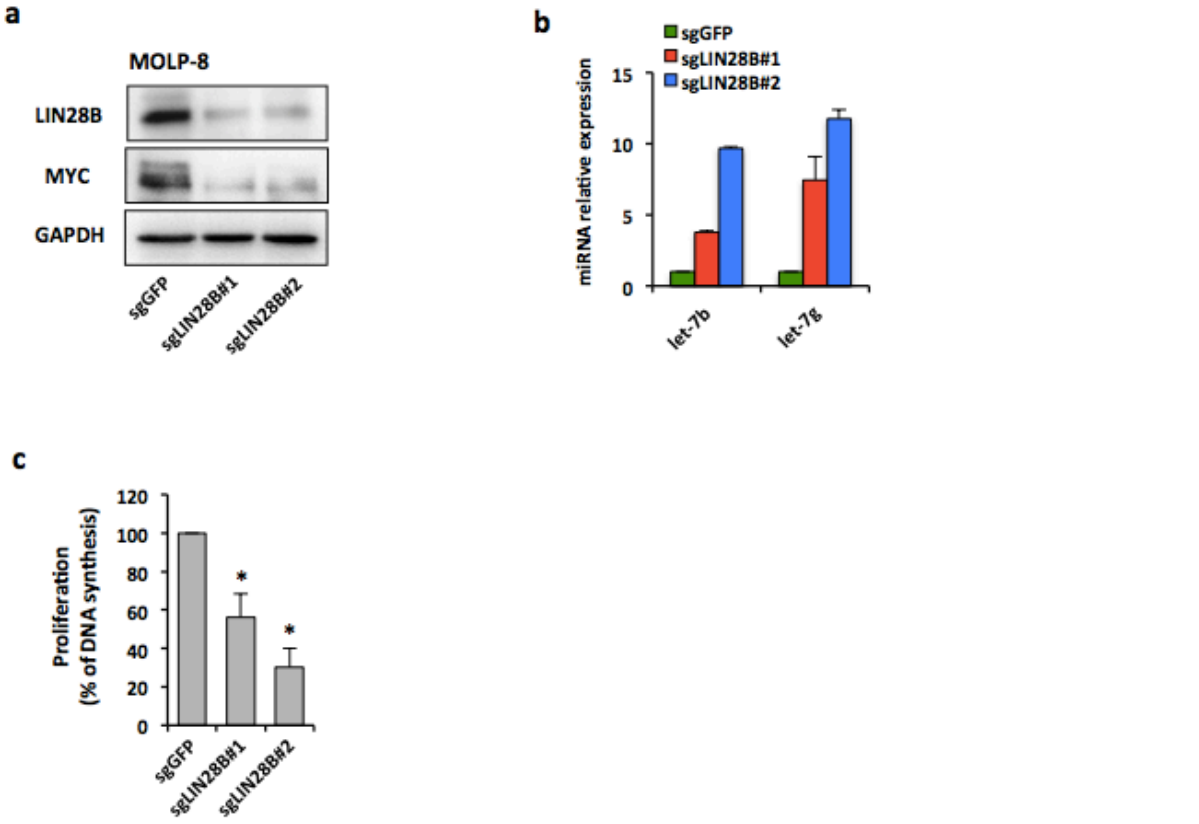

Figure 5

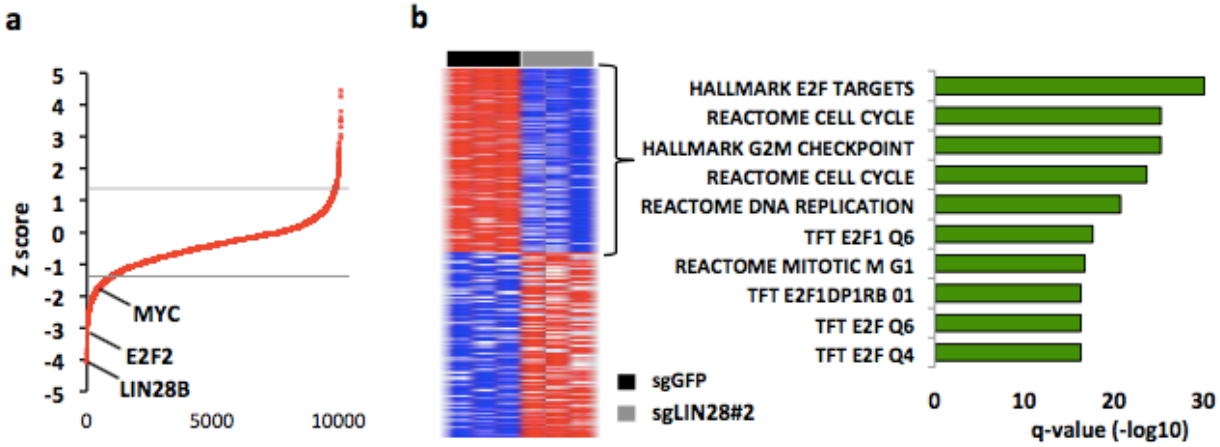

Figure 6

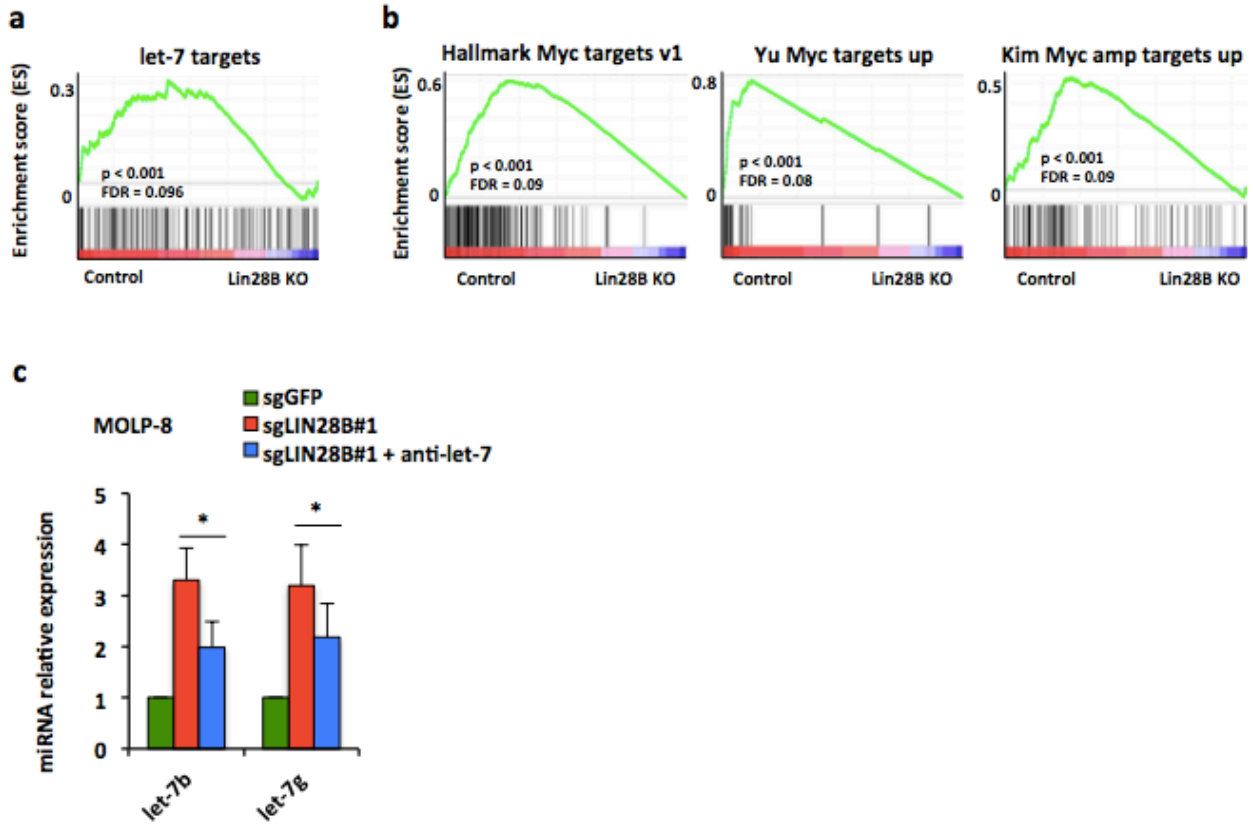
a
let-7 targets
Enrichment score (ES)
0.3
0
p < 0.001
FDR = 0.096
Control
Lin28B KO
b
Hallmark Myc targets v1
0.6
0
p < 0.001
FDR = 0.09
Control
Lin28B KO
Yu Myc targets up
0.8
0
p < 0.001
FDR = 0.08
Control
Lin28B KO
Kim Myc amp targets up
0.5
0
p < 0.001
FDR = 0.09
Control
Lin28B KO
c
MOLP-8
sgGFP
sgLIN28B#1
sgLIN28B#1 + anti-let-7
miRNA relative expression
5
4
3
2
1
0
*
*
let-7b
let-7g

Figure 7

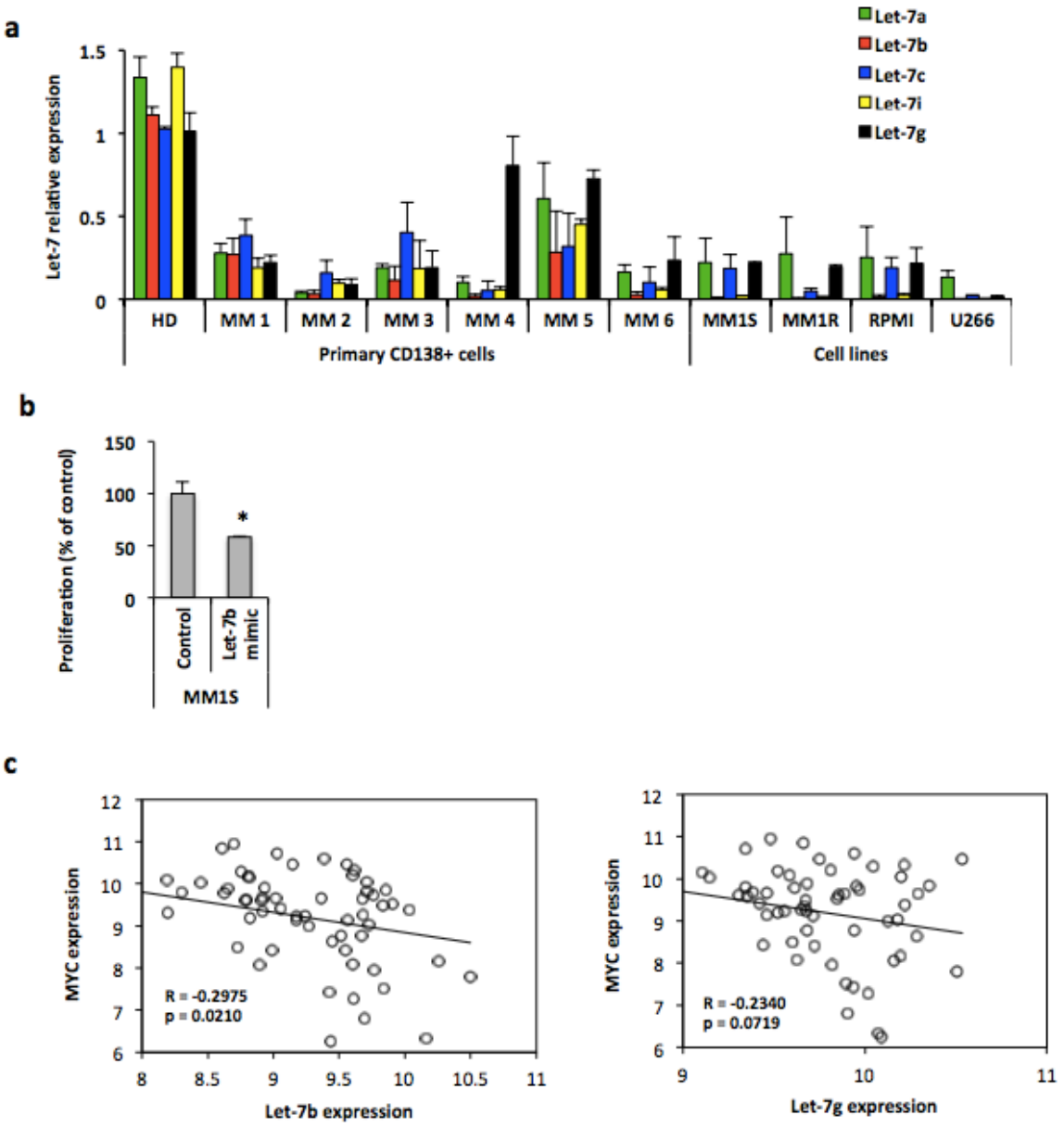
a
Let-7a
Let-7b
Let-7c
Let-7i
Let-7g
Let-7 relative expression
1.5
1
0.5
0
HD
MM 1
MM 2
MM 3
MM 4
MM 5
MM 6
MM1S
MM1R
RPMI
U266
Primary CD138+ cells
Cell lines
b
Proliferation (% of control)
150
100
50
0
*
Control
Let-7b mimic
MM1S
c
MYC expression
12
11
10
9
8
7
6
R = -0.2975
p = 0.0210
8
8.5
9
9.5
10
10.5
11
Let-7b expression
MYC expression
R = -0.2340
p = 0.0719
9
10
11
Let-7g expression

Figure 8

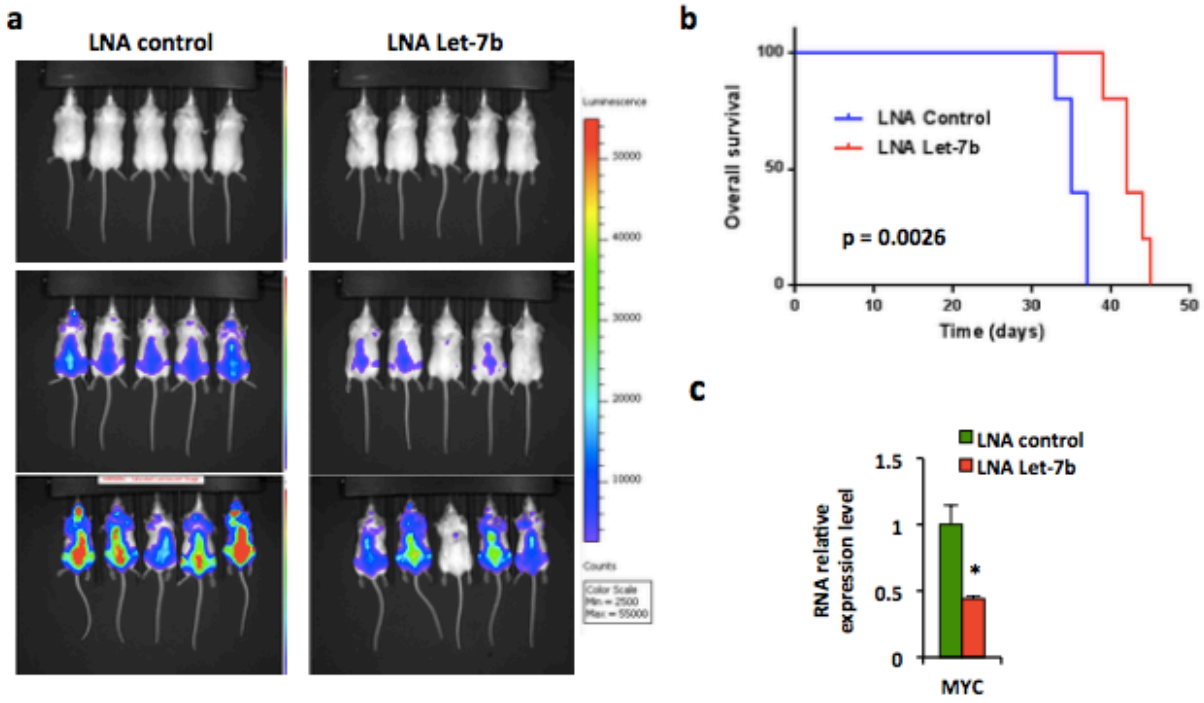
a
LNA control
LNA Let-7b
Luminescence
50000
40000
30000
20000
10000
Counts
Color Scale
Min = 2500
Max = 55000
b
Overall survival
100
50
0
LNA Control
LNA Let-7b
p = 0.0026
0
10
20
30
40
50
Time (days)
c
LNA control
LNA Let-7b
RNA relative expression level
1.5
1
0.5
0
*
MYC

Supplemental Figures

Supplemental Figure 1. *LIN28B* expression level and knockdown in MM.

(**a)** Relative expression of primary *let-7g* in MOLP-8. **(b)** Scatter plot showing the correlation between *LIN28B* and *MYC* from GSE16558 and GSE2658. A Pearson correlation coefficient and a two-tailed p value were computed for each of them. **(c)** *MYC* expression ex-vivo from mice injected with *LIN28B* knockdown or scrambled control cells. P values were obtained by two-tailed Student t test (**P* < 0.05).

Supplemental Figure 2. *LIN28B* CRISPR knockout in MM.

(a) MOLP-8 cell line was infected with a lentiCRISPR control (sgGFP) or 2 different sgLIN28B and studied for western blot and proliferation. **(b)** proliferation by thymidine uptake assay of MOLP-8 cells. Bars indicate mean ± SD (n = 3), P values were obtained by two-tailed Student t test (**P* < 0.05).

Supplemental Figure 3. *Let-7* is down-regulated in MM, and regulates *MYC*.

(a) qRT-PCR analysis for *let-7b* and **(b)** protein blot analysis of *MYC*, 72 hours after transfection of a *let-7b* mimic or a control probe in MM.1S cells. Bars indicate mean ± SD (n = 3). P values were obtained by two-tailed Student t test (**P* < 0.05).

Supplemental Figure 4. Increased expression of *let-7 in vivo* decreases MM proliferation.

(a) qRT-PCR analysis of *let-7* target genes in MM.1S cultured for 48 hours in presence of 10nM, 100nM or 1uM of either control LNA GapmeR or *let-7* LNA GapmeR. **(b)** BLI

quantification in the 2 groups of SCID/bg mice (5 per group) after injection of 5 million of MM.1S $GFP^{+}Luc^{+}$ cells followed by i.p. injection 2 times a week with 20mg/kg of LNA control or LNA *let-7* mimic. P values were obtained by two-tailed Student t test (*P < 0.05).

Supplemental Figure 5. Schematic representation of the mechanisms proposed for *LIN28B/let-7* regulation in MM. The *let-7* biogenesis inhibitor *LIN28B* correlates with *MYC* expression in MM and is associated with adverse outcome. *LIN28B/let-7* axis modulates the expression of *MYC*, itself a *let-7* target. Perturbation of the axis through LIN28 knockdown regulates the proliferation of MM cells *in vivo* in a xenograft tumor model. We provide proof of principle for therapeutic regulation of *MYC* through *let-7* with an LNA-GapmeR containing a *let-7b* mimic *in vivo*, demonstrating that high levels of *let-7* expression repress tumor growth by regulating *MYC* expression. These findings reveal a novel mechanism of therapeutic targeting of *MYC* through the *LIN28B/let-7* axis in MM.

Suppl. Figure 1

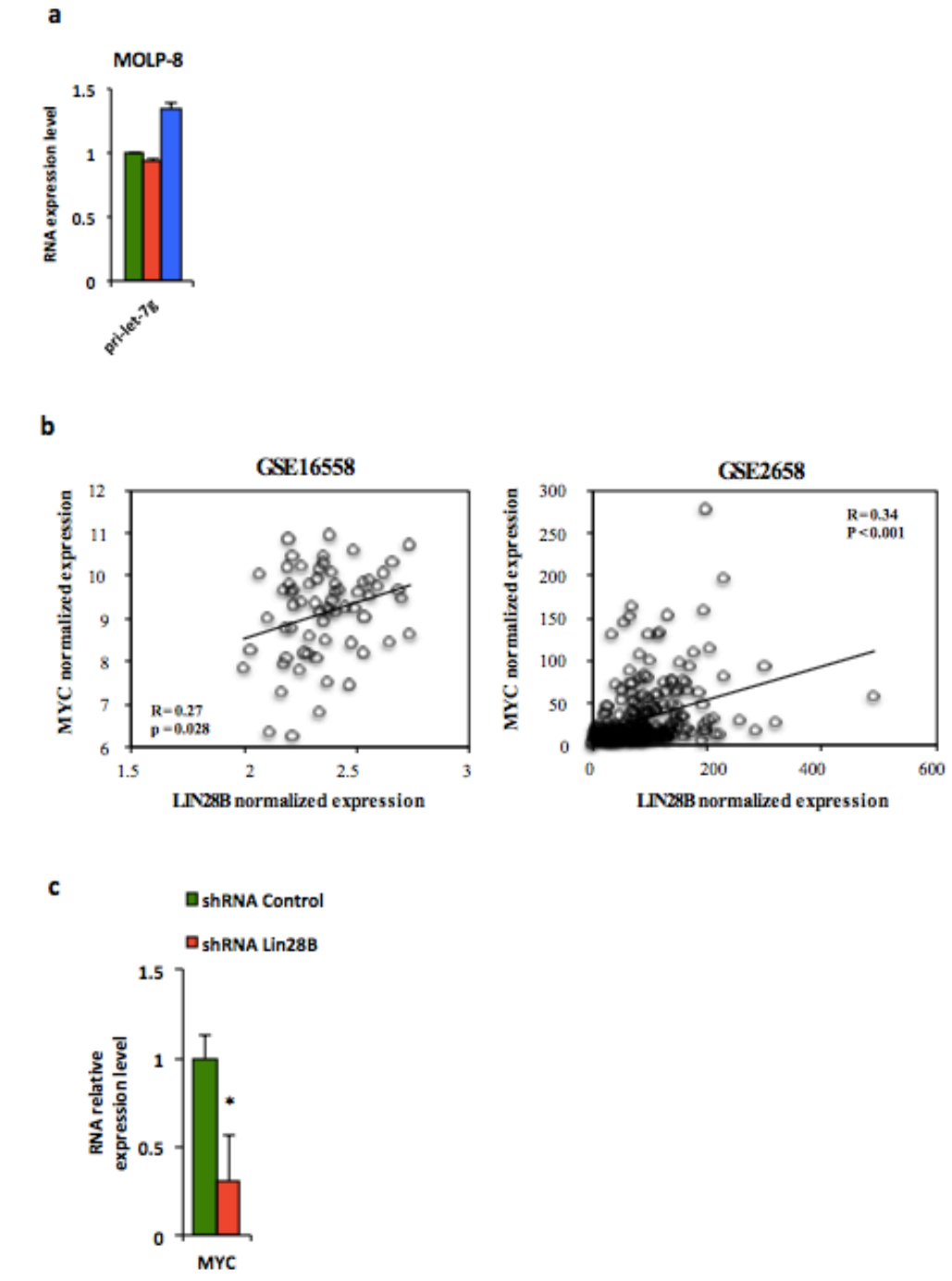

Suppl. Figure 2

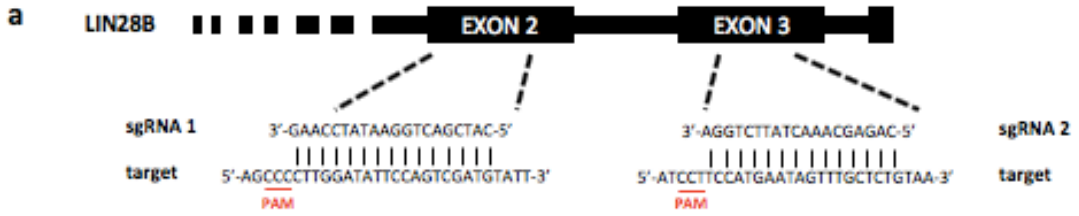

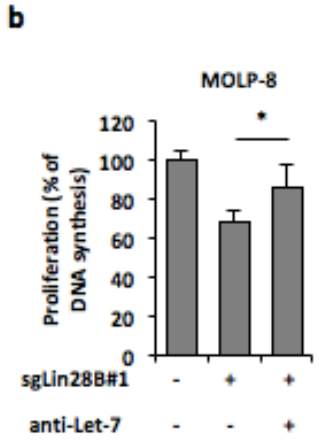

Suppl. Figure 3

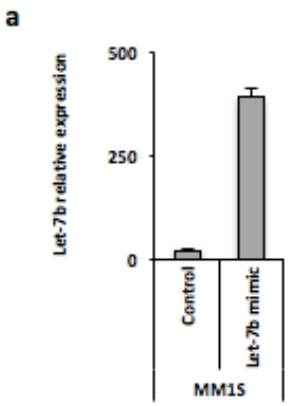

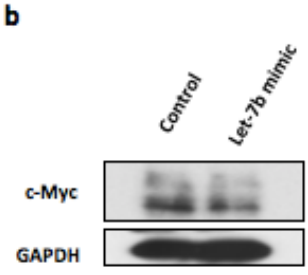

Suppl. Figure 4

a

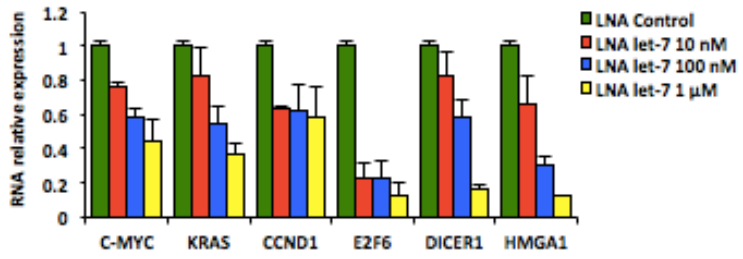

b

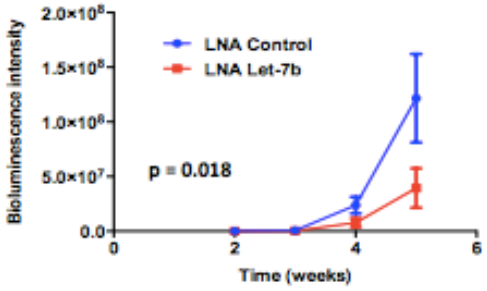

Suppl. Figure 5

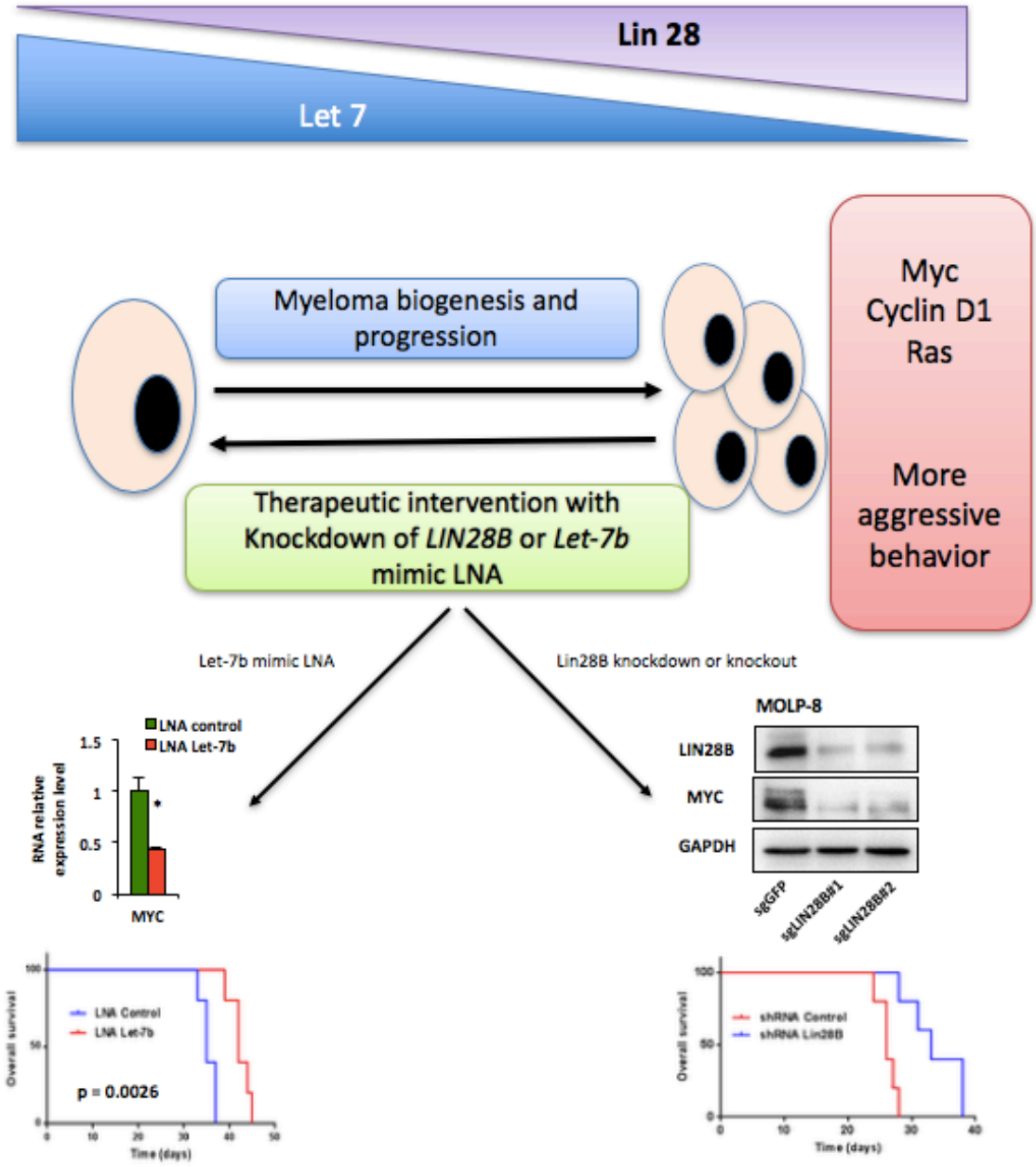

ARTICLE 2

Prognostic role of circulating exosomal miRNAs in multiple myeloma

Résumé

Dans ce deuxième travail, nous avons évalué la valeur pronostic des miARNs des exosomes circulants dans le MM. Nous avons isolé les miARN des exosomes circulants d'une cohorte de 156 échantillons de patients uniformément traités pour un MM au diagnostic. Après analyse du profil de miARN exosomaux par séquençage de nouvelle génération pour 10 échantillons de MM et 5 échantillons contrôles, nous avons utilisé une technique de qRT-PCR array pour étudier la corrélation entre le niveau d'expression de 22 miARN et les survies sans progression (SSP) et globale (SG). Deux miARN, à savoir let-7b et miR-18a, étaient significativement associés à la SSP et SG en analyse univariée et en analyse multivariée, après ajustement pour le système de stratification international (ISS) et les marqueurs cytogénétique de mauvais pronostic (délétion 17p et translocation 4 ;14). Nos résultats montrent que le niveau d'expression des miARN let-7b et miR-18a au sein des exosomes circulants permettent d'améliorer la stratification du risque chez les patients atteints de MM.

Contribution de l'auteur

Salomon Manier a participé à l'ensemble du design et à la réalisation des expériences du travail présenté : extraction des exosomes à partir de sérum, isolation des miARN, qRT-PCR par emploi de la technologie TLDA (*Taqman Low Density Array*). Il a interprété les résultats et participé à l'analyse statistique. Salomon Manier a généré les figures et écrit le manuscrit.

Prognostic role of circulating exosomal miRNAs in multiple myeloma

Salomon Manier[1,2,3*], Chia-Jen Liu,[1,4,5,*], Hervé Avet-Loiseau[6], Jihye Park[1], Jiantao Shi[7], Federico Campigotto[7], Karma Z. Salem[1], Daisy Huynh[1], Siobhan V. Glavey[1], Bradley Rivotto[1], Antonio Sacco[1,8], Aldo M. Roccaro[1,8], Juliette Bouyssou[1], Stéphane Minvielle[9], Philippe Moreau[10], Thierry Facon[2], Xavier Leleu[11], Edie Weller[6], Lorenzo Trippa[6], and Irene M. Ghobrial[1]

[1]Department of Medical Oncology, Dana-Farber Cancer Institute, Harvard Medical School, Boston MA, USA; [2]Department of Hematology, University Hospital Center of Lille, France; [3]INSERM UMR-S1172, Lille 2 University, France; [4]Division of Hematology and Oncology, Department of Medicine, Taipei Veterans General Hospital, Taipei, Taiwan; [5]School of Medicine, National Yang-Ming University, Taipei, Taiwan; [6]Laboratory for Genomic in Myeloma, INSERM U1037, Toulouse University Hospital, France; [7]Department of Biostatistics and Computational Biology, Dana-Farber Cancer Institute, Harvard Medical School, Boston, MA, USA; [8]ASST Spedali Civili di Brescia, Coordinamento e Progettazione Ricerca Clinica, CREA Laboratory, Brescia, BS, Italy; [9]Center for Cancer Research Nantes-Angers, UMR892 INSERM - 6299 CNRS, University Hospital Center of Nantes, France; [10]Department of Hematology, University Hospital Center of Nantes, France, and [11]Department of Hematology, University Hospital Center of Poitiers, France.

[*]S.M. and C-J.L. contributed equally to this study.

Running title: Circulating exosomal miRNAs in multiple myeloma

Corresponding author:

Dr. Irene M. Ghobrial

Dana-Farber Cancer Institute

450 Brookline Avenue

Boston, MA 02215

Tel: (617) 632-6777

Fax: (617) 632-6069

E-mail: Irene_ghobrial@dfci.harvard.edu

Word count for abstract: 211

Word count for main text: 3519

Figure count: 3 (and 4 supplemental figures)

Table count: 2 (and 2 supplemental tables)

Reference count: 40

The authors declare no conflict of interest.

Key points

- Two circulating exosomal microRNAs, namely let-7b and miR-18a, improved survival prediction in patients with multiple myeloma.
- Circulating exosomal miRNAs enhanced the stratification of patients with high-risk factors.

Abstract

Exosomes, secreted by several cell types, including cancer cells, can be isolated from the peripheral blood and have been shown to be powerful markers of disease progression in cancer. In this study, we examined the prognostic significance of circulating exosomal microRNAs (miRNAs) in multiple myeloma (MM). A cohort of 156 patients with newly diagnosed MM, uniformly treated and followed, was studied. Circulating exosomal miRNAs were isolated and used to perform small RNA sequencing analysis on 10 samples and a qRT-PCR array on 156 samples. We studied the relationship between miRNA levels and patient outcomes including progression-free survival (PFS) and overall survival (OS). We identified miRNAs as the most predominant small RNAs present in exosomes isolated from the serum of MM patients and healthy controls by small RNA sequencing of circulating exosomes. We then analyzed exosomes isolated from serum samples of 156 patients using a qRT-PCR array for 22 miRNAs. Two of these miRNAs, namely let-7b and miR-18a, were significantly associated with both PFS and OS in the univariate analysis, and were still statistically significant after adjusting for the International Staging System (ISS), and adverse cytogenetics in the multivariate analysis. Our findings support the use of circulating exosomal miRNAs improves the identification of patients with newly diagnosed MM with poor outcomes. The results require further validation in other independent prospective MM cohorts.

Introduction

Multiple myeloma (MM) is a hematological malignancy characterized by a clonal proliferation of plasma cells in the bone marrow microenvironment.[1] The clinical and biological heterogeneity of this malignancy leads to variable responses to therapy and outcomes.[124] With a vast increase in therapeutic choices in MM and improved outcomes, the issue of risk stratification to dissect this heterogeneity is becoming more critical as it may lead to tailored therapies for different groups of patients.

A large number of prognostic biomarkers has been identified, including markers that reflect tumor burden and stage of the disease, tumor biology (such as chromosomal abnormalities and gene expression signatures), or factors present in the host that indicate fitness to therapy.[124] The most widely used prognostic factors in MM are currently the International Staging System[4] (ISS)—based on albumin and beta-2 microglobulin levels in the peripheral blood at the time of diagnosis—and chromosomal abnormalities such as translocation t(4;14), 17p deletion and 1q21 amplification.[125] A revised ISS (R-ISS) system has been proposed that includes high-risk cytogenetics for improved characterization of patients with poor survival.[9] However, despite these advances, patients within similar prognostic groups display heterogeneous outcomes, indicating that current prognostic factors used in MM are suboptimal in stratifying patients with high-risk features. Combining information about cytogenetic abnormalities and ISS with other molecular markers may therefore further improve their prognostic value.

Exosomes are 50–140 nm nanovesicles that contain proteins and nucleic acids, such as microRNAs (miRNAs).[126] They are actively secreted by several cell types,

including cancer cells, and can be isolated from the peripheral blood, making them attractive for use as biomarkers of disease progression and risk stratification. Exosomes have been reported to promote tumorigenesis in many cancer types, in particular through transfer of miRNAs.[127-129] Remarkably, tumor-derived exosomes contain their own miRNA-associated machinery and display a cell-independent capacity for processing precursor miRNAs into mature miRNAs. This phenomenon mediates an efficient and rapid silencing of mRNA in target cells, thus promoting oncogenesis.[129]

Of note, miRNAs are small non-coding RNAs that are assumed to regulate more than 50% of all protein-coding genes.[130] They predominantly act as translational repressors by binding to the 3'-UTR region of their targeted mRNAs, which are deregulated in most cancer types,[90] including MM[131,132], and have a role in the development and progression of many cancers.[133-137]

Circulating miRNAs are generated via two main mechanisms: cell death by apoptosis or necrosis, leading to the release of miRNAs bound to AGO proteins, and an active process by secretion of exosomes containing miRNAs.[138] Thus, exosomal miRNAs could represent a more specific molecular biomarker than cell-free miRNAs. However, the clinical significance of circulating exosomal miRNAs in MM has not been examined. In this study, we aimed to characterize circulating exosomal miRNAs in MM and to determine their impact on patient outcomes.

Material and Methods

Plasma samples from patients with MM

We obtained 156 serum samples from the Intergroupe Francophone du Myélome (IFM), collected between June 14, 2006 and December 16, 2008 for this study. All patients were newly diagnosed with MM, uniformly followed and treated with a combination of bortezomib and dexamethasone, followed by high-dose melphalan and autologous hematopoietic stem cell transplantation. None of the patients received therapy before the collection of blood samples. Criteria of diagnosis, clinical staging and risk stratification were assessed according to the International Myeloma Working Group (IMWG) guidelines.[139] Patients provided written informed consent in accordance with the Declaration of Helsinki. In addition, samples from five healthy volunteers (for age-matched comparison) were used for the preliminary RNA sequencing study.

Circulating exosome isolation

We isolated circulating exosomes as described previously.[140] Serum was extracted from blood drawn on dry tubes. The starting volume of serum was 0.5mL, which was diluted into 2mL of PBS before differential centrifugation and precipitation reagent. Exosomes were isolated from frozen serum samples using a combined centrifugation and exosome isolation reagent method (Figure S1A). Serum was isolated by centrifugation at 300 *g* for 10 min, and further spun down at 2,000 *g* for 10 min, and 10,000 *g* for 10 min, to remove dead cells and cell debris, respectively. We harvested exosomes by adding an exosome isolation reagent for 30 min (ExoQuick solution) before centrifugation at 1,500 *g* for 30 min. We used a differential centrifugation protocol

combined with an exosome isolation reagent where the exosome pellet was washed before RNA extraction, thus limiting potential contamination by cell-free/exosomes-free miRNA.

Electron microscopy

Exosomes were characterized by electron microscopy using CD63 and CD81 as follows: pelleted exosomes were fixed in 0.1 M phosphate buffer (pH 7.4) with 2% paraformaldehyde, then processed for ultrathin sectioning and immunogold labeling by using anti-CD63 and anti-CD81 antibodies and protein A coupled with 10- or 15-nm gold particles. Sections were observed at 80 kV on a TecnaiGβ Spirit BioTWIN transmission electron microscope (FEI), and images were recorded with an AMT 2k CCD camera. We confirmed the presence of exosomes by transmission electron microscopy and NanoSight analysis in MM samples before proceeding with the rest of the samples for exosome isolation.

RNA extraction and RNA sequencing

Total RNA was extracted from exosome pellets using the miRNeasy Micro Kit (Qiagen). Small RNA libraries were prepared and amplified using the NEBNext small RNA Library Prep Set (New England BioLabs). Amplified libraries were resolved on a 10% polyacrylamide gel for size selection. The 140 to 160 nucleotide bands corresponding to adapter-ligated constructs derived from the 21 to 40 nucleotide RNA fragments were excised and recovered in a DNA elution buffer. The average size distribution of each library was determined using Agilent Bioanalyzer with High

Sensitivity Chip Kit (Agilent) and quantified on ABI 7900HT Fast RT-PCR instrument using the KAPA Library Quantification kit (Kapa Biosystems). Each library was adjusted to final concentration of 2 nM, pooled and sequenced on an Illumina HiSeq 2000 sequencer for single-read 50 cycles at the Center for Cancer Computational Biology at Dana-Farber Cancer Institute. The BCL files were demultiplexed using CASAVA 1.8.2 (Illumina) into FASTQ files. Raw sequencing reads were then analyzed using miRDeep2 to quantify known small RNA species. RNA sequencing was performed for circulating exosomes obtained from the serum of 10 MM patients and 5 healthy individuals.

TaqMan Low-Density Array

For quantitative RT-PCR, we designed a custom TaqMan Low-Density Array (TLDA, Applied Biosystems). Twenty-two miRNAs were selected based on biological relevance in prior studies of tumor samples in MM.[131,132] RNA concentrations were measured with a Qubit miRNA assay and 5 ng of miRNA was reverse transcribed to cDNA using a miRNA reverse transcription kit (TaqMan, Applied Biosystems) and pre-amplified with a custom pool of primers and a PreAmp Master Mix (TaqMan, Applied Biosystems). Quantitative PCR reactions were done with the TaqMan Universal Master Mix II reagent in Custom TaqMan Array Cards (384-well plate preloaded with 22 specific primers of interest) on a ViiA™ 7 Real-Time PCR System (Applied Biosystems). TLDA quantification was performed based on the manufacturer's protocol and based on prior publications.[141] All cards were run on the Applied Biosystems 7900HT Fast Real-Time PCR System using the AgPath-ID One-Step kit (Applied Biosystems). All assays were

performed in duplicate in each card. A subset of samples was run in two different cards to test reproducibility. The gene expression levels were determined and relatively quantified by using the comparative cycle threshold (Ct) method. All Ct values above 35 cycles were considered as undetectable. We normalized qRT-PCR data using a robust global median normalization as described previously (Figure S2).[142] Each plate was adjusted by a normalization factor as the difference between the global median Ct value and the plate median Ct value. We calculated the expression of miRNAs with ΔCt, in which the maximal Ct value for a miRNA was subtracted from the specific value for this miRNA. The average of the replicate expression values of the miRNAs was used in the analysis. In our experimental design, we controlled our data quality by having technical replicates of plates and technical replicates of each sample in each plate. Technical replicates of plates were used to assess the variability to measurement in two plates; we had two control plates in which the same set of samples were analyzed. We observed a high correlation with Ct values from the duplicate plate, which indicated good concordance between technical replicates of plates. We indeed observed that Ct values in some plates was higher and this was corrected after global normalization. In addition, we calculated the Ct difference for all technical replicates for each sample in each plate.

Statistical analysis

The primary outcomes of interest were progression-free survival (PFS) and overall survival (OS). To illustrate the impact of the miRNAs graphically, the miRNAs were dichotomized at the median based on a low-versus-high expression. The PFS and

OS were plotted and compared using the Kaplan–Meier method and the log-rank test. A Cox proportional hazards model was employed to compute the hazard ratios (HRs) and accompanying 95% confidence intervals (CIs). The multivariate Cox proportional hazards model was used to identify independent outcome predictors after adjustment for confounders, such as ISS and cytogenetics.

We compared miRNA expressions between MM patients and healthy adults by using the Mann–Whitney *U* test in the preliminary study, then further analyzed the effect of each miRNA expression in the serum samples of 156 newly diagnosed untreated MM patients on outcomes. We dichotomized the expression levels of miRNAs according to the median level of all samples and further analyzed their clinical impact. We defined a miRNA with clinical significance when it significantly correlated with both PFS and OS in the multivariate analysis. Correction for multiple comparisons was performed by using Benjamini-Hochberg correction in the univariate analysis. The miRNAs that were significant after correction were adjusted for ISS and cytogenetics in the multivariate analysis.

The area under the receiver operating characteristic curve (AUC) was used to evaluate the predictive values of miRNA expressions for the patients' PFS and OS. We compared the curves between the miRNA expressions alone, ISS with cytogenetics, and both to evaluate the predictive value of the miRNA expressions. In order to avoid overfitting, cross-validation was applied to this analysis. We evenly divided the study cohort into a training part and a validation part by random sampling. We used the Cox proportional hazards model to find the most significant two miRNAs in the training

cohort. The two miRNAs were used to calculate the AUC in the validation cohort. We iterated 1,000 times and reported the mean of the results.

All statistical analyses were performed in R (version 3.1.1), SAS 9.2 software (SAS Institute Inc., Cary, North Carolina), and STATA statistical software (version 12.1; StataCorp). Those statistical analyses with *p*-values < 0.05 in the univariate model were further analyzed in the multivariate analysis.

Results

Characterization of circulating exosomes in MM

We first characterized peripheral blood circulating exosomes from MM patients and healthy adults. After isolation of circulating exosomes (Figure S1A), we confirmed the presence of exosomes by transmission electron microscopy with immunogold labeling for CD63 and CD81, which are specific markers of exosomes (Figure S1B).[126] The diameter of isolated exosomes was confirmed to be around 120nm by NanoSight analysis (Figure S1C).

To define the content of exosomes in terms of small RNAs, we next performed a small RNA sequencing from circulating exosomes of 10 newly diagnosed MM patients and five healthy individuals. The large majority of mappable RNAs were miRNAs (88.0% in MM samples and 86.7% in healthy donor samples). The rest of the RNAs were represented by small nuclear and nucleolar RNA (sno/snRNA), ribosomal RNA (rRNA), messenger RNA (mRNA), long intergenic non-coding RNA (lincRNA) and unclassified RNA (miscRNA). Importantly, we found no difference in distribution of small RNA between MM and healthy donors' exosomes. The distribution of small exosomal RNAs between MM and healthy donor samples is shown in Figures 1A and S3.

Exosomal miRNAs and survival in MM

Given that the majority of the RNA content was miRNAs, we focused on miRNAs that could be differentially expressed between MM patients and could be predictive of prognosis. We sought to design a panel of miRNAs that is specific for MM pathogenesis

based on prior studies in tumor cells, and thereby restricted our prognostic studies of exosomal miRNAs to those that should be critical for MM-tumor derived miRNAs. This helped us avoid detecting miRNAs that are derived from other non-tumor cells as well as having to perform comparisons of circulating exosomal miRNAs to tumor derived miRNAs given that did not have access to matched tumor cells from this cohort of patients. In this respect, we focused on 22 miRNAs that were selected based on their biological relevance in prior studies of tumor samples in MM and their presence in the RNA sequencing study performed (Figure S4).[131,132] We developed a custom-made TaqMan assay using these miRNAs to perform a screening of the prognostic relevance of exosomal miRNAs in patients with MM. The expression levels of these 22 miRNAs were further confirmed using RT-PCR in the same samples that were profiled by RNA sequencing. The expression levels of these 22 miRNA were significantly lower in MM patients compared to healthy individuals (Figure 1B).

We aimed to identify whether circulating exosomal miRNAs are of clinical prognostic significance in patients with newly diagnosed MM. Therefore, we obtained serum samples of 156 patients with newly diagnosed MM who were uniformly treated with bortezomib and dexamethasone (from the IFM group). The clinical characteristics of the patients are listed in Table 1. All serum samples were harvested at diagnosis, before the initiation of therapy. The median follow-up of the cohort was 5.4 years (interquartile range, 4.6–5.8). We performed a custom quantitative RT-PCR TLDA to assess the clinical significance of the 22 selected miRNAs. The association between the miRNAs and patients' outcomes were analyzed in the univariate and multivariate Cox regression models. We performed Benjamini-Hochberg correction for multiple

comparisons. After correction, let-7b, let-7e, miR-106a, miR-106b, miR-155, miR-16, miR-17, miR-18a, and miR-20a were significant risk factors for PFS in the univariate analyses. All of these miRNAs were still significant after adjustment for ISS and specific cytogenetic abnormalities. After Benjamini-Hochberg correction, let-7b, miR-155, and miR-18a were significantly associated with patients' survival in the univariate analyses. However, only let-7b and miR-18a were the significant predictors for OS in the multivariate models (Table 2). We further analyzed the association between let-7b and miR-18a and patients' characteristics since only the two exosomal miRNAs demonstrated independent predictors for both PFS and OS in the univariate and multivariate analysis. Lower expression of let-7b or miR-18a was significantly associated with a high ISS stage (Tables S1–2). However, both let-7b and miR-18a were independent predictors after adjusting for ISS and specific cytogenetic abnormalities. The effect of the two miRNAs on PFS and OS was illustrated by Kaplan–Meier curves with dichotomized miRNAs at the median (Figure 2). These data indicate that specific miRNAs can be critical in defining worse prognosis in patients with newly diagnosed MM.

The area under the receiver operating characteristic curve (AUC)

To further assess the prognostic value of the miRNAs signature in addition to clinical value, we performed an AUC analysis with cross-validation. The combination of the two miRNAs signature with ISS and cytogenetics status had a better prediction for PFS and OS than those without the miRNA signature (Figure 3). Together, these data

indicate that circulating exosomal miRNAs could improve on the prognostic stratification of patients with MM, in addition to ISS and cytogenetics.

Discussion

To our knowledge, this is the first large study that proves the clinical significance of circulating exosomal miRNAs in a uniformly treated newly diagnosed MM cohort. Indeed, miRNAs have recently emerged as promising biomarkers of different pathological conditions including cancer and their inherent stability in the serum/exosomes and reproducible levels across many individuals make miRNAs attractive biomarkers. Unlike current conventional genomic approaches that require a bone marrow biopsy, exosomal miRNAs can be obtained from the peripheral blood making them candidates for use as non-invasive biomarkers. In the study, we examined a novel prognostic biomarker from patients' serum samples to improve the prediction of PFS and OS in patients with MM. Our results show that two miRNAs, let-7b and miR-18a, from circulating exosomes can predict PFS and OS in patients with newly diagnosed MM in an independent manner, and improves on the prognostic value of ISS and cytogenetic status in MM.

Cell-free miRNAs have emerged as appealing biomarkers because they are non-invasive and have been reported as prognostic tools in many cancer types,[143] including MM.[144-146] However, many circulating miRNAs are passively released from apoptotic and necrotic cells,[138,143] and therefore may not truly reflect the biological changes that occur in these tumor cells. In contrast, exosomes are actively secreted in the peripheral blood by different cell types, including cancer cells, and are biologically relevant as they promote tumorigenesis through miRNA transfer.[138] Recent studies show that cancer exosomes are capable of cell-independent miRNA processing and transfer of mature miRNAs into recipient cells; they thus mediate significant transcriptome alterations in

target cells and lead to the induction of proliferation and conversion of non-tumorigenic cells into tumor-forming cells.[129] This indicates that exosomes carry specifically selected miRNAs as well as their own miRNA biogenesis machinery.[129] Therefore, exosomal miRNAs may truly represent specific molecular biomarkers, in contrast to cell-free miRNAs.

Peripheral blood exosomes are reported to be strong diagnostic and prognostic markers in cancer. Indeed, patients with stage IV melanoma and a high protein concentration in circulating exosomes have a shorter survival.[127] Specifically, markers of melanoma, such as TYRP2, VLA-4 and HSP70, are significantly higher in stage IV patients compared to those at other stages. More recently, circulating exosomal miRNAs were studied in castration-resistant prostate cancer (CRPC), and two (miR-1290 and miR-375) were shown to be independent predictive markers of overall survival in patients with CRPC, improving the predictive value of the standard clinical staging system.[147] Melo *et al.* identified the presence of glypican-1 on circulating exosomes in patients with pancreatic cancer, which could serve as a powerful marker for both the diagnosis and prognosis of this disease.[148] Future studies to determine the source of exosomes present in the peripheral blood and whether the level of miRNAs in circulating exosomes correlates with tumor derived miRNAs should be performed. However, it is well known that circulating exosomal miRNAs can be prognostic in many cancer types without the need of profiling the tumor cellular counterparts.[127,147,148]

In this study, we used the mean expression value for normalization instead of RNU6B normalization. Xiang *et al*. reported that U6 is not a suitable endogenous control for the quantification of circulating microRNAs, especially in frozen samples.[149]

Mestdagh *et al*. demonstrated that using the mean expression value was better than other small non-coding RNAs for normalization.[150] Cui *et al*. reported that normalization based on the global mean of each plate superior to normalization based on mammalian U6 or spiked-in miR159.[151] Our study shows high concordance across plates and for replicates of each sample and the inter-plate variability has been corrected by global normalization.

Established markers of prognosis in MM include the ISS and cytogenetics.[4] The ISS classification is based on non-clonal markers instead that are albumin and beta-2 microglobulin (B2M). Although B2M is a useful marker of the tumor burden, it may not be specific enough to define the clinical and biological heterogeneity of patients with MM.[124] Cytogenetics and several gene expression signatures are truly reflective of the molecular and biological characteristics of the tumor clone. However, these are performed only on tumor cells obtained from bone marrow biopsies. Therefore, there is a need to develop non-invasive biomarkers that reflect the molecular aspect of the disease.

We identified two exosomal miRNA signatures, namely let-7b and miR-18a, that were associated with poor outcomes in regards to PFS and OS. The let-7 family is one of the most studied groups of miRNAs in cancer.[89] We and others have recently published that there is a significant decrease in the expression of let-7 family members in MM tumor cells compared to normal plasma cells.[131,132,152] Indeed, we demonstrated that let-7 acted as a tumor suppressor miRNA in MM.[152] This miRNA family is notably processed by the RNA-binding protein LIN28B, which is often deregulated in cancer.[100,153] Low levels of let-7 induce cell proliferation and growth by de-repressing

oncogenes such as *CCND1*, *MYC* and *RAS*.[154] MiR-18a is a component of the miR-17-92 cluster on chromosome 13q31.3, which undergoes amplification in lymphomas and solid tumors.[155] Krutilina *et al.* reported that miR-18 inhibited hypoxia-inducible factor 1α (HIF1A) activity in breast cancer and repressed tumor dissemination through a HIF1A-dependent pathway.[156] Teng *et al.* found that miR-18a mediated induction of M1 macrophages by directly targeting *IRF2*. NK and NKT cells activated by miR-18a play a critical role in the inhibition of tumor metastasis.[157]

The results of this study need to be confirmed in large series of MM patients. In addition, the prognostic relevance of these miRNAs in patients treated with other therapeutic agents may be different, indicating the need for larger studies to be performed in different therapeutic settings. However, this large study provides evidence of the association between exosomal miRNAs and outcomes in newly diagnosed MM patients. We have identified an unprecedented prognostic significance for circulating exosomal miRNAs in MM patients, which requires further validation in other independent prospective MM cohorts.

Acknowledgments

The authors thank Sonal Jhaveri-Schneider (Office for Postdoctoral Training & Career Development, Dana-Farber Cancer Institute) for the English editing of the manuscript. This work was supported by a grant from the National Cancer Institute (R01CA154648). The RNA sequencing data is publicly available at http://www.ncbi.nlm.nih.gov/geo/ (GEO accession number is GSE94564).

Authorship Contributions

S.M. and I.M.G. designed the study. S.M., K.Z.S., D.H., S.V.G., B.R., A.S., and J.B. obtained and assembled the data. H.A.-L., S.Mi., P.M., T.F., and X.L. collected the samples and clinical information. S.M., C.-J.L., J.P., J.S., F.C., K.Z.S., A.M.R., E.W., L.T,. and I.M.G. analyzed and interpreted the data. S.M., C.-J.L., and I.M.G. wrote the report. All authors revised the report and approved the final version.

Conflicts of Interest Disclosure

The authors declare no conflict of interest.

Table 1. Clinical characteristics of patients.

	***N* = 156**	
Characteristics	***N***	**%**
Age, median (range)	56	(34–73)
Sex, male	89	57
IGH		
IgG	81	52
IgA	36	23
IgD	2	1
No heavy chain	22	14
No data	15	10
IGL		
Kappa	94	60
Lambda	41	26
No data	21	14
ISS		
I	63	40
II	56	36
III	33	21
No data	4	3
FISH*		
del(13q)	59	40
t(4;14)	14	10
del(17p)	5	3
High-risk**	17	12
Progression-free survival		
Relapse or death	111	71
3-year PFS, (95% CI)	50	(42–28)
Overall survival		
Death	27	17
3-year OS, (95% CI)	97	(95–99)
Follow-up		
Median, years (IQR)	5.6	(5.4–5.9)

* del(13q): unknown for seven subjects; t(4;14): unknown for 13 subjects; del(17p): unknown for eight subjects; CI, confidence interval; IQR, interquartile range.

** High-risk cytogenetics include t(4;14) and/or del(17p).

Table 2. Risk factors for mortality and progression among multiple myeloma patients

	Progression-free survival				Overall survival			
	Crude HR (95% CI)	*P* value	Adjusted* HR (95% CI)	*P* value	Crude HR (95% CI)	*P* value	Adjusted* HR (95% CI)	*P* valu
ow let-7b	1.78 (1.21–2.60)	0.003†	1.90 (1.22–2.94)	0.004	4.57 (1.90–10.97)	0.001†	2.83 (1.07–7.50)	0.036
ow let-7c	1.22 (0.84–1.78)	0.302			2.28 (1.04–4.99)	0.039		
ow let-7e	1.73 (1.19–2.53)	0.005†	2.01 (1.30–3.11)	0.002	2.39 (1.09–5.24)	0.030		
ow miR-106a	1.90 (1.30–2.78)	0.001†	2.34 (1.52–3.61)	< 0.001	2.67 (1.21–5.88)	0.015		
ow miR-106b	2.52 (1.72–3.69)	< 0.001†	3.54 (2.21–5.68)	< 0.001	2.76 (1.25–6.10)	0.012		
ow miR-10b	1.23 (0.85–1.80)	0.273			1.82 (0.83–3.98)	0.133		
ow miR-125a	1.28 (0.88–1.86)	0.203			2.31 (1.05–5.08)	0.037		
ow miR-125b	1.02 (0.70–1.49)	0.906			1.27 (0.60–2.72)	0.533		
ow miR-155	1.64 (1.12–2.40)	0.011†	1.76 (1.15–2.69)	0.009	3.19 (1.42–7.14)	0.005†	2.41 (0.96–6.05)	0.061
ow miR-15a	1.37 (0.94–2.00)	0.101			2.27 (1.02–5.06)	0.046		
ow miR-16	1.86 (1.27–2.72)	0.001†	2.21 (1.41–3.47)	0.001	2.37 (1.09–5.17)	0.030		
ow miR-17	1.83 (1.25–2.67)	0.002†	2.29 (1.48–3.55)	< 0.001	2.21 (1.01–4.83)	0.046		
ow miR-181a	1.45 (0.99–2.12)	0.054			2.15 (1.00–4.63)	0.051		
ow miR-18a	2.01 (1.37–2.94)	< 0.001†	2.76 (1.79–4.26)	< 0.001	4.62 (1.85–11.50)	0.001†	4.52 (1.57–12.98)	0.005
ow miR-19a	0.13 (0.02–0.99)	0.049	Ω		Ω	0.990		
ow miR-19b	0.83 (0.56–1.22)	0.335			0.48 (0.22–1.03)	0.060		
ow miR-20a	2.00 (1.37–2.92)	< 0.001†	2.31 (1.52–3.53)	< 0.001	2.91 (1.29–6.54)	0.010		
ow miR-21	1.53 (1.05–2.23)	0.028			1.88 (0.88–4.06)	0.106		
ow miR-223	1.33 (0.91–1.94)	0.147			1.77 (0.83–3.76)	0.140		
ow miR-25	1.20 (0.82–1.76)	0.344			2.56 (1.16–5.65)	0.020		
ow miR-744	1.32 (0.91–1.93)	0.144			2.10 (0.97–4.53)	0.059		
ow miR-92a	1.39 (0.95–2.02)	0.089			2.15 (1.00–4.65)	0.051		

HR, hazard ratio; CI, confidence interval; *Adjusted for ISS stage, del(17q) and t(4;14); ΩData didn't converge

†Significance by using Benjamini-Hochberg correction (corrected significance level = 0.020 for progression-free survival and 0.006 for overall survival)

Figure legends

Figure 1. Circulating exosomes characterization in patients with multiple myeloma (MM). (A) Distribution of mappable small RNAs by next-generation sequencing in circulating exosomes from 10 MM patients and five healthy donors. (B) Quantitative RT-PCR of circulating exosomal miRNAs in 10 MM patients and five healthy donors. Box plots represent the median and standard deviation of the normalized expression level of 22 miRNAs. *miRNA (microRNA), mt-rRNA and mt-tRNA (ribosomal and transfer RNA located in mitochondrial genome), snoRNA and snRNA (small nucleolar and nuclear RNA), rRNA (ribosomal RNA), lincRNA (long intergenic non-coding RNA), misc_RNA (miscellaneous other RNA), mRNA (messenger RNA).*

Figure 2. Kaplan–Meier survival curves according to different levels of circulating exosomal miRNAs in multiple myeloma. Kaplan-Meier survival curves of (A) progression-free survival (PFS) and (B) overall survival (OS) in patients with multiple myeloma. The miRNAs were dichotomized at the median based on a low-versus-high expression.

Figure 3. The area under the receiver operating characteristic curve (AUC). The comparisons between the AUC curves of the ISS and cytogenetics, the two miRNAs signature, and the combination for (A) progression-free survival (PFS) and (B) overall survival (OS). Cross-validation has been applied to this analysis to avoid overfitting.

Figures

A

Figure 1

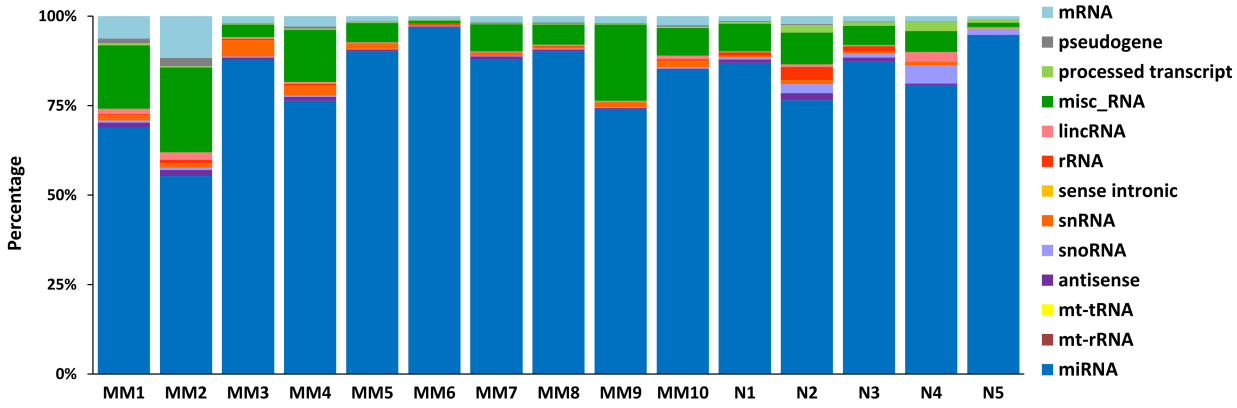

B

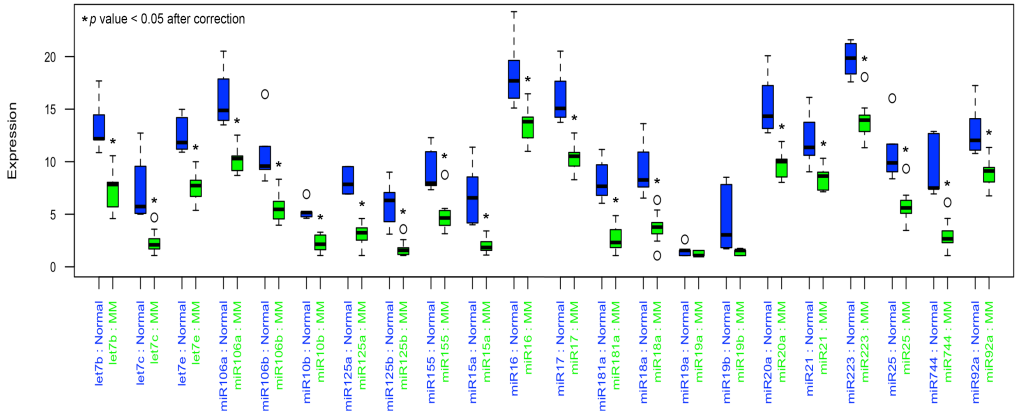

A **Figure 2**

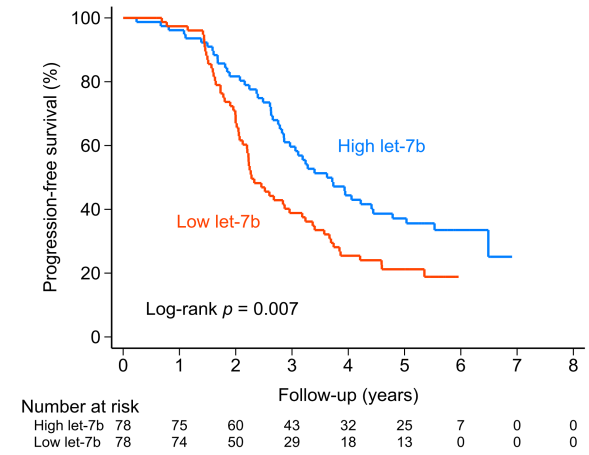

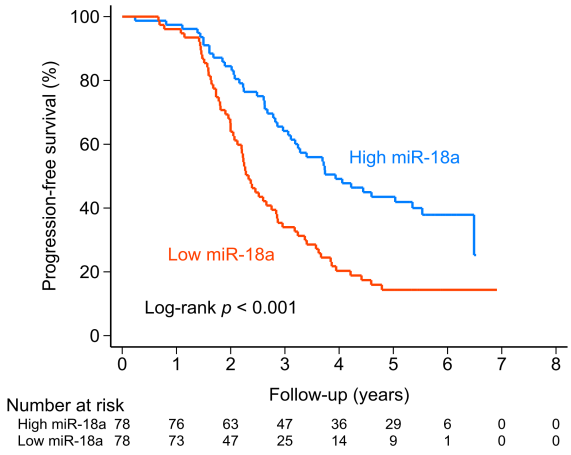

B

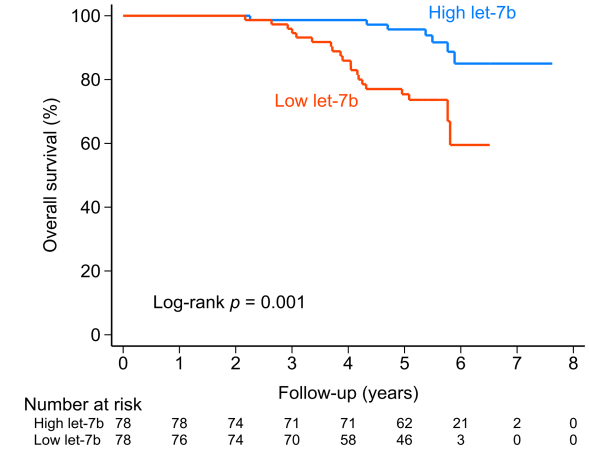

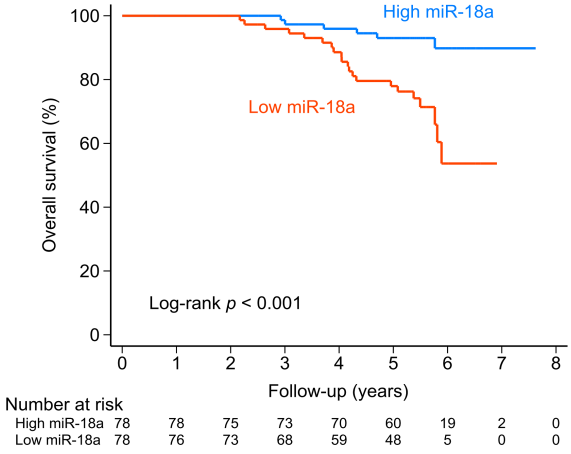

A **Figure 3**

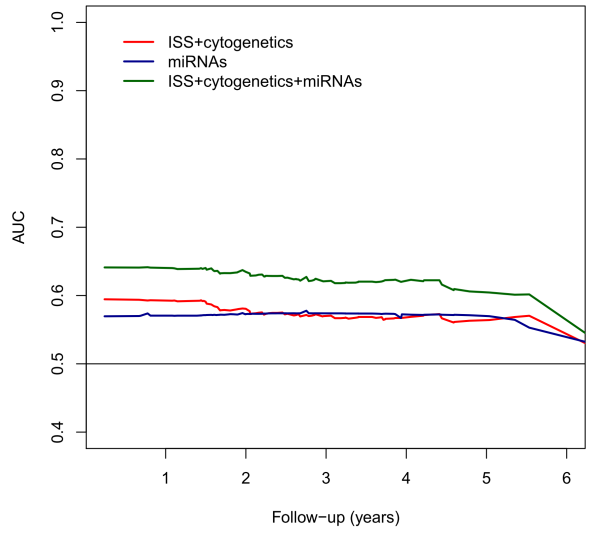

B

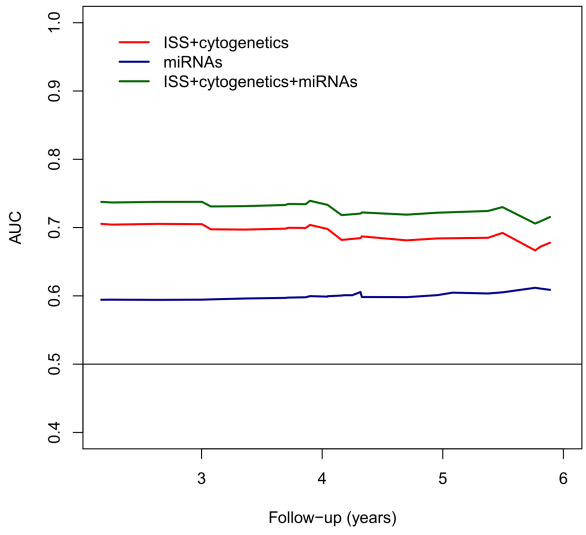

Supplemental material

Table S1. Baseline patient characteristics of multiple myeloma patients with different expressions of let-7b

	Total ***n*** **= 156**	**High let-7b** ***n*** **= 78**	**Low let-7b** ***n*** **= 78**	
Characteristics	***n*** **(%)**	***n*** **(%)**	***n*** **(%)**	***P*** **value**
ISS stage				0.022
I	63 (40.4)	40 (51.3)	23 (29.5)	
II	56 (35.9)	25 (32.1)	31 (39.7)	
III	33 (21.2)	12 (15.4)	21 (26.9)	
Unknown	4 (2.6)	1 (1.3)	3 (3.9)	
FISH*				
del(13q)	59 (37.8)	28 (35.9)	31 (39.7)	0.761
t(4;14)	14 (9.0)	7 (9.0)	7 (9.0)	0.978
del(17p)	5 (3.2)	2 (2.6)	3 (3.9)	1.000
High risk**	17 (10.9)	8 (10.3)	9 (11.5)	1.000
IGH				0.515
IgG	81 (51.9)	38 (48.7)	43 (55.1)	
IgA	36 (23.1)	16 (20.5)	20 (25.6)	
IgD	2 (1.3)	2 (2.6)	0 (0.0)	
No heavy chain	22 (14.1)	12 (15.4)	10 (12.8)	
Unknown	15 (9.6)	10 (12.8)		
IGL				0.265
Kappa	94 (60.3)	47 (60.3)	47 (60.3)	
Lambda	41 (26.3)	16 (20.5)	25 (32.1)	
Unknown	21 (13.5)	15 (19.2)	6 (7.7)	
β2-microglobulin, μg/mL, median (IQR)	3.4 (2.4–5.0)	3.0 (2.3–4.5)	4.0 (2.5–6.2)	0.041
Albumin, g/L, median (IQR)	39.0 (34.0–42.0)	39.0 (36.0–42.0)	37.0 (33.0–42.0)	0.119
Creatinine, μmol/L, median (IQR)	78.0 (72.0–106.0)	79.0 (72.0–97.0)	77.5 (74.0–111.5)	0.883
Hemoglobin, g/dL, median (IQR)	11.0 (9.1–13.2)	11.0 (9.1–13.3)	11.3 (9.1–13.1)	0.763

* del(13q): unknown for seven subjects; t(4;14): unknown for 13 subjects. del(17p): unknown for eight subjects.

** high-risk cytogenetics include t(4;14) and/or del(17p).

Table S2. Baseline patient characteristics of multiple myeloma patients with different expressions of miR-18a

	Total ***n*** **= 156**	**High miR-18a** ***n*** **= 78**	**Low miR-18a** ***n*** **= 78**	
Characteristics	***n*** **(%)**	***n*** **(%)**	***n*** **(%)**	***P*** **value**
ISS stage				0.005
I	63 (40.4)	42 (53.9)	21 (26.9)	
II	56 (35.9)	24 (30.8)	32 (41.0)	
III	33 (21.2)	12 (15.4)	21 (26.9)	
Unknown	4 (2.6)	0 (0.0)	4 (5.1)	
FISH*				
del(13q)	59 (37.8)	28 (35.9)	31 (39.7)	0.483
t(4;14)	14 (9.0)	5 (6.4)	9 (11.5)	0.205
del(17p)	5 (3.2)	3 (3.9)	2 (2.6)	1.000
High risk**	17 (10.9)	7 (9.0)	10 (12.8)	0.441
IGH				0.932
IgG	81 (51.9)	40 (51.3)	41 (52.6)	
IgA	36 (23.1)	17 (21.8)	19 (24.4)	
IgD	2 (1.3)	1 (1.3)	1 (1.3)	
No heavy chain	22 (14.1)	12 (15.4)	10 (12.8)	
Unknown	15 (9.6)	8 (10.3)	7 (9.0)	
IGL				0.032
Kappa	94 (60.3)	51 (65.4)	43 (55.1)	
Lambda	41 (26.3)	14 (18.0)	27 (34.6)	
Unknown	21 (13.5)	13 (16.7)	8 (10.3)	
β2-microglobulin, μg/mL, median (IQR)	3.4 (2.4–5.0)	2.7 (2.1–4.3)	4.1 (2.7–6.5)	< 0.001
Albumin, g/L, median (IQR)	39.0 (34.0–42.0)	40.5 (36.0–45.0)	36.0 (31.0–40.0)	< 0.001
Creatinine, μmol/L, median (IQR)	78.0 (72.0–106.0)	74.0 (72.0–98.0)	81.0 (75.0–108.0)	0.046
Hemoglobin, g/dL, median (IQR)	11.0 (9.1–13.2)	11.7 (10.2–13.5)	10.5 (8.0–12.2)	0.022

* del(13q): unknown for seven subjects; t(4;14): unknown for 13 subjects. del(17p): unknown for eight subjects.

** high-risk cytogenetics include t(4;14) and/or del(17p).

Figure S1. Exosome isolation protocol. Exosome isolation protocol using sequential centrifugation and an exosome isolation reagent (A). Isolated exosomes were further studied by electron microscopy with immunogold labeling for CD63 and CD81 (B) and Nanosight analysis for the diameter (*n* = 3 patients with MM) (C).

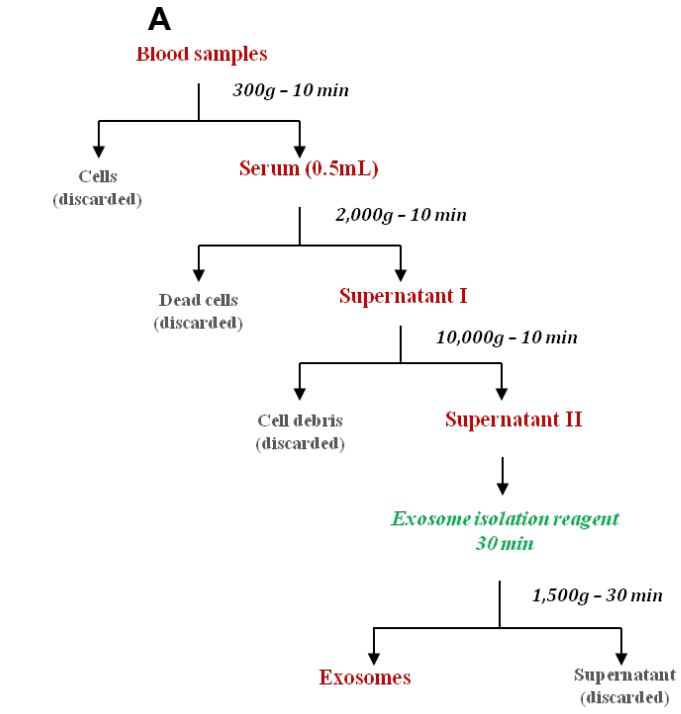

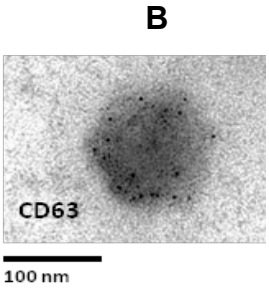

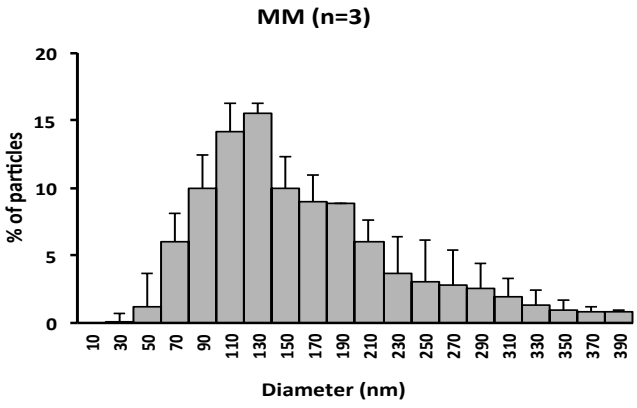

Figure S2. Global median normalization for the TaqMan Low-Density Array (TLDA). Box plot representing 20 TLDA cards, each containing eight samples in duplicate before and after normalization using a global median normalization. Each plate was adjusted by a normalization factor as the difference between the global median Ct value and the plate median Ct value.

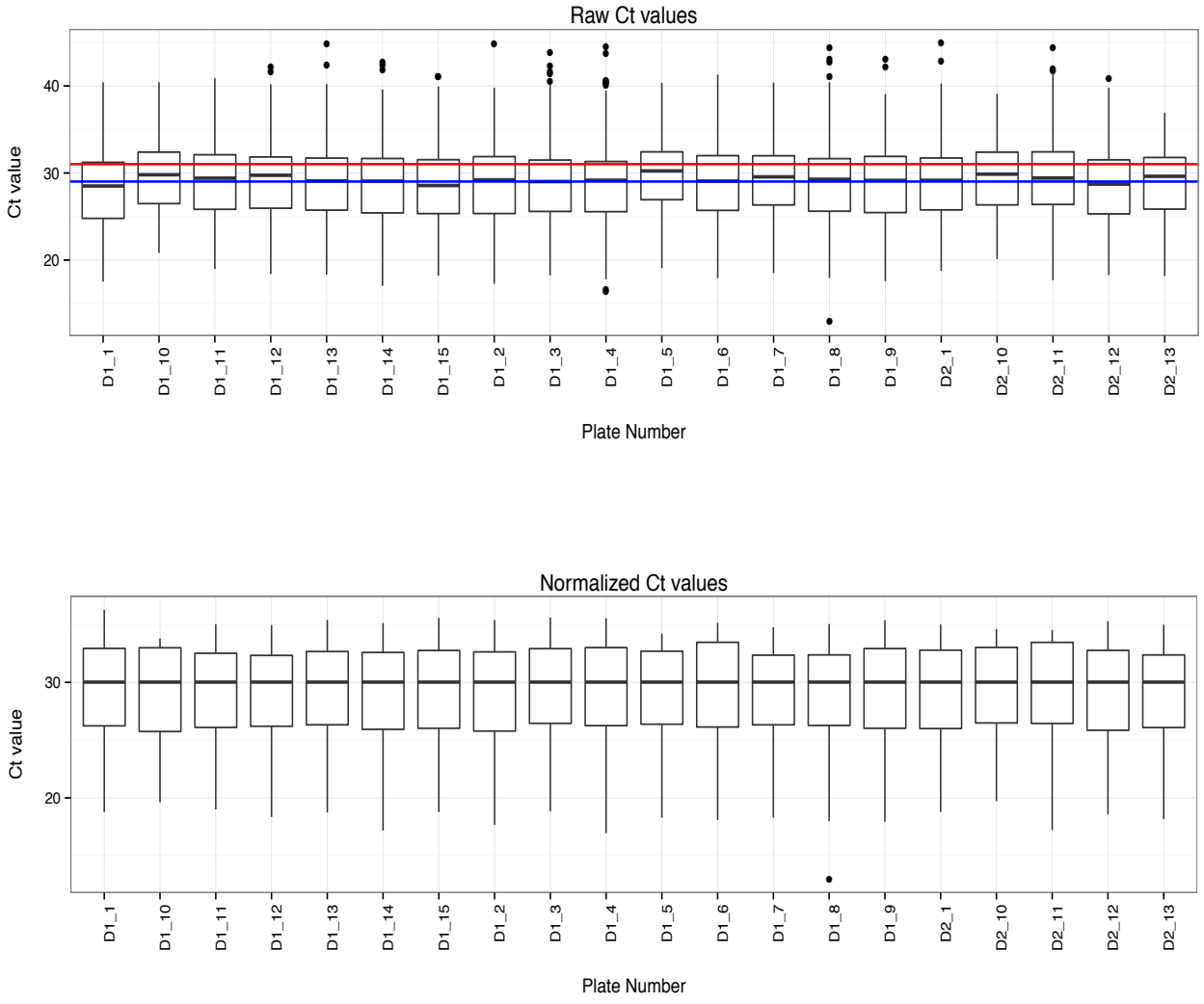

Figure S3. Pie chart of small RNA species and their distributions in the plasma-derived exosomes.

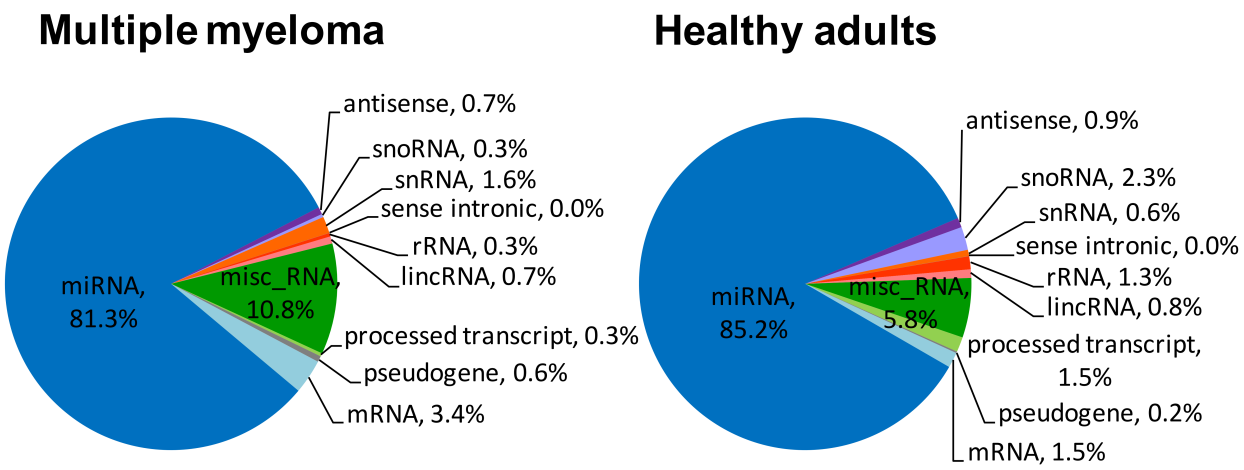

Figure S4. Panel of 22 selected microRNAs and their corresponding clusters.

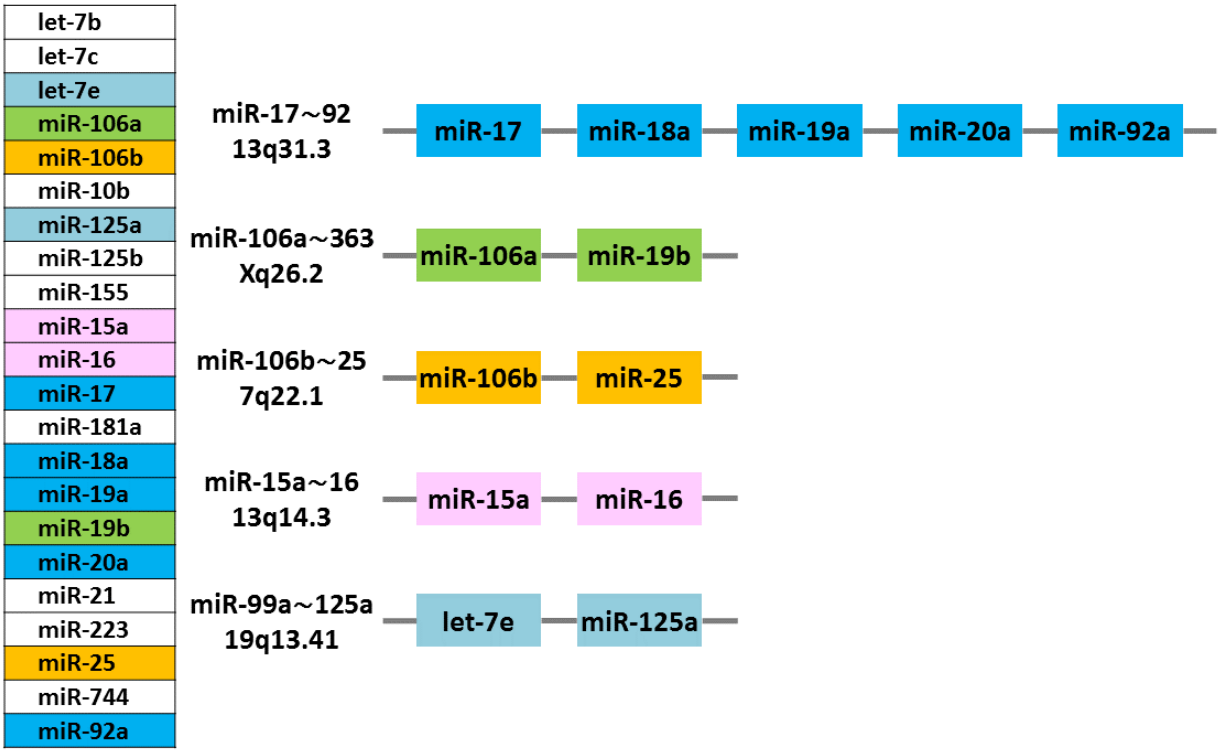

ARTICLE 3

Inhibiting the oncogenic translation program is an effective therapeutic strategy in multiple myeloma

Résumé

Dans ce troisième travail, nous avons étudié les possibilités thérapeutiques de cibler MYC en testant une librairie de molécules sur des lignées cellulaires ayant une expression élevée de MYC. Les résultats ont permis d'identifier les rocaglates, une famille de composés inhibant l'initiation de la traduction, comme étant les plus actifs. Nous avons par ailleurs montré qu'il existe une corrélation entre le niveau d'expression de MYC et l'activité traductionnelle par étude de la base d'une base de données comportant plus de 1000 lignées cellulaires (CCLE – *Cancer Cell Line Encyclopedia*). Parmi les différents composés de la famille rocaglate étudiés, CMLD010509 présentait l'efficacité la plus importante avec des IC50 aux alentours de 10 nM pour les lignées de MM. L'étude du profil transcriptionnel par séquençage de l'ARN de lignées cellulaires de MM traitées par CMLD010509 ou DMSO a révélé la présence d'une signature caractérisant les cellules traitées par rocaglate avec l'activation de gènes implqués dans le transcription et l'inhibition de gènes impliqués dans la traduction. Cette signature est caractéristique de l'inactivation de HSF1 secondaire à l'inhibition du flux traductionnel. Afin d'étudier l'impact de CMLD010509 sur les lignées cellulaires traitées et de déterminer si l'inhibition de la traduction est générale ou spécifique à un sous-

groupe de protéines, nous avons étudié le profile traductionnel des cellules traité par CMLD010509 ou DMSO par spectrométrie de masse quantitative (Tandem Mass Tag System). Nous avons identifié un ensemble de protéines, dont MYC, MDM2, CCND1, MAF et MCL-1, spécifiquement affectées par l'inhibition de la traduction liée au composé CMLD010509 dans le MM. Par marquage au S^{35}, nous avons confirmé que la réduction du niveau d'expression de ces protéines est liée à une diminution de leur traduction. Ces études de transcriptomiques et protéomiques ont été validées par qRT-PCR et Western Blot. De plus, nous avons montré que le composé induit l'apopotose des lignées cellules traitées, sans affecter la prolifération des cellules mononuclées périphériques de donneurs sains. Nous avons ensuite évalué l'efficacité et la tolérance de CMLD010509 dans différents modèles murins, dont deux modèles de xénogreffe utilisant les lignées cellulaires MM.1S et KMS11 et un modèle de souris transgéniques (Vk*Myc). Dans l'ensemble de ces modèles murins, on constatait une augmentation de la survie des souris traitées par CMLD010509 comparativement aux souris contrôles (DMSO), sans toxicité apparente. Ces résultats montrent la possibilité de cibler MYC en inhibant son le programme de traduction oncogénique dans MM.

Contribution de l'auteur

Salomon Manier a participé au design et à la réalisation de l'ensemble des expériences *in vitro* et *in vivo* : screening de la librairie de molécules complète, screening de validation, mesure des IC50, prolifération par Cell Titer Glo, apoptose par Caspase Glo, qRT-PCR, Western Blot, extraction des protéines pour la spectrométrie de masse, préparation des librairies d'ARN pour séquençage à haut débit, injection et suivi des

souris, lecture des lames d'histologie. Il a aussi réalisé l'ensemble des analyses bioinformatiques à partir des base de données CCLE (*Cancer Cell Line Encyclopedia*) , GSEA (Gene Set Enrichment Analysis), LINCSCloud, Cytoscape. Salomon Manier a interprété les résultats, généré les figures et écrit le manuscrit.

Inhibiting the oncogenic translation program is an effective therapeutic strategy in multiple myeloma

One Sentence summary: Targeting translation initiation in multiple myeloma induces inhibition of a specific oncogenic translation program.

Salomon Manier[1,2,3*#], Daisy Huynh[1*], Yujia J. Shen[1], Jia Zhou[1], Timur Yusufzai[1], Karma Z. Salem[1], Richard Y. Ebright[1], Jiantao Shi[1], Jihye Park[1], Siobhan V. Glavey[1], William G. Devine[4], Chia-Jen Liu[1], Xavier Leleu[5], Bruno Quesnel[3], Catherine Roche-Lestienne[3], John K. Snyder[4], Lauren E. Brown[4], Nathanael. Gray[1], James. Bradner[1], Luke. Whitesell[6], John A. Porco, Jr.[4], Irene M. Ghobrial[1#]

[1]Dana-Farber Cancer Institute, Harvard Medical School, Boston, MA 02215, USA; [2]Department of Hematology, Lille Hospital, 59000 Lille, France; [3]INSERM UMR1172, University of Lille 2, 59000 Lille, France; [4]Boston University Center for Molecular Discovery (BU-CMD), Boston, MA 02215, USA; [5]Department of hematology, Poitiers Hospital, 86021 Poitiers, France; [6]Whitehead Institute, Cambridge, MA 02142, USA.

Corresponding authors:

Irene M. Ghobrial, irene_ghobrial@dfci.harvard.edu

Salomon Manier, salomon_manier@dfci.harvard.edu

*These authors contributed equally to this work

Abstract

Multiple myeloma (MM) is a frequently incurable hematological cancer in which overactivity of MYC plays a central role, notably through upregulation of ribosome biogenesis and translation. To better understand the oncogenic program driven by MYC and investigate its potential as a therapeutic target, we screened a chemically diverse small molecule library for anti-MM activity. The most potent hits identified were rocaglate-scaffold inhibitors of translation initiation. Expression profiling of MM cells revealed reversion of the oncogenic MYC-driven transcriptional program by CMLD010509, the most promising rocaglate. Proteome-wide, reversion correlated with selective depletion of short-lived proteins that are key to MM growth and survival, most notably MYC, MDM2, CCND1, MAF, and MCL-1. The efficacy of CMLD010509 in mouse models of MM confirmed the therapeutic relevance of these findings *in vivo* and supports the feasibility of targeting the oncogenic MYC-driven translation program in MM with rocaglates.

Introduction

Multiple myeloma (MM) is a hematological malignancy characterized by a clonal proliferation of plasma cells in the bone marrow microenvironment [1]. According to the National Cancer Institute, the prevalence of MM was estimated at 89,650 people in the United States in 2012, with an annual incidence of 6.3 new cases per 100,000 individuals and a 5-year overall survival of 46.6% [85]. Despite notable therapeutic advances, MM remains a frequently incurable hematological malignancy. Therefore, there is an urgent unmet need for the development of therapeutic options with new mechanisms of action in MM.

The transcription factor MYC plays a central role in the progression of the disease. Approximately two thirds of patients who are newly diagnosed with MM harbor MYC activation, which correlates with adverse clinical outcome [24]. In about 20 to 40% of the patients, this is explained by translocations that involve the *MYC* locus [26,29]. Another 10% of patients harbor a gain of 8q24 comprising *MYC* [30]. MYC is centrally positioned in cell growth- and cancer-regulatory networks. MYC heterodimerizes with MAX, to bind the E-box element CACGTG. Functional categories of MYC-induced genes include cell growth (ribosome biogenesis and protein synthesis), cell cycle control, energy production (glycolysis, glutaminolysis, and mitochondrial biogenesis), anabolic metabolism (synthesis of amino acids, nucleotides, and lipids), and DNA replication [42].

Alterations in ribosome synthesis and translation activity are a defining feature of most cancer cells, satisfying the increased anabolic demands associated with malignant transformation and tumor growth. MYC directly enhances transcription genes encoding ribosomal proteins, ribosomal RNA, and proteins of the translation initiation complex.

The ribosome and translation initiation complexes have historically been perceived as passive complexes, supporting protein synthesis without having an active role in directing functional expression of the genome. However, recent studies have revealed that ribosome biogenesis and translation activity are in fact highly regulated to drive specific translation programs, independent of the genetic make-up of the cancer [158-160], and represent a crucial node for hyperactivation of oncogenic downstream signaling in cancer cells [161]. Accordingly, ribosome biogenesis and translation initiation potentially provide very attractive targets for cancer therapy.

In this study, we sought to identify chemical compounds that disrupt ribosome biogenesis and translation activation in MM. Herein, we describe analogs of the rocaglate natural product class as very potent compounds, which inhibit the oncogenic translation program supporting MM.

Results

MYC and translation activation in MM

To examine potential correlation between *MYC* expression and translation activation in MM, we analyzed the Cancer Cell Line Encyclopedia (CCLE), a large database of gene expression profiling for more than 1,000 human cancer cell lines. We first generated a Z score for each cell line by combining 2 KEGG (Kyoto Encyclopedia of Genes and Genomes) canonical pathway gene sets: ribosomal biogenesis and translation. We found a significant correlation between *MYC* expression and translation activation across the ~ 1,000 CCLE cell lines ($R=0.478$, $p<0.001$), (Fig. 1A). In particular, many MM cell lines had increased *MYC* expression and an enrichment of ribosomal biogenesis and translation (high Z score), which was also observed in other hematological malignancies (fig. S1). We used MM patient tumor cell-derived gene expression profiling (GSE6477 and GSE16558) to further confirm enrichment of translation and ribosomal biogenesis in the context of high *MYC* expression (Fig. 1B and 1C, respectively). These results establish a strong correlation between *MYC* expression and translation activity in MM.

Identification of rocaglate derivatives

To identify a chemical biological probe with which to perturb lymphoid malignancies in the context of *MYC* overexpression, we screened a diverse small molecule library (2,812 compounds) provided by the Boston University Center for Molecular Discovery (BU-CMD). The BU-CMD screening collection is comprised largely of compounds synthesized using diversity-oriented synthesis (DOS) techniques, as well as synthetic

analogs of bioactive natural product scaffolds, assembled with the goal of accessing greater structural complexity and a broader coverage of chemical space than is possible with conventional combinatorial chemistry-based libraries [162]. Two lymphoid cell lines with high expression of *MYC* were used: NCI-H929 (Multiple Myeloma) and NAMALWA (Burkitt lymphoma). We identified 45 compounds, which potently inhibited proliferation of at least one of the cell lines (Fig. 2A and fig. S2). We validated these 45 hits in 5 MM cell lines and 1 Burkitt lymphoma cell line (Fig. 2B). Based on their structure-activity relationships (SAR), this secondary validation highlighted 3 compounds (CMLD010331, CMLD010332, and CMLD009433), all totally synthetic analogs of the rocaglate natural product class (fig. S2B). These three compounds were the most active, inhibiting proliferation of MM cells to a level similar to that of bortezomib (Fig. 2B).

Rocaglate (flavagline) natural products (and synthetic analogs) are recognized to inhibit protein synthesis [163,164]. To better define the activity of rocaglate derivatives against MM cells, we performed a follow-up SAR study involving 40 additional structurally related compounds (Fig. 3A and fig. S2C). These included synthetic samples of both natural and non-natural rocaglates. Of the set, the compound CMLD010509 (SDS-1-021, [163,165]) was identified as the most potent compound, with an IC_{50} below 10 nM for most MM cell lines tested (Fig. 3B and Fig. 3C). The compound was relatively ineffective against lung and breast cancer cell lines, with an IC_{50} of ≈30 nM (Fig. 3D).

Gene expression altered by CMLD010509 inhibiting translation in MM

To further define the mode of action for CMLD010509 against MM, we performed RNA-seq on drug- *vs*. DMSO-treated cells in 5 different MM cell lines. We identified 845 and 475 genes significantly up- and downregulated, respectively, with a fold change higher than 2 and a p-value < 0.05 (Fig. 4A and tables S1A and S1B, respectively). Several zinc finger transcription factors were among the top up-regulated genes, while ribosomal proteins and heat shock proteins were among the most significantly downregulated (Fig. 4A). Furthermore, we defined four clusters by arranging the significantly altered gene sets in a network enrichment map [166]. The transcription and post-translational clusters were enriched in CMLD010509-treated cells, whereas oxidative phosphorylation and translation clusters were enriched in control cells, indicating down-regulation in CMLD010509-treated cells (Fig. 4B and table S1C). Indeed, the most significantly upregulated genes were highly enriched for transcriptional activation, and the most significantly downregulated genes were highly enriched for ribosome components and translation (Fig. 4C and tables S1D and S1E). This transcriptome profile has been associated with low translational flux and consequent inactivation of heat shock factor 1 (HSF1) [167]. In this model, inhibition of translation reverses constitutive HSF1 activation in cancers, thereby leading to extensive remodeling of the transcriptome. We confirmed that CMLD010509 inhibits the heat shock response in MM cells, as indicated by decreased *HSP70* and *HSP90* mRNA and down-regulation of the HSF1 program in CMLD010509-treated cells by pathway analysis (fig. S3A). To assess whether HSF1 is constitutively activated in MM, we used a previously published HSF1 activation signature [168] to interrogate publicly available datasets. We observed that this HSF1 activation signature was increased in MM cells

compared to normal plasma cells [169,170] and correlated with poor clinical outcome in MM [170,171], (fig. S3B and S3C).

To further characterize the link between CMLD010509 and translation inhibition, we used our CMLD010509 expression signature to query the Library of Integrated Network-based Cellular Signatures (LINCS) NIH program (www.lincscloud.org). The LINCS database is a large catalog of perturbational gene expression profiles across 77 cell lines. It includes over 20,000 chemical compounds and over 22,000 genetic perturbations (knockdown and overexpression of genes). The most significant positive correlations with the CMLD010509 signature were represented by known translation inhibitors such as emetine, omacetaxine, and cephaeline, as well as knockdown of ribosome subunits and translation initiation factors (Fig. 4D and table S1F). These results are consistent with the potent activity of CMLD010509 as a translation inhibitor.

More interestingly, *MYC* knockdown was one of the perturbations with the most positive correlation with our compound signature. The gene set enrichment analysis of our compounds' effects using RNA sequencing data revealed that several *MYC* gene sets were among the most significantly enriched compared to the DMSO-control cells, indicating a down-regulation of the entire *MYC* pathway in CMLD010509-treated cells (Fig. 4E). Several *MYC* target genes were indeed downregulated by the drug; however, the amounts of *MYC* transcript were not decreased in CMLD010509-treated cells, indicating post-transcriptional regulation of *MYC* activity (Fig. 4F). Together these results reinforce the role of *MYC* in translation activation in MM and the mechanistic action of CMLD010509 as a translation inhibitor in MM cells.

Disruption of the oncogenic translation program in MM by CMLD010509

To better define the consequences of CMLD010509-induced translation inhibition, we performed an unbiased, proteome-wide experiment in a quantitative and highly parallel format [172]. We compared the immediate impact of CMLD010509 treatment (100 nM) to that of vehicle control in NCI-H929 cells. Exposure for 2 hours was selected to identify primary, immediate consequences of compound action and to mitigate expected, confounding effects of suppressed CMLD010509-target proteins. Each treatment condition was prepared in three biological replicates and individually labeled using isobaric tagging. We identified 7,312 proteins, of which 54 were significantly depleted by more than 2-fold after CMLD010509 exposure ($p < 0.05$ and FC > 2), (Fig. 5A and table S2A). Several key oncoproteins in MM were among the proteins most depleted by the compound, including MYC, MDM2, CCND1, MCL-1, and MAF. *MYC* is overexpressed in about 40% of MM by either translocations or gain of 8q24, among other potential epigenetic regulations [26,29]. *CCND1* is overexpressed in about 20% of MM in case of t(11;14) or focal gain in 11q13 [26,122]. *MDM2* is an ubiquitin ligase (E3) that acts as a negative regulator of p53 [173]. *MCL-1* belongs to the Bcl-2 family and is one of the driver oncogenes in gain-of-1q cancers [174]. *MAF* is frequently overexpressed in MM in relation to t(14;16) [175].

To further study the mechanism of action of CMLD010509, we compared the protein fold changes to the transcript fold changes in CMLD010509-treated vs. vehicle-treated cells (Fig. 5B). The large majority of depleted proteins had a change in transcript amount less than 2-fold, indicative of a selective translation inhibitory mode of action for CMLD010509. To validate these findings, we measured MYC, MDM2, CCND1, MCL-1,

and MAF by immunoblot and qRT-PCR after compound treatment as above (100 nM, 2 hours). All five genes were depleted at the protein level, whereas the amounts of each transcript were unchanged or slightly increased (Fig. 5C and D), consistent with post-transcriptional effects of CMLD010509. Similar results were observed in six additional MM cell lines (fig. S4A-G). To assess whether the targeted proteins were directly depleted by inhibiting their synthesis, we pulse-labeled cells with S35-cysteine/methionine and immunoprecipitated the proteins of interest. In the presence of CMLD010509, we observed selective inhibition of new translation for MYC, CCND1, and MCL-1 as opposed to housekeeping proteins such as GAPDH (fig. S4H).

To further establish pathways affected by CMLD010509, we queried the 54 proteins with more than 2-fold depletion against the KEGG (Kyoto Encyclopedia of Genes and Genomes) database. Cancer pathways were highly enriched among these depleted proteins, representing a distinct cluster by network enrichment analysis (Fig. 6A and table S2B). Moreover, when interrogating the whole MSigDB C2 canonical pathway database (representing 1330 gene sets), we found that the most highly enriched pathways consisted of MM pathways: *IRF4* and *MYC* targets. This result indicates that a significant number of CMLD010509-depleted proteins are present in the IRF4 and MYC pathways ($p < 0.001$), as defined by GSEA transcriptional pathways. *IRF4* is a key transcription factor essential for plasma cell differentiation, upon which MM cells are dependent [38], (Fig. 6B and table S2C), suggesting that CMLD010509 inhibits translation of key oncoproteins in MM. To determine whether this translational program is specific for MM, we used the signature of 54 proteins to calculate Z scores for over 1000 cell lines across the CCLE database. The CMLD010509 signature was

enriched in MM cell lines at the transcriptional level compared to other cancer cell lines (Fig. 6C). Furthermore, the signature was also significantly enriched in plasma cells of patients with MM compared to those of healthy donors ($p<0.05$), in two independent gene expression profiling experiments including patients at diagnosis (GSE16558) and at relapse (GSE6477) (Fig. 6D). Together these results demonstrate that CMLD010509 inhibits the translation of key oncoproteins, supporting the proliferation and survival of MM.

Induction of apoptosis in MM cells by CMLD010509

We next explored the antiproliferative consequences of inhibiting the oncogenic translation program in MM cells with CMLD010509. The drug was associated with a strong induction of an apoptotic response in NCI-H929 and MM1S cells, as measured by caspase-3 and -7 activation (Fig. 7A) and cleavage of both poly(ADP-ribose) polymerase (PARP) and caspase-3 (Fig. 7B). Kinetic studies revealed a rapid apoptotic response to CMLD010509 at 3 hours, associated with depletion of MYC and MCL-1 even at low concentrations (10 nM), (Fig. 7C). We next assessed the *in vitro* activity of CMLD010509 against human peripheral blood mononuclear cells (PBMCs) and found no cytotoxicity, suggesting the potential for a useful therapeutic window for this agent against MM (fig. S5).

In vivo suppression of MM by CMLD010509

Based on the mechanism of action of CMLD010509 in MM, we assessed whether the drug would be effective and tolerable in animal models. We first established

a xenograft model by intravenous (i.v.) injection of MM1S cells expressing luciferase into severe combined immunodeficient (SCID) mice. After engraftment, the mice were randomized to vehicle and compound treatment groups, with equal amount of bioluminescence imaging (BLI) intensity in each group. CMLD010509 or vehicle control was administered by intraperitoneal (i.p.) injection at 0.7 mg/kg twice a week (Fig. 8A). CMLD010509 caused a marked reduction in tumor burden despite the very rapid growth of this aggressive MM cell line, as monitored by BLI and prolonged survival (median OS 35 vs. 47 days, $p<0.001$), (Fig. 8B and C). Of note, 4 weeks of CMLD010509 treatment were well tolerated with preservation of body weight and normal complete blood counts (fig. S6A-C). To confirm the *in vivo* efficacy of CMDL010509, we used a second xenograft model consisting of SCID mice inoculated intravenously with KMS11 cells. The mice were treated with i.p. injections of either CMLD010509 at 0.7 mg/kg or vehicle control twice a week, starting at week 4, and the mice were sacrificed at week 8. Immunohistochemistry studies were conducted on bone marrow samples to assess the presence of CD138+ tumor cells as well as amounts of MYC and Ki67 protein. A decrease of CD138+ plasma cells, depletion of MYC, and inhibition of proliferation (Ki67 staining) were observed with CMLD010509 compared to vehicle control (Fig 8D), further validating the activity of CMLD010509 on MM cell lines *in vivo*.

Finally, to complete the assessment of CMLD010509's effects on *MYC*-driven MM cells *in vivo,* we used an immunocompetent mouse model, in which transplantable mouse MM cells were injected into C57BL/6J mice. The tumor cells are driven by plasma cell-specific *MYC* overexpression (Vk*Myc cells), [25]. Mice were treated with either CMLD010509 at 0.7 mg/kg or vehicle control i.p. twice a week, beginning 1 week

after cell tumor inoculation. Treatment was well tolerated, as indicated by normal transthyretin and albumin serum concentrations at 6 weeks (fig. S6D). Serum electrophoresis proteins (SPEP) revealed a robust decrease of M-spike in CMLD010509-treated mice as shown at week 4 (Fig. 8E), which was associated with a significantly prolonged survival - median survival of 39 days in the control group *vs.* not reached (NR) in the CMLD010509-treated group after 85 days of experiment ($p = 0.0019$), (Fig. 8F). Together, these data indicate that CMLD010509 is highly active and well tolerated *in vivo* in several mouse models of MM.

Discussion

The oncogenic translation program of tumors is supported by aberrant activation of ribosome biogenesis and dysregulation of the translation initiation machinery [158-160]. In this study, we report the correlation between *MYC* activation and the translation of an oncogenic program in MM, which can be inhibited by the rocaglate derivative CMLD010509. We identified the rocaglate derivative CMLD010509 (SDS-1-021) as a highly specific inhibitor of the oncogenic translation program supporting MM – including key oncoproteins such as MYC, MDM2, CCND1, MAF, and MCL1.

Although ribosome biogenesis and translation initiation complex function have historically been perceived as passive processes, recent studies have revealed that they are actively regulated to support specific translation programs [158,159]. Here, using a proteome-wide approach, we report that targeting translation initiation in MM selectively depletes multiple oncoproteins, while leaving other housekeeping proteins largely unperturbed. The selective inhibition of translation initiation for oncogenic mRNA in the context of cancer can be explained by several mechanisms. First, some messengers are translated in a cap-dependent manner while others are translated through the internal ribosome entry site (IRES) process. Cap-dependent translation relies on the ability of the eukaryotic translation initiation factor 4F (eIF4F) complex to bind to the 5' 7-methylguanosine cap present on mature mRNAs [176]. Moreover, the presence of complex secondary structures within the 5'UTR influences mRNA translation. Transcripts with complex 5'UTR secondary structures are subject to greater dependence on the initiation machinery and therefore might be more sensitive to its inhibition. Subsequent studies have shown that the limiting factor is often eIF4E, mainly

through its ability to recruit the eIF4A helicase [177-180]. Complex 5'UTR structures have been identified in several pro-oncogenic mRNAs such as those encoding *MYC, MDM2,* and cyclins [160].

Rocaglate natural products, including silvestrol and rocaglamide A, comprise a class of protein synthesis inhibitors [164,167] that interact with the eukaryotic translation initiation factor 4A (eIF4A) - a protein subunit of the translation initiation complex [164,181]. These compounds increase the affinity between eIF4A and mRNA and specifically clamp eIF4A onto polypurine sequences in mRNA 5'UTR, thus blocking ribosome subunit scanning and reducing protein expression from transcripts bearing the rocaglamide A–eIF4A target sequence [182]. The compound CMLD010509 is a potent and selective translation inhibitor through an eIF4E phosphorylation–independent mechanism [165]. In this work, we demonstrate that CMLD010509 inhibits translation of a key suite of oncoproteins in MM that constitute an oncogenic translation program supporting MM oncogenesis. Moreover, this compound is highly effective *in vivo* in several mouse models, suggesting an effective therapeutic approach toward targeting *MYC* in MM.

The present work was aimed to assess the translational potential of rocaglates in MM. We did not focus on the specific relationship between *MYC* and translation activation in MM. Moreover, the specific effect of CMLD010509 on the translational oncogenic program in MM could be further explored to fully determine its mechanism of action.

In summary, we present an indirect, but highly effective mechanism for targeting an oncogenic translation program frequently driven by *MYC* in MM. Even with the most

recent advances in the management of plasma cell dyscrasias, MM remains a frequently incurable disease. Therefore, there is an urgent need for additional treatment options with new modes of activity. As shown here, rocaglates inhibit a specific translation oncogenic program related to high expression of MYC, with a very potent activity *in vitro* and *in vivo*. Thus, targeting dysregulated translation initiation with rocaglates rather than targeting the elongation machinery with other translation inhibitors might be less toxic to normal tissues. Indeed, several characteristics of CMLD010509 support its further preclinical development. First, the compound can be made by total synthesis from simple starting materials, which avoids reliance on limited bioresources [183]. Second, its mode of action suggests a simple strategy for therapeutic drug monitoring to minimize toxicity in patients based on routinely available measurements of short-lived serum proteins such as prealbumin (transthyretin) or Factor VII. Finally, successful clinical development might be improved by use of the oncogenic signature we have proposed as a potential companion diagnostic to identify patients most likely to benefit from rocaglate treatment. The targeting of protein degradation in MM with proteasome inhibitors has become a mainstay in the management of this disease. Based on the preclinical data presented here, we suggest that targeting protein homeostasis in the opposite way, through selective inhibition of protein synthesis, is worthy of further development and may provide an equally effective approach in the management of MM and possibly other hematological malignancies.

Materials and Methods

Study design. The objectives of this study were as follows: (i) to identify compounds able to interfere with *MYC* activation in MM, (ii) to assess the mechanistic role of rocaglate compounds in MM, and (iii) to determine the preclinical efficacy of CMLD010509 as an effective treatment against MM. Cell-titer Glo was used to evaluate the efficacy of a small-molecule screen against 2 cell lines with high expression of *MYC*, to validate the best hits against 6 cell lines, and to generate IC50s of rocaglate compounds. Functional evaluations of CMLD010509 was performed by RNA sequencing of 5 MM cell lines and Tandem-Mass-Tag mass spectrometry using NCI-H929 exposed to CMLD010509 or DMSO in both cases. Further, qRT-PCR and Western blotting were performed to validate the data. We used Gene Set Enrichment Analysis and the LINCS cloud databases for pathway analyses. The effect of CMLD010509 *in vitro* was assessed on MM cell lines by Caspase3/7 Glo and Western blotting for Caspase 3 and PARP. To determine the preclinical efficacy of CMLD010509, we used three different mouse models. The first one was a xenograft model where MM1S luc/GFP cells were injected i.v. into SCID mice. After 2 weeks of engraftment, tumor formation was monitored by BLI. To allocate animals to experimental groups, we measured BLI using Living Image 4.0 software and randomized mice to obtain equal amounts of BLI intensity in each group. Mice were treated with either CMLD010509 or DMSO and monitored weekly for BLI, blood count, and body weight and for survival. The second xenograft model consisted of injecting KMS11 cells into SCID mice and treating them with either CMLD010509 or DMSO. The mice were all sacrificed at week 6 and studied for IHC of the bone marrow with CD138,

MYC, and Ki67 antibodies. Finally, we developed an immunocompetent mouse model by injecting Vk*Myc cells into C57BL/6 mice. After 1 week of engraftment, mice were randomized into 2 groups and treated with either CMLD010509 or DMSO. Mice were monitored for SPEP and survival. The experiment was terminated after 3 months of follow up.

Cell lines and primary cells. NCI-H929, NAMALWA, MM1S, MM1R, U266, and RPMI8226 were purchased from ATCC, OPM2 from DSMZ, and KMS11 and KMM-1 from JCRB Cell Bank. MM1S luc/GFP cells were kind gifts from Dr. Andrew Kung, Dana-Farber Cancer Institute, and CAL51, NCI-1650, NCI-1750, NCI-23, DU4475 and ZR-751 cells were kind gifts from the Dr. Pasi Jänne lab, Dana-Farber Cancer Institute. Vk*Myc cells used in this study were isolated from late stage Vk*Myc mice (kind gift from Drs. Leif Bergsagel and Marta Chesi) and expanded *in vivo*. All cells were maintained under 5% CO_2 in medium according to their specifications. Peripheral blood mononuclear cells (PMBCs) were obtained from the peripheral blood of healthy volunteers by Ficoll gradient centrifugation.

Small-Molecule Screen. MM cell lines were treated with 2,812 compounds provided by the Boston University Center for Molecular Discovery (BU-CMD, cmd.bu.edu). A microplate dispenser, Matrix Wellmate (ThermoFisher Scientific), was used to dispense 2,000 adherent cells or 5,000 suspension cells per well into 384-well microplates. Compounds were added using Biomek FX pin tool (Beckman Coulter). After treatment, cytotoxicity was measured by Cell-Titer-Glo (Promega) according to manufacturer's

protocol, and luminescence signals were read using EnSpire (Perkin Elmer), a plate reader.

Cell Viability Assay. Relative cell growth and survival were measured in 96-well microplate format by using luminescent detection of CellTiter-Glo or Caspase-Glo as an endpoint. For IC_{50}, 5,000 adherent cells and 30,000 suspension cells were plated and incubated with compounds for 72 hours. Each analysis was performed three times.

Protein and RNA isolation. Harvested cells were lysed using lysis buffer (Cell Signaling) supplemented with 5 mM NaF and 1 mM PMSF (phenylmethylsulfonyl fluoride) for 30 minutes on ice, and lysates were centrifuged at 14,000x*g* for 30 minutes. Protein concentration was measured using Bio-Rad Protein Assay kit (Bio-Rad).
Total RNA was isolated from cells using RNeasy Mini Kit (Qiagen) according to manufacturer's protocol and evaluated for quantity and quality by NanoDrop spectrophotometer.

qRT-PCR. For qRT-PCR, 100 ng of total RNA per sample was used for reverse transcription using SuperScript III First-Strand Synthesis Kit (Invitrogen). Quantitative real-time PCR was done on a StepOnePlus Real-Time PCR System (Applied Biosystems) using Sybr Green I Mastermix. Gene expression was normalized to 18S. The primer sequences are provided below:

human *MYC*	F: TCCGTCCTCGGATTCTCTGCTCT
	R: GCCTCCAGCAGAAGGTGATCCA

human *MDM2*	F: CCCAAGACAAAGAAGAGAGTGTGG
	R: CTGGGCAGGGCTTATTCCTTTTCT
human *CCND1*	F: GCTGCGAAGTGGAAACCATC
	R: CCTCCTTCTGCACACATTTGAA
human *MAF*	F: CTGGCAATGAGCAACTCCGA
	R: AGCCGGTCATCCAGTAGAGT
human *MCL1*	F: TGCTTCGGAAACTGGACATCA
	R: TAGCCACAAAGGCACCAAAAG
human 18S	F: TCAACTTTCGATGGTAGTCGCCGT
	R: TCCTTGGATGTGGTAGCCGTTTCT

RNA-Sequencing. NCI-H929, NAMALWA, U266, MM1S, and OPM2 cells were treated with 50 nM CMLD010509 or vehicle control for 6 hours. RNA was prepared as mentioned earlier. A starting amount of 500 ng of RNA was used to prepare poly-A enriched, single barcoded libraries using the NEBNext kit. Quality control of the libraries was evaluated by Bioanalyzer analysis with High Sensitivity chips (Agilent Technologies). Sequencing was performed on a HiSeq 2500 (Illumina) by 2 X 50 bp paired-end reads at the Biopolymers Facility of Harvard Medical School. We used Bcbio_nextgen (https://github.com/chapmanb/bcbio-nextgen/) to process the RNA-seq data. Briefly, cutadapt (https://github.com/marcelm/cutadapt/) was used to trim adapters; trimmed reads were aligned to human reference genome (GRCh37) with tophat2; read count for each gene was calculated by HT-seq. Genes with low expression (FPKM < 1 across all samples) were filtered out. Gene set enrichment

analysis (GSEA) was used to identify significantly enriched pathways [166], with false discovery rate (FDR) <0.25 and p value < 0.05. Gene sets were downloaded from the Broad Institute's MSigDB (http://www.broadinstitute.org/gsea/index.jsp).

Immunoblotting. Cell lysates (50 µg) were subjected to sodium dodecyl sulfate-polyacrylamide gel electrophoresis, transferred to a polyvinylidene fluoride membrane, blocked with 5% non-fat dry milk, and incubated with primary antibodies overnight at 4C. Primary antibodies used included anti-MYC, anti-MCL1, anti-CCDN1 (all Cell Signaling), anti-MDM2, anti-MAF (all Santa Cruz), and anti-tubulin (Sigma Aldrich).

Tandem Mass Tag Spectrometry. NCI-H929 cells were treated in triplicate with CMLD010509 (100 nM) or vehicle control for 2 hours. Proteins were isolated and further processed for quantitative proteomic analysis by Tandem Mass Tag (TMT) (Thermo Fisher Scientific) as per manufacturer protocol, with mass spectrometry (MS).

^{35}S Labeling. NCIH929 and MM1S cells were pre-incubated in methionine-free RPMI medium supplemented with dialyzed Fetal bovine serum (FBS) and Pen Strep (Thermo Scientific) for 10 minutes. ^{35}S-methione was added to the medium at a final concentration of 100 µCi/ml (~9 µM methionine), and the cells were labeled for 20 minutes at 37°C. An equal volume of complete RPMI medium (containing an excess of unlabeled methionine; ~50 µM final) was added and the cells incubated for an additional 10 min at 37°C. The cells were then collected by centrifugation and washed with cold 1X PBS. Whole cell extracts were prepared by resuspending the cells in 1X Cell Lysis

Buffer (Cell Signaling) supplemented with HALT protease and phosphatase inhibitors (Thermo Scientific) followed by 30 min incubation on ice. The extracts were centrifuged for 15 min at 18000 g to remove the insoluble material. For the IP experiments, the whole cell extracts were incubated with primary antibodies (anti-MYC (Abcam #ab32), anti-Cyclin D1 (Abcam #ab134175), anti-MCL1 (Cell Signaling #94296), anti-GAPDH (Abcam #ab181602), or anti-control IgG (Cell Signaling #3900)) overnight at 4^{o}C with rotation. The following morning, 40 µl of DynaBeads-Protein G (Invitrogen) were added, and the samples were rotated for an additional hour. The beads were separated using a magnetic rack and washed three times with Cell Lysis Buffer. The immunoprecipitated material was eluted in 25 µl of 1x SDS sample buffer. The whole cell extracts and the IP samples were resolved by SDS-PAGE and transferred to a nitrocellulose membrane (GE healthcare). The membrane was stained with Ponceau S to visualize total proteins in samples. The membrane was then air-dried and exposed to a phosphorimager screen to visualize the 35S-labeled proteins.

***In Vivo* Studies.** SCID mice (n=10/group) used for xenograft experiments were injected intravenously with 5x10^{6} MM1S-GFP-Luc+ and monitored by blood cell count, body weight, bioluminescence imaging (BLI), and survival. After engraftment, the mice were randomized into two groups based on bioluminescence imaging (BLI), and CMLD010509 or vehicle control were administered by i.p. injection at 0.7 mg/kg twice a week. Similar studies were performed in SCID mice (n=10/group) by injecting 7x10^{6} KMS11, but because these cells are not luc+, the mice were sacrificed at week 6, and the bone marrow of femurs was subjected to immunohistochemistry as described

below. For the immunocompetent mouse model, C57BL/6 mice were purchased from Jackson Laboratories (Bar Harbor, Maine). The transplantable Vk*MYC cell line, which was a kind gift of Dr. Marta Chesi and Dr. P. Leif Bergsagel (Mayo Clinic, Scottsdale AZ), was maintained and expanded *in vitro* using RPMI-1640 containing 10% fetal bovine serum FBS (Sigma Chemical), 2 mM L-glutamine, 100 U/mL penicillin, and 100 μg/mL streptomycin (GIBCO). 3.5×10^6 Vk*Myc cells were injected i.v. into C57BL/6 mice, and the peripheral blood from the mice was collected for SPEP measurement at serial time points by sub-mandibular bleeding. SPEP was performed using QuickGel Protein Kit (Helena Laboratories) according to manufacturer's protocol. After 1 week of vk*Myc cell injection, the mice were randomized to therapy or vehicle control - i.p. injection at 0.7 mg/kg twice a week, n=10 mice per group.

Study approval. All mice were treated, monitored, and sacrificed in accordance with an approved protocol of the Dana-Farber Cancer Institute Animal Care and Use Committee.

Immunohistochemistry. Murine tissues were fixed overnight in 10% buffered formalin and stored in 70% ethanol before proceeding to paraffin-embedding, sectioning, and staining with hematoxylin-eosin (H.E.). Immunohistochemistry was performed using anti-CD138, anti-Ki-67, anti-c-Myc, as previously reported [184].

Statistical Analysis. The unpaired Student's t-test was used to compare two independent groups. One-way ANOVA was used when three or more independent

groups were compared. For survival data, Kaplan–Meier curves were plotted and compared using a log-rank test. All tests were two-sided. A p value of less than 0.05 was considered statistically significant. Pearson coefficient was used to assess the correlation between 2 groups. Analysis was performed with GraphPad Prism Software (GraphPad Software Inc.). Mann–Whitney U test was used to quantify the enrichment of a given signature in a ranked list of genes, which was represented as a Z-score. GSEA was performed as described previously using GSEA v2.0.10 (http://www.broadinstitute.org/gsea/) [166]. MSigDB collections (http://software.broadinstitute.org/gsea/msigdb/index.jsp) and specific gene sets (KEGG Translation and Ribosome and several MYC gene sets) were tested for their enrichment in datasets – MM patients with high expression of MYC vs. low or MM cell lines treated with CMLD010509 *vs*. DMSO. Investigate_GeneSets (http://software.broadinstitute.org/gsea/msigdb/annotate.jsp) was used to investigate pathways enriched in a list of genes against MSigDB collections. The analysis was performed by applying the two-tailed Fisher test method as implemented in the Investigate_GeneSets module at MSigDB. For network enrichment mapping, gene sets with significant enrichment in CMLD010509- or DMSO-treated cells by GSEA were selected on the basis of $P<0.05$ and $FDR<0.25$ and visualized with Cytoscape v3.3.0 (http://www.cytoscape.org/cy3.html). This software organizes the significant gene sets into a network, where nodes correspond to gene sets and the edges reflect significant overlap between the nodes according to a Fisher's test. The size of the nodes is proportional to the number of genes in the gene set, as previously described [185].

Acknowledgements: We are thankful to Dr. Marc Mendillo (Northeastern University, Boston MA) for his analysis of the HSF1 activation signature in MM datasets, to Dr. Andrew Kung (Dana-Farber Cancer Institute, Boston MA) for providing MM1S luc/GFP cells, to Dr. Pasi Jänne (Dana-Farber Cancer Institute, Boston MA) for providing lung and breast cell lines and to Drs. Leif Bergsagel and Marta Chesi (Mayo Clinic, Scottsdale AZ) for providing Vk*Myc cells.

Funding: This work was supported in part by NCI R01 CA181683-01A1. Work at Boston University is supported by R35GM118173 and R24GM111625. We thank Mr. Steve Stone for the initial synthesis of CMLD010509. R.Y.E. was supported by National Institute of General Medical Sciences T32GM007753.

Authors contribution: S.M., N.G., J.B., L.W. and I.M.G. designed the study; S.M., D.H., Y.S., K.Z.S., R.E., S.V.G., T.Y. and J.Z. performed experiments; S.M., D.H., J.P., J.S., L.W. and I.M.G. analyzed the data; W.D., L.B., J.S. and J.P. generated reagents; all authors wrote-reviewed and edited the manuscript; I.M.G. provided funding.

Competing Interests: The authors declare that they have no competing interests.

Data and materials availability: RNA-seq data have been deposited to the Gene Expression Omnibus (http://www.ncbi.nlm.nih.gov/geo/), GSE94827. All compounds tested are from Dr. John Porco under a material agreement with Boston University.

Figure legends

Figure 1. Correlation of *MYC* expression with ribosomal biogenesis and translation activity. (A) Correlation analysis of *MYC* expression on the Y axis and the Z-score enrichment across over 1000 cell lines from the Cancer Cell Line Encyclopedia (CCLE) database. A Z-score was generated for each cell line by combining 2 KEGG canonical pathway gene sets: ribosomal biogenesis and translation. Red dots indicate multiple myeloma (MM) cell lines, and black dots indicate all CCLE cell lines except MM. A significant correlation between *MYC* expression and the translation activation was observed, R= 0.478, $p<0.0001$. Gene Set Enrichment Analysis (GSEA) of MM patient tumor cell-derived gene expression profiling (GSE6477 and GSE16558) shown in (**B**) and (**C**), respectively, confirming enrichment of translation and ribosomal biogenesis in context of high expression of *MYC*.

Figure 2. Chemical library screen. (**A**) Small molecule library generated by the Boston University Center (~ 3,000 synthetic compounds) against NCI-H929 (multiple myeloma) and NAMALWA (Burkitt lymphoma). We identified 45 compounds with a potent inhibition of proliferation for at least one of the cell lines. (**B**) Validation of 45 hits in 6 cell lines harboring diverse MM driver genomic features of MM, showing that the most effective compounds to inhibit proliferation were the rocaglate derivative class, namely CMLD010331, CMLD010332, and CMLD09433 (red dots). These compounds had similar potency as bortezomib.

Figure 3. High potency of rocaglate inhibitors in MM. (A) Heat map of the effects of 40 rocaglate derivatives on relative survival of MM cells (NCI-H929, KMS-18, MM1R, MM1S, OPM-2, RPMI8226, and U266) along with lymphoma cell lines (NAMALWA and MEC1) shows strong activity with low doses of the rocaglate compounds in these cell lines. (**B**) IC_{50} of these 40 compounds in NCI-H929 showing that CMLD010509 was the most potent compound, with an IC_{50} below 10 nM. (**C**) IC_{50} of CMLD010509 showing an IC_{50} below 10 nM for most MM cell lines tested (indicated in red), while it was relatively resistant in lung and breast cancer cell lines (in black) with an IC50 of ≈30 nM. **(D**) CMLD010509 is a synthetic rocaglamide derivative characterized by a cyclopenta(b)tetrahydrobenzofuran core structure.

Figure 4. Transcription activation and translation inhibition induced by the rocaglate derivative CMLD010509. (A) Volcano plot of RNA sequencing of drug- *vs*. DMSO-treated cells in 5 different MM cell lines showing 845 and 475 genes significantly up- and down-regulated, respectively, with a fold change higher than 2. **(B**) Network enrichment map identifying 2 clusters enriched in CMLD010509-treated cells (transcription and post-translational modification clusters) and 2 clusters enriched in control cells (oxidative phosphorylation and translation clusters). (**C**) Bar graphs showing the most significantly up-regulated and down-regulated genes in CMLD010509-treated cells determined by querying the MSigDB C5 gene sets. (**D**) Connectivity score using Library of Integrated Network-based Cellular Signatures (LINCS) NIH program with the gene signature of CMLD010509 against 10,000 ‘pertubagen’ signatures (corresponding to shRNA, open reading frame and

compounds). **(E)** GSEA analysis of CMLD010509 using RNA sequencing data. Several *MYC* gene sets were among the most significantly enriched compared to DMSO-control cells. **(F)** Bar graphs of *MYC* transcript expression in MM cell lines and NAMALWA in CMLD010509-treated cells, normalized to DMSO control.

Figure 5. Regulation of the oncogenic translation program of MM by CMLD010509. (A) Expression proteomics showing the impact of CMLD010509 treatment (100 nM) relative to vehicle control in NCI-H929 cells after a 2-hour incubation (3 biological replicates were used and individually tagged using isobaric tagging). We identified 7312 proteins, of which 54 were significantly depleted more than 2-fold by CMLD010509 exposure ($p<0.05$ and $FC>2$). The most depleted proteins included MYC, MDM2, CCND1, MCL-1, and MAF (red dots). (**B**) Comparison of the protein fold changes to the transcript fold changes in CMLD010509-treated vs. vehicle-treated cells. A large majority of depleted proteins had a transcript fold change lower than 2-fold, suggestive of a specific translational mechanism of action for CMLD010509. (**C**) Immunoblots and (**D**) qRT-PCR analysis of MYC, MDM2, CCND1, MCL-1, and MAF in compound-treated (100 nM, 3 hours) or vehicle-treated NCI-H929. All five genes were depleted at the protein level, whereas their transcripts were unchanged or slightly over expressed.

Figure 6. Pathway analysis of CMLD010509. (**A**) Network enrichment analysis of 54 depleted proteins with more than 2 fold change analyzed in the KEGG database, showing that cancer pathways were highly enriched among these depleted proteins. (**B**)

The 54 depleted proteins were queried against MSigDB C2 canonical pathway database, showing an enrichment of MM specific oncoproteins including *IRF4* pathway. (**C**) Z-scores of the 54 proteins evaluated on 1000 cell lines of the CCLE database. (**D**) Z-scores of the 54 proteins evaluated on two independent gene expression profiles including patients at diagnosis (GSE16558) and at relapse (GSE6477).

Figure 7. **Induction of apoptosis by CMLD010509.** (**A**) Apoptosis assay measured by caspase 3 and 7 activation (Caspase 3/7 Glo) at 3 hrs and 24 hrs in NCI-H929 and MM1S cells treated with 3 concentrations of CMLD010509 *vs.* vehicle control. (**B**) Immunoblots for cleavage of both poly(ADP-ribose) polymerase (PARP) and caspase-3 in response to 3 concentrations of CMLD010509 in NCI-H929 and MM1S cells, at 3 hrs and 24 hrs. (**C**) Immunoblots for MYC and MCL-1 in response to 3 concentrations of CMLD01010509 in NCI-H929 and MM1S cells at 3 hrs and 24 hrs.

Figure 8. In vivo suppression of MM by CMLD010509. (A). Diagram of *in vivo* studies performed. SCID mice were injected with MM1S GFP-Luc+. After engraftment, the mice were randomized to two groups based on bioluminescence imaging (BLI), and CMLD010509 or vehicle control was administered by i.p. injections at 0.7 mg/kg two times a week. Tumor growth was assessed by weekly bioluminescence (BLI) counts, (**B**) showing a significant difference in tumor growth between the DMSO-treated group and the CMLD010509 group, $p<0.001$. (**C**) Kaplan Meier curve showing a significant survival difference between vehicle and drug-treated mice, with a median OS 35 vs. 47 days, $p<0.001$. (**D)** Immunohistochemistry for CD138, Ki67, and MYC in bone marrow

samples from the KMS11-injected mice. Scale bars represent 50 μm. (**E**) Electrophoresis of serum proteins from transplantable Vk*Myc, mice indicating the presence of a gammaglobulin (M-spike) in the DMSO control group (arrow) at 4 weeks. C57BL6 syngeneic mice were injected with 3.5×10^6 VK*Myc cells intravenously. At Day 7 after tumor cells injection, mice were randomized into 2 groups and received DMSO (n=10) or CMLD010509 drug (n=10, 0.7 mg/kg/mouse) through i.p. injections twice a week. (**F**) Kaplan-Meier curve showing a significant survival difference between vehicle and drug-treated mice, with a median OS of 39 days vs. NR, p=0.0019. Statistical analyses were performed using log-rank test.

Figures

Figure 1

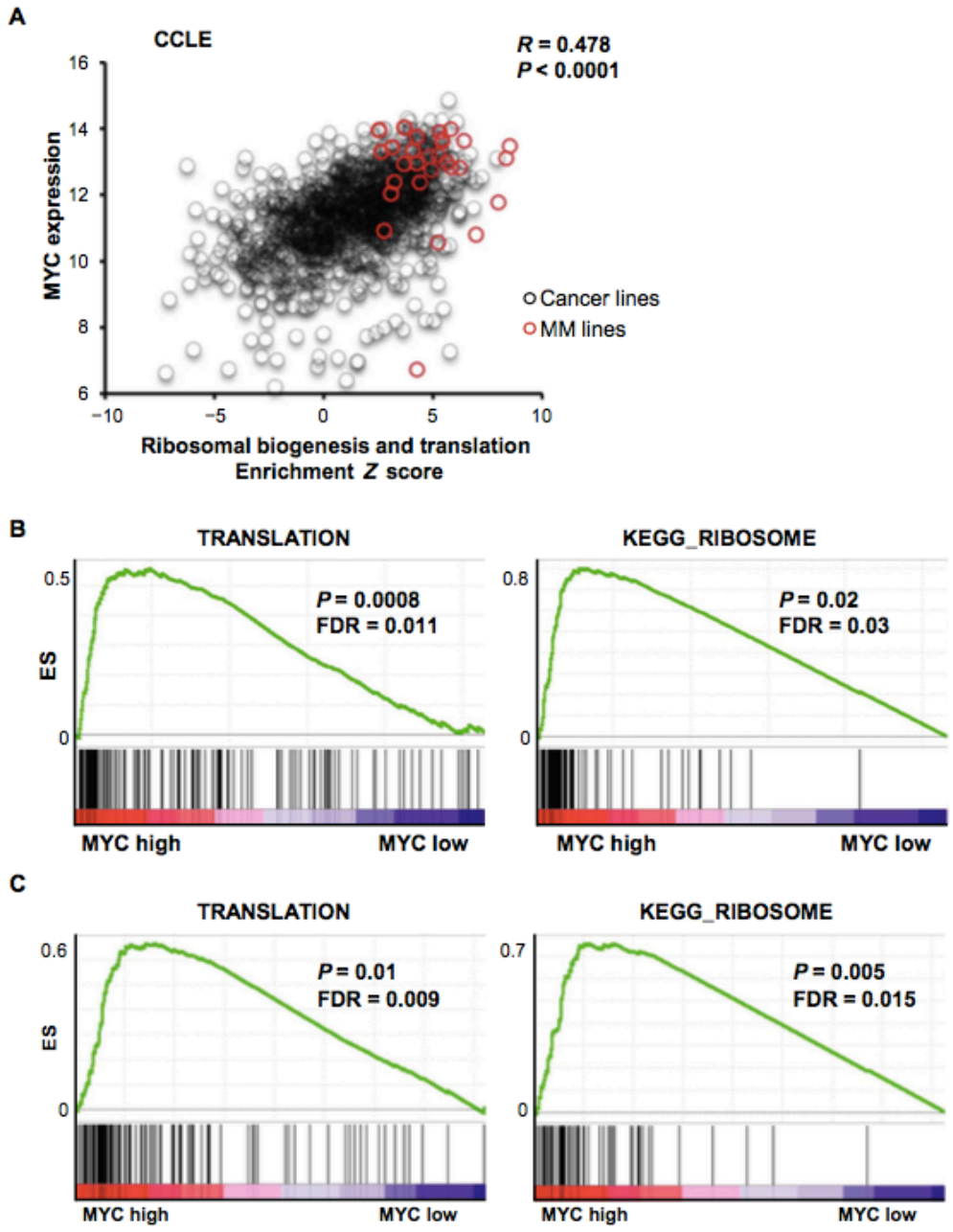

Figure 2

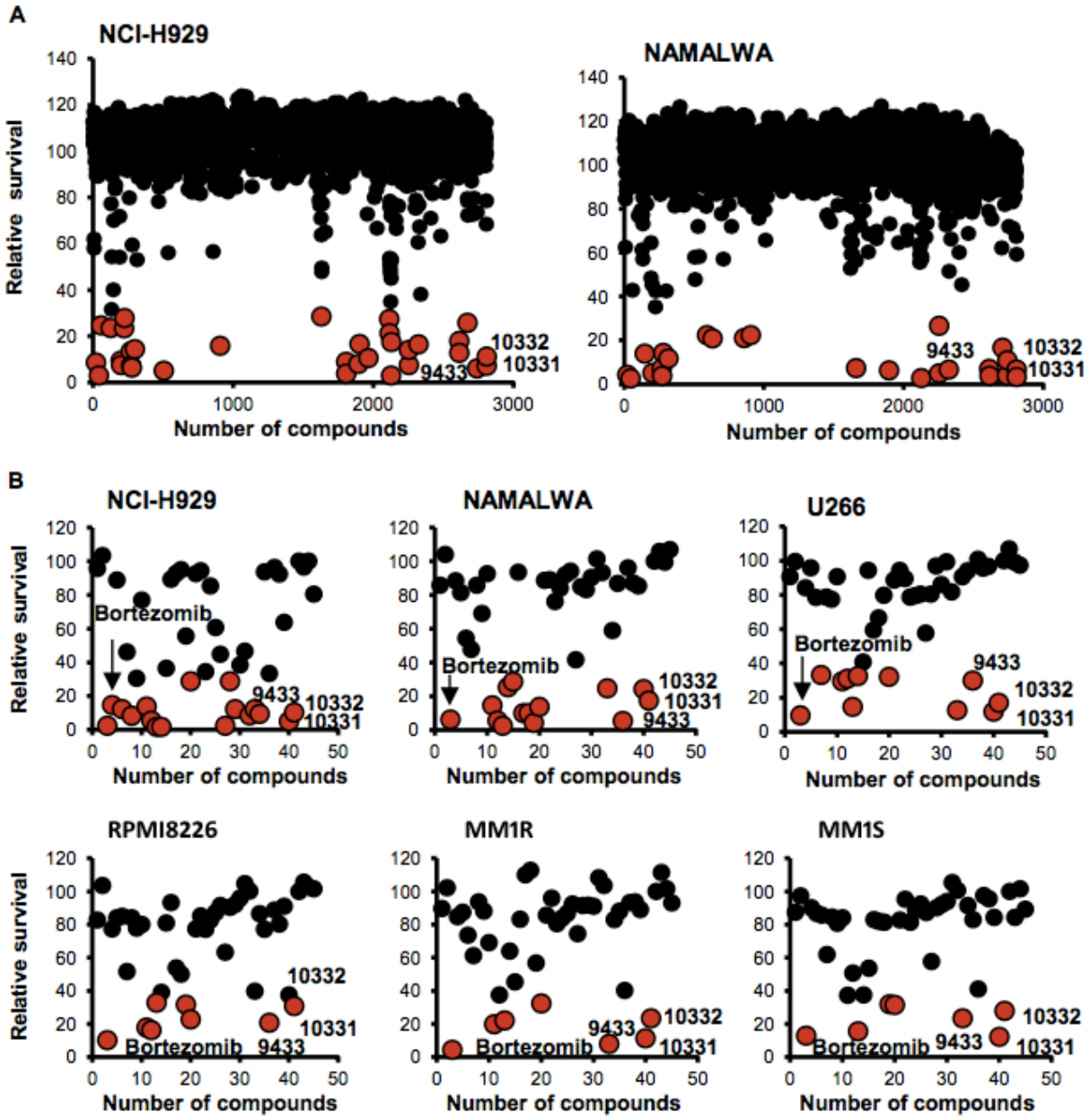
A
NCI-H929
NAMALWA
Relative survival
Number of compounds
10332
10331
9433
B
NCI-H929
NAMALWA
U266
RPMI8226
MM1R
MM1S
Bortezomib
Relative survival
Number of compounds

Figure 3

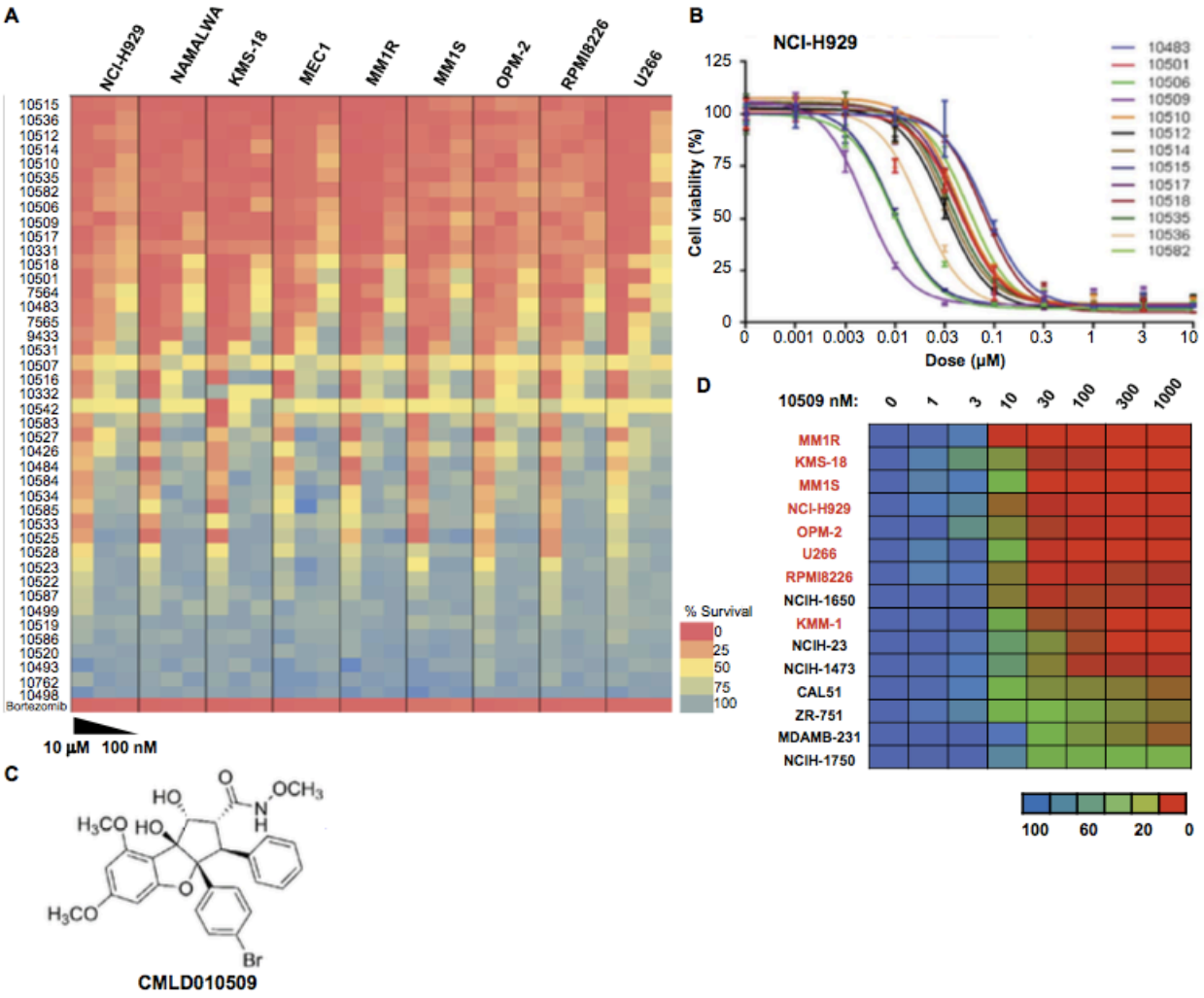
A
NCI-H929
NAMALWA
KMS-18
MEC1
MM1R
MM1S
OPM-2
RPMI8226
U266
Bortezomib
10 µM
100 nM
% Survival
0
25
50
75
100
B
NCI-H929
Cell viability (%)
Dose (µM)
0.001
0.003
0.01
0.03
0.1
0.3
1
3
10
C
CMLD010509
D
10509 nM:
0
1
3
10
30
100
300
1000
MM1R
KMS-18
MM1S
NCI-H929
OPM-2
U266
RPMI8226
NCIH-1650
KMM-1
NCIH-23
NCIH-1473
CAL51
ZR-751
MDAMB-231
NCIH-1750
100
60
20
0

Figure 4

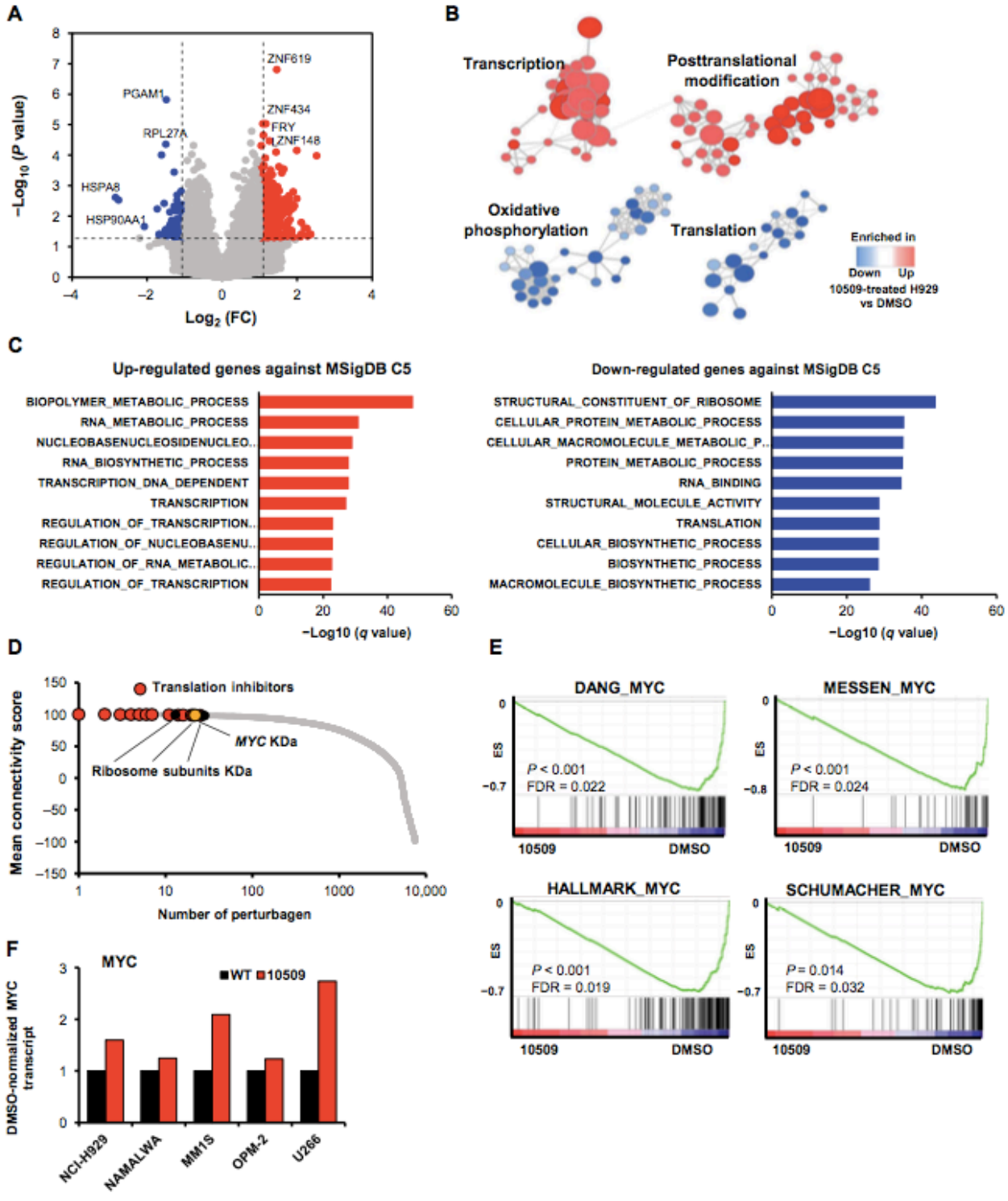
A
ZNF619
PGAM1
ZNF434
FRY
RPL27A
ZNF148
HSPA8
HSP90AA1
−Log10 (P value)
Log2 (FC)
B
Transcription
Posttranslational modification
Oxidative phosphorylation
Translation
Enriched in
Down Up
10509-treated H929 vs DMSO
C
Up-regulated genes against MSigDB C5
BIOPOLYMER_METABOLIC_PROCESS
RNA_METABOLIC_PROCESS
NUCLEOBASENUCLEOSIDENUCLEO..
RNA_BIOSYNTHETIC_PROCESS
TRANSCRIPTION_DNA_DEPENDENT
TRANSCRIPTION
REGULATION_OF_TRANSCRIPTION..
REGULATION_OF_NUCLEOBASENU..
REGULATION_OF_RNA_METABOLIC..
REGULATION_OF_TRANSCRIPTION
−Log10 (q value)
Down-regulated genes against MSigDB C5
STRUCTURAL_CONSTITUENT_OF_RIBOSOME
CELLULAR_PROTEIN_METABOLIC_PROCESS
CELLULAR_MACROMOLECULE_METABOLIC_P..
PROTEIN_METABOLIC_PROCESS
RNA_BINDING
STRUCTURAL_MOLECULE_ACTIVITY
TRANSLATION
CELLULAR_BIOSYNTHETIC_PROCESS
BIOSYNTHETIC_PROCESS
MACROMOLECULE_BIOSYNTHETIC_PROCESS
−Log10 (q value)
D
Translation inhibitors
MYC KDa
Ribosome subunits KDa
Mean connectivity score
Number of perturbagen
E
DANG_MYC
P < 0.001
FDR = 0.022
MESSEN_MYC
P < 0.001
FDR = 0.024
HALLMARK_MYC
P < 0.001
FDR = 0.019
SCHUMACHER_MYC
P = 0.014
FDR = 0.032
ES
10509
DMSO
F
MYC
WT 10509
DMSO-normalized MYC transcript
NCI-H929
NAMALWA
MM1S
OPM-2
U266

Figure 5

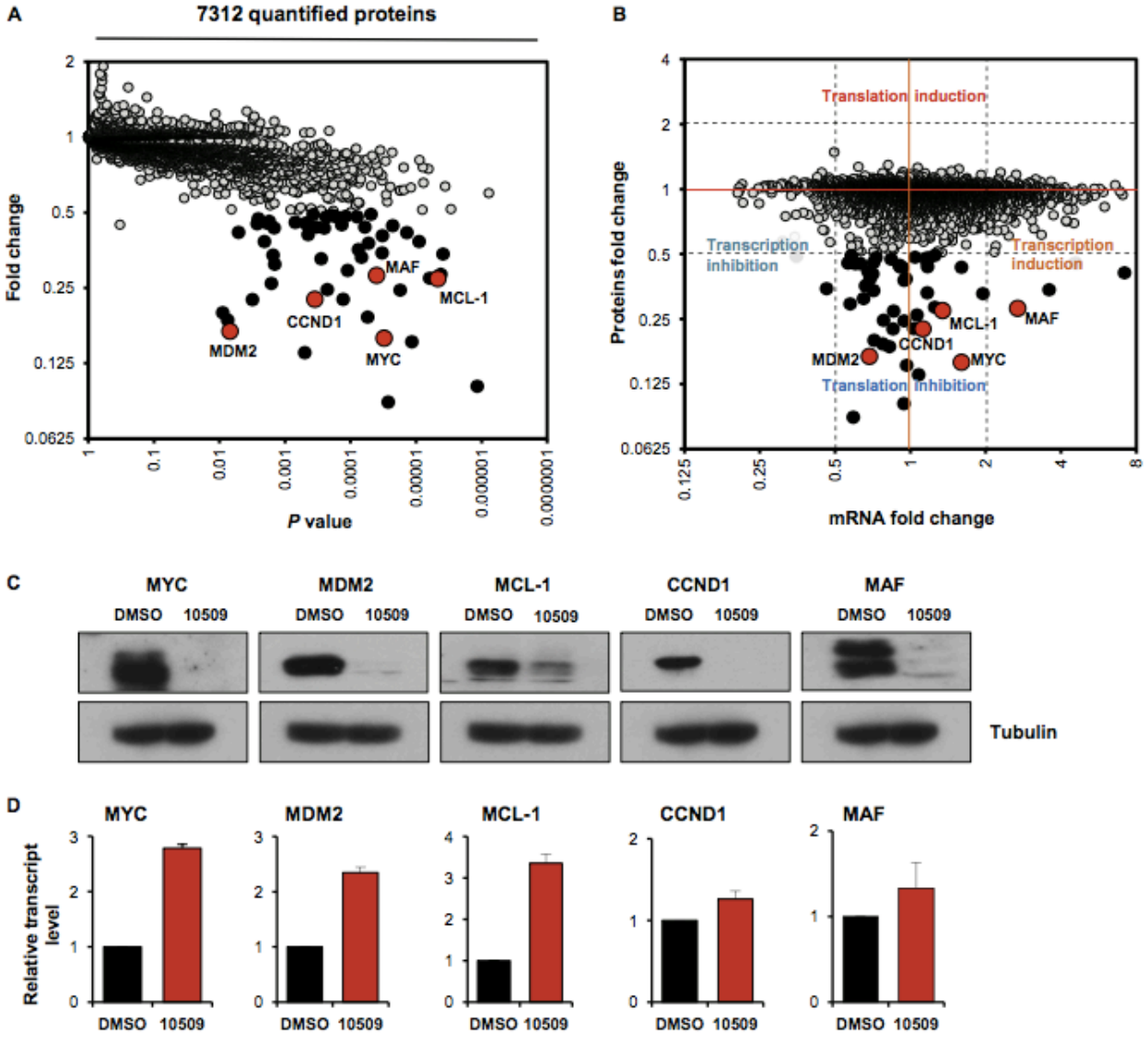
A
7312 quantified proteins
Fold change
P value
MAF
MCL-1
CCND1
MDM2
MYC
B
Translation induction
Transcription inhibition
Transcription induction
Translation inhibition
Proteins fold change
mRNA fold change
C
MYC
MDM2
MCL-1
CCND1
MAF
DMSO 10509
Tubulin
D
Relative transcript level
DMSO 10509

Figure 6

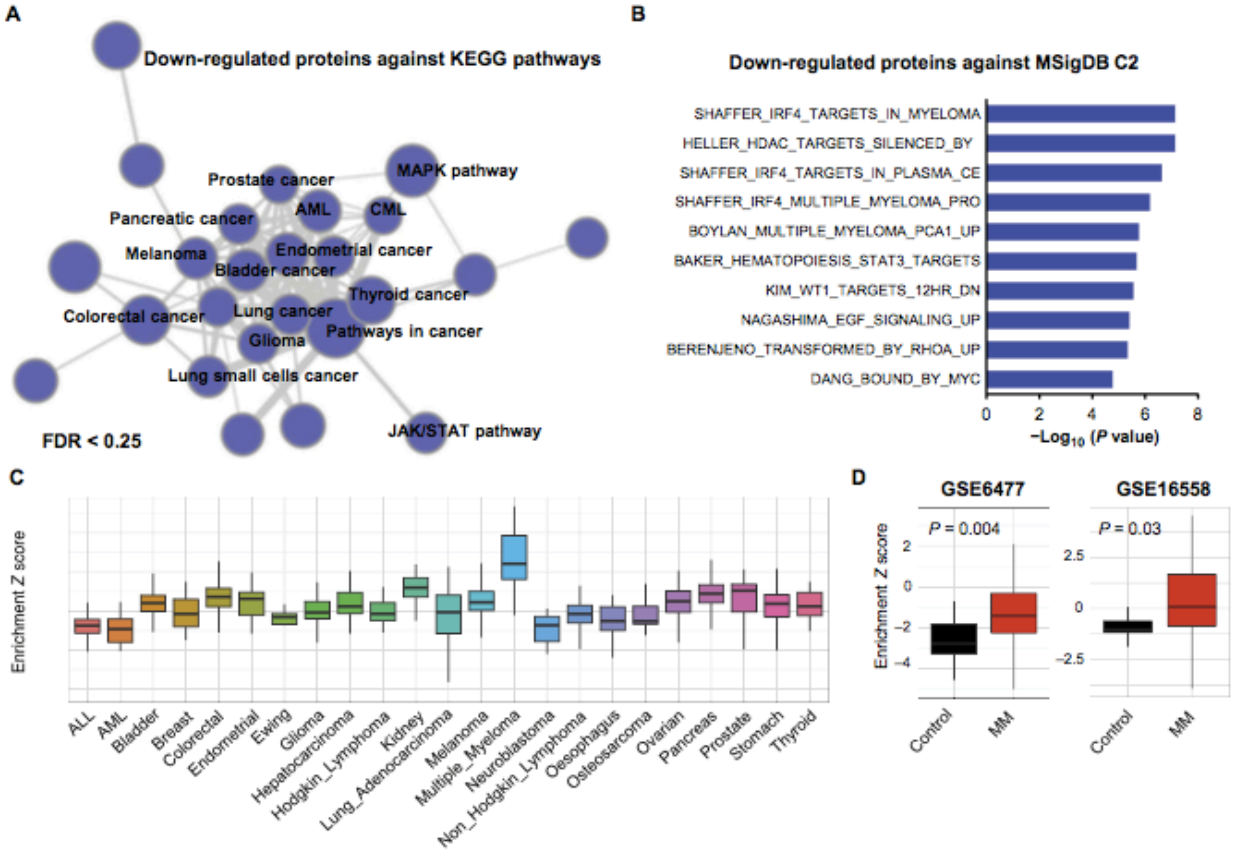
A
Down-regulated proteins against KEGG pathways
Prostate cancer
MAPK pathway
Pancreatic cancer
AML
CML
Melanoma
Endometrial cancer
Bladder cancer
Thyroid cancer
Colorectal cancer
Lung cancer
Pathways in cancer
Glioma
Lung small cells cancer
JAK/STAT pathway
FDR < 0.25
B
Down-regulated proteins against MSigDB C2
SHAFFER_IRF4_TARGETS_IN_MYELOMA
HELLER_HDAC_TARGETS_SILENCED_BY
SHAFFER_IRF4_TARGETS_IN_PLASMA_CE
SHAFFER_IRF4_MULTIPLE_MYELOMA_PRO
BOYLAN_MULTIPLE_MYELOMA_PCA1_UP
BAKER_HEMATOPOIESIS_STAT3_TARGETS
KIM_WT1_TARGETS_12HR_DN
NAGASHIMA_EGF_SIGNALING_UP
BERENJENO_TRANSFORMED_BY_RHOA_UP
DANG_BOUND_BY_MYC
0
2
4
6
8
−Log10 (P value)
C
Enrichment Z score
ALL
AML
Bladder
Breast
Colorectal
Endometrial
Ewing
Glioma
Hepatocarcinoma
Hodgkin_Lymphoma
Kidney
Lung_Adenocarcinoma
Melanoma
Multiple_Myeloma
Neuroblastoma
Non_Hodgkin_Lymphoma
Oesophagus
Osteosarcoma
Ovarian
Pancreas
Prostate
Stomach
Thyroid
D
GSE6477
P = 0.004
GSE16558
P = 0.03
Enrichment Z score
Control
MM
Control
MM

Figure 7

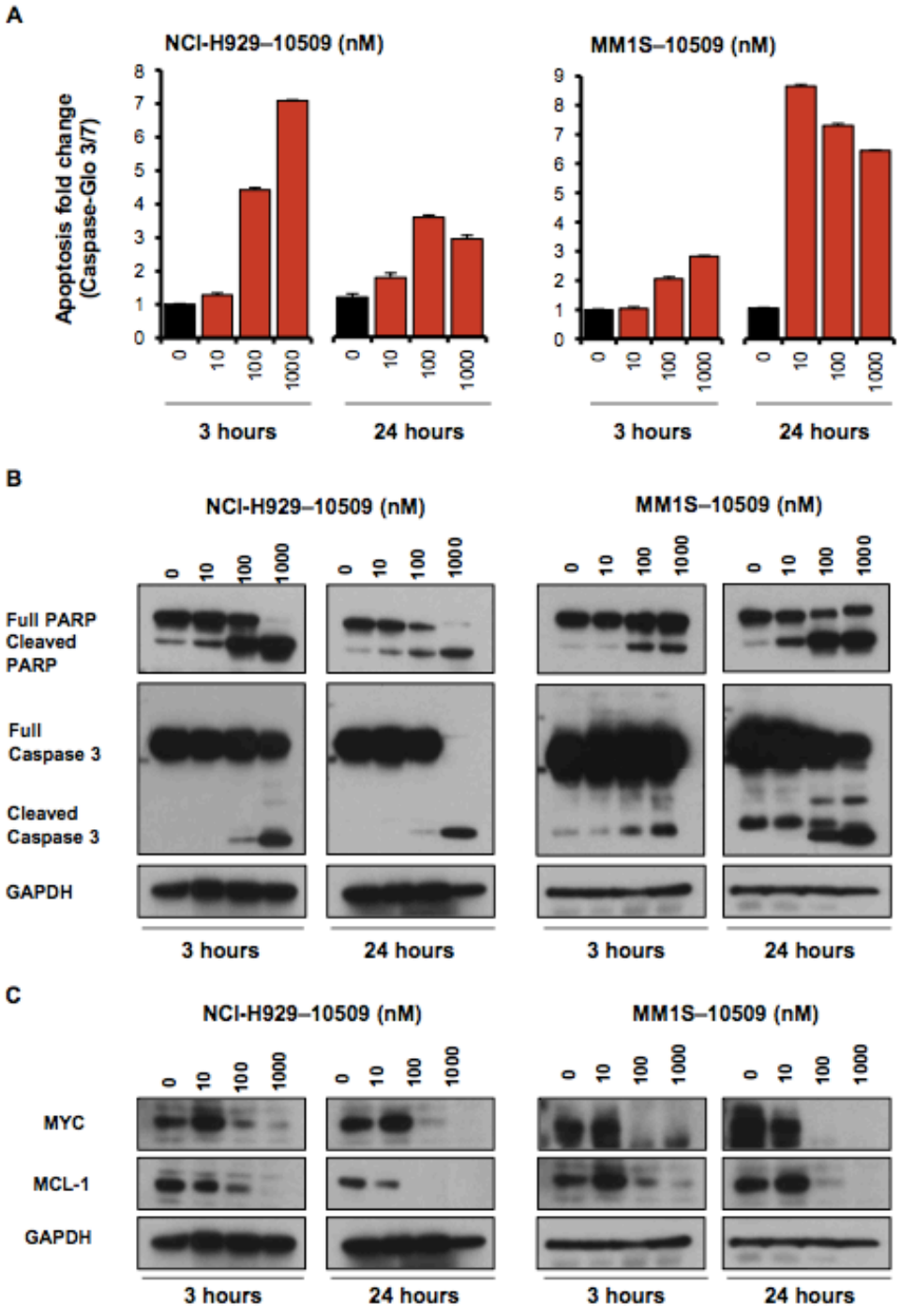
A
NCI-H929–10509 (nM)
MM1S–10509 (nM)
Apoptosis fold change (Caspase-Glo 3/7)
0
10
100
1000
3 hours
24 hours
B
NCI-H929–10509 (nM)
MM1S–10509 (nM)
Full PARP
Cleaved PARP
Full Caspase 3
Cleaved Caspase 3
GAPDH
C
NCI-H929–10509 (nM)
MM1S–10509 (nM)
MYC
MCL-1
GAPDH

Figure 8

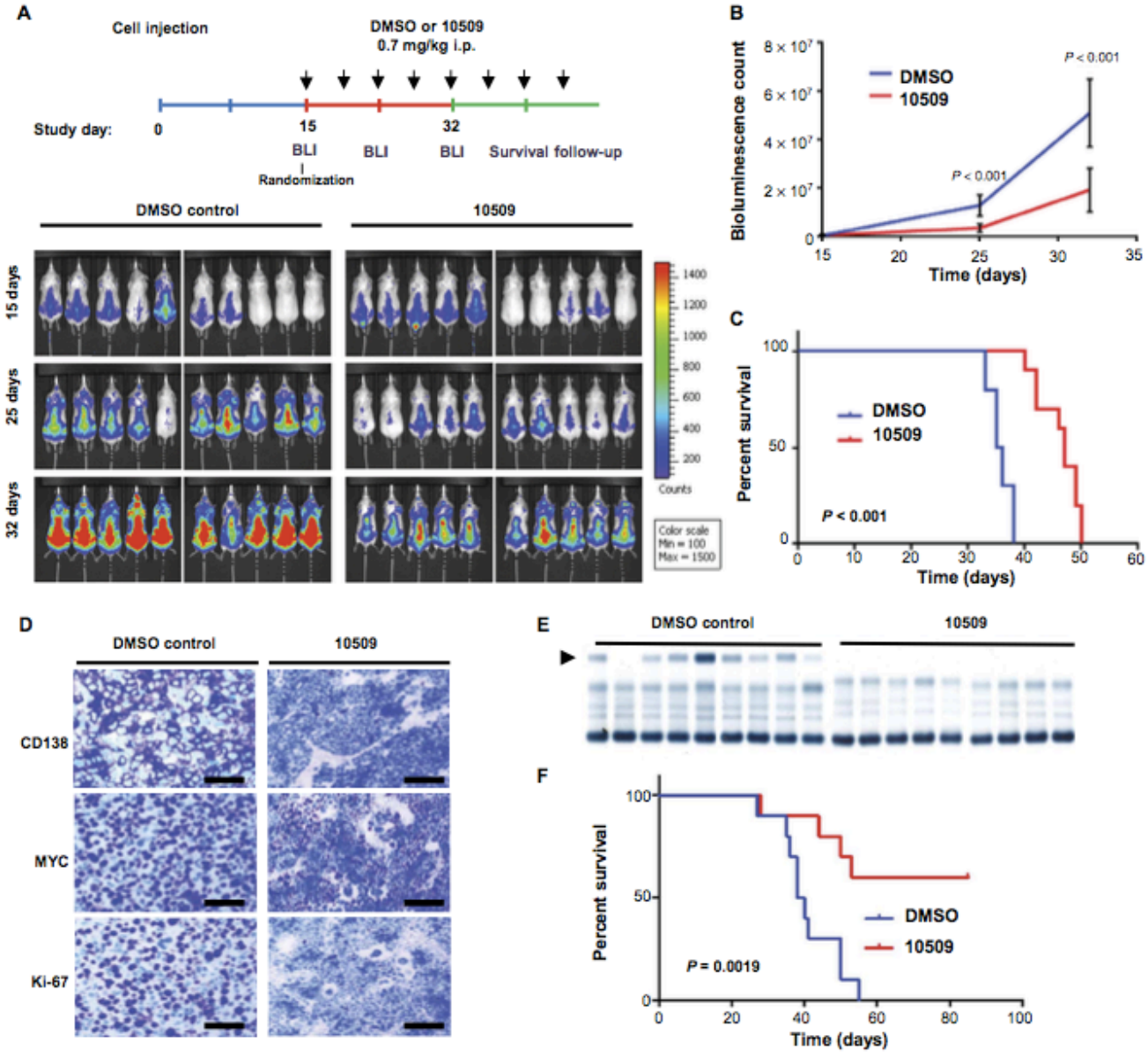
A
Cell injection
DMSO or 10509
0.7 mg/kg i.p.
Study day:
0
15
32
BLI
BLI
BLI
Survival follow-up
Randomization
DMSO control
10509
15 days
25 days
32 days
Counts
Color scale
Min = 100
Max = 1500
B
Bioluminescence count
DMSO
10509
P < 0.001
P < 0.001
Time (days)
C
Percent survival
DMSO
10509
P < 0.001
Time (days)
D
DMSO control
10509
CD138
MYC
Ki-67
E
DMSO control
10509
F
Percent survival
DMSO
10509
P = 0.0019
Time (days)

Supplemental Materials

Fig. S1. Correlation between *MYC* expression and translation activation in different hematologic malignancies.

Fig. S2. Three potent rocaglate derivatives identified by an initial drug screen of a small-molecule compound library.

Fig. S3. Association of HSF1 activation in MM with poor outcomes.

Fig. S4. RNA-seq and TMT proteomic data validations in several MM cell lines.

Fig. S5. Assessment of CMLD010509 toxicity on PBMCs.

Fig. S6. Evaluation of CMLD010509 toxicity *in vivo*.

Table S1: RNA-sequencing of MM cells treated by CMLD010509 (provided as an Excel file).

Table S2. TMT proteomic analysis of NCI-H929 treated by CMLD010509 (provided as an Excel file).

Supplemental Figure 1

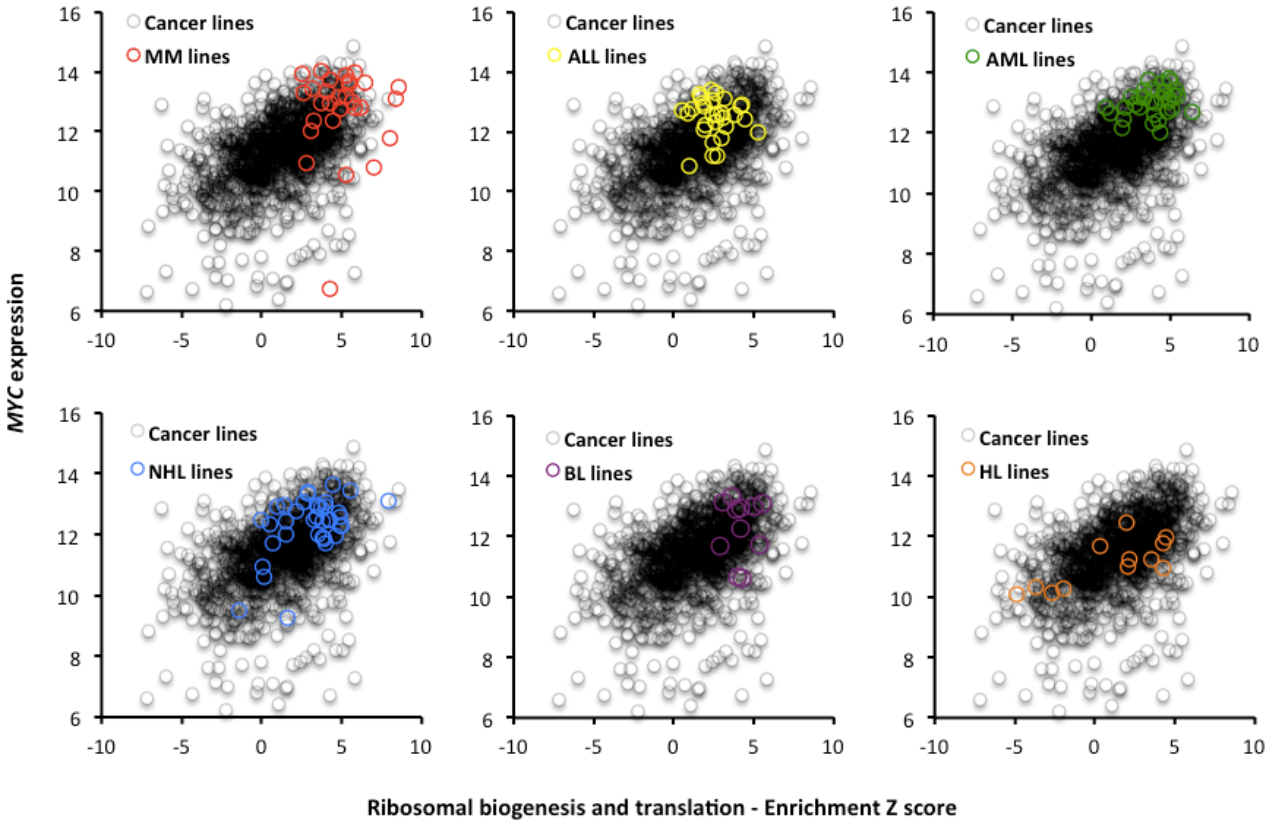

Fig. S1. Correlation between *MYC* expression and translation activation in different hematologic malignancies. Correlation analysis of *MYC* expression on the Y axis and the Z-score enrichment across over 1000 cell lines from the Cancer Cell Line Encyclopedia (CCLE) database. A Z-score was generated for each cell line by combining 2 KEGG canonical pathway gene sets: ribosomal biogenesis and translation.

Supplemental Figure 2

A

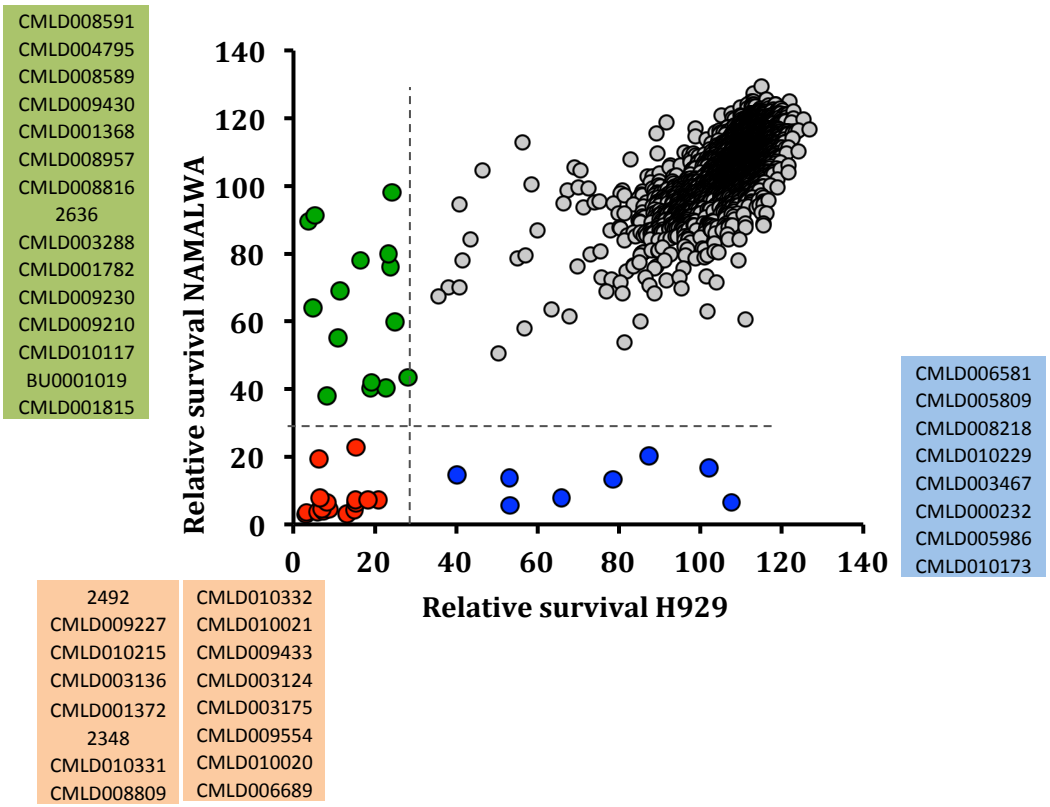

B

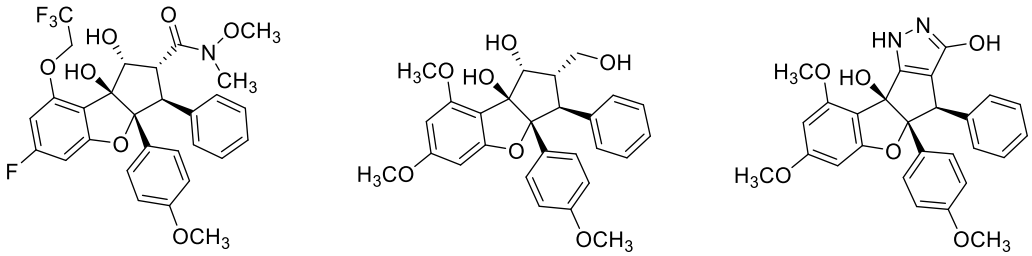

C

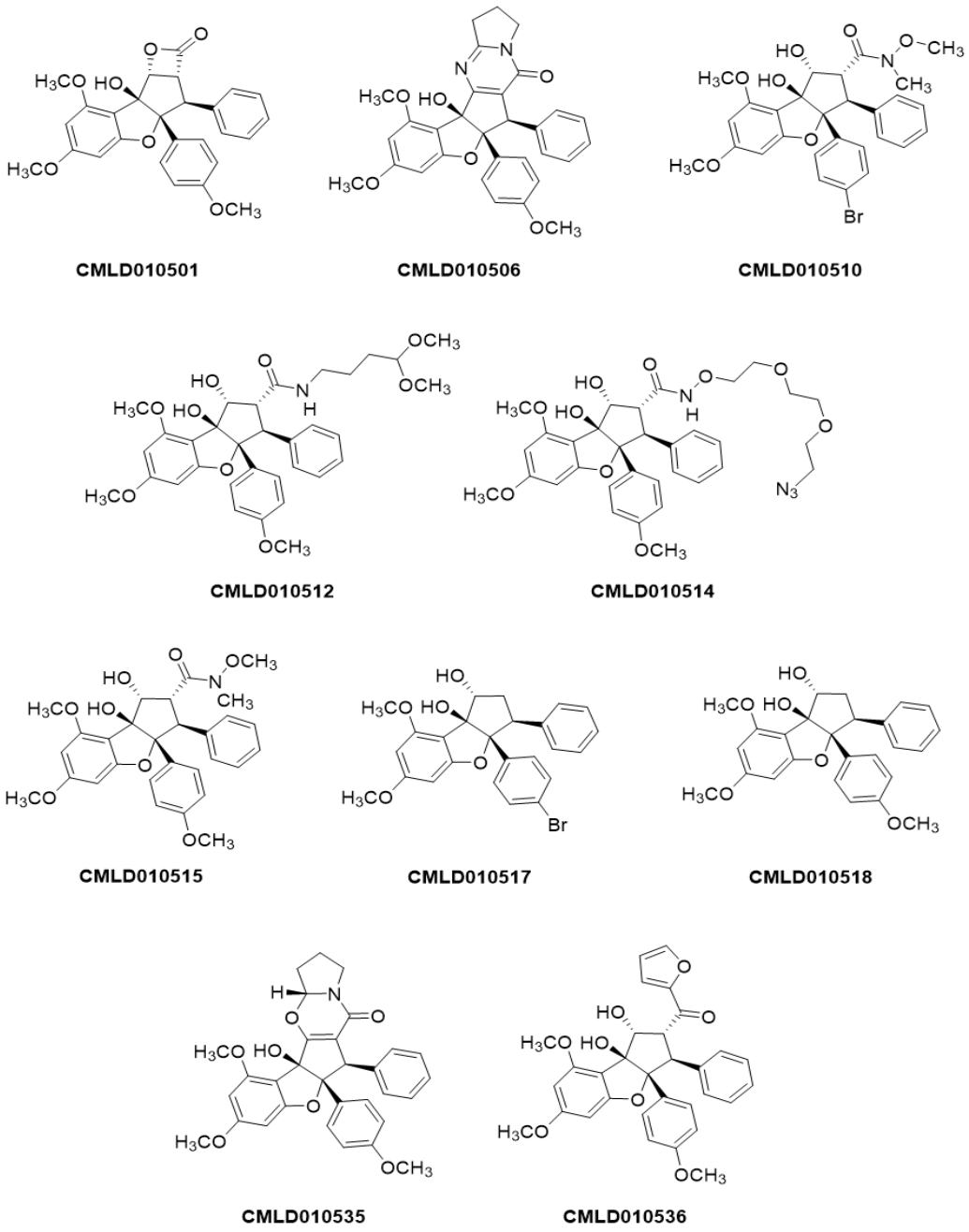

Fig. S2. Initial drug screen of a small-molecule compound library identifies 3 potent rocaglate derivatives. (A) Comparison of the relative survival of lymphoid cell lines, NAMALWA *vs*. NCI-H929 after 72 h treatment with a library of 3000 small compounds. Compounds found effective in decreasing survival of NAMALWA and NCI-H929 cells are depicted respectively as green and blue dots along with the names of compounds shown in a box, while compounds effective in both cell lines are shown as red dots. In total, 45 compounds were found to potently inhibit proliferation in at least one of the cell lines. **(B)** Chemical structures of the 3 rocaglates identified by the validation screen. **(C)** Chemical structures of the 10 top rocaglates from the validation screen in addition to CMLD010509.

Supplemental Figure 3

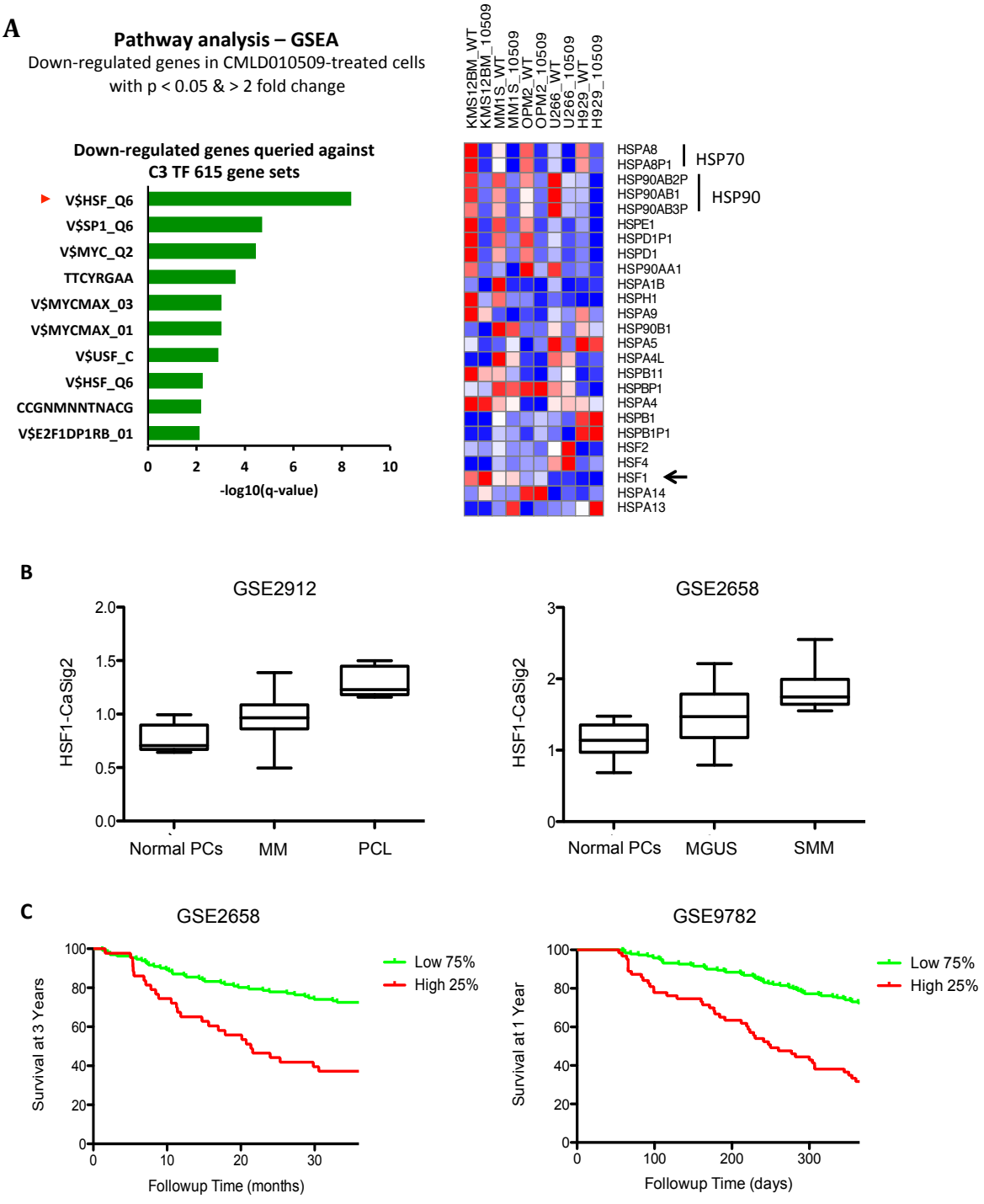

Fig. S3. HSF1 activation in MM is associated with a poor outcome. (A) Pathway analysis (RNA-seq) of genes downregulated in CMLD010509-treated cells identified by interrogating the MSigDB C3 Transcription Factor Dataset. Genes involved in heat shock

response are represented in a heat map. Red arrow indicates HSF1 pathway and black arrow indicates *HSF1* gene. **(B)** HSF1 activation signature (HSF1-CaSig2)[18] was evaluated in 2 publicly available datasets of MM patients (GSE2912[19] and GSE2658[20]). This signature represents the mean expression of 323 HSF1-bound genes identified through ChIP-seq of multiple human breast cancer cell lines. **(C)** High HSF1 activation signature is strongly correlated with poor clinical outcome in MM (GSE2658[20] and GSE9782[21]). PCs: plasma cells; MM: Multiple Myeloma; PCL: plasma cell leukemia; SMM: smoldering multiple myeloma.

Supplemental Figure 4

A. NAMALWA

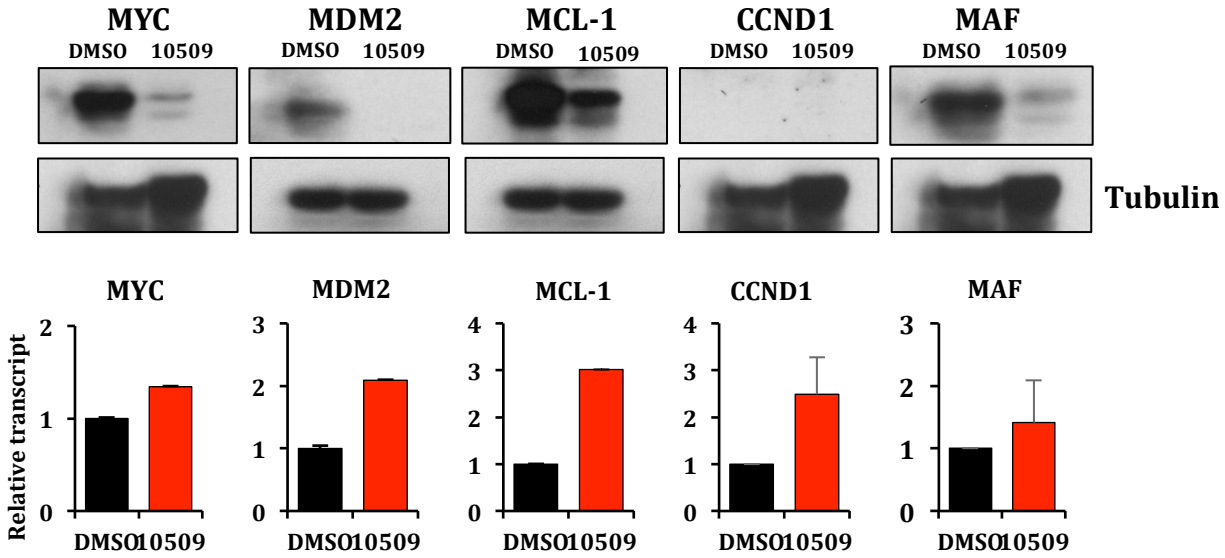

B. KMS18

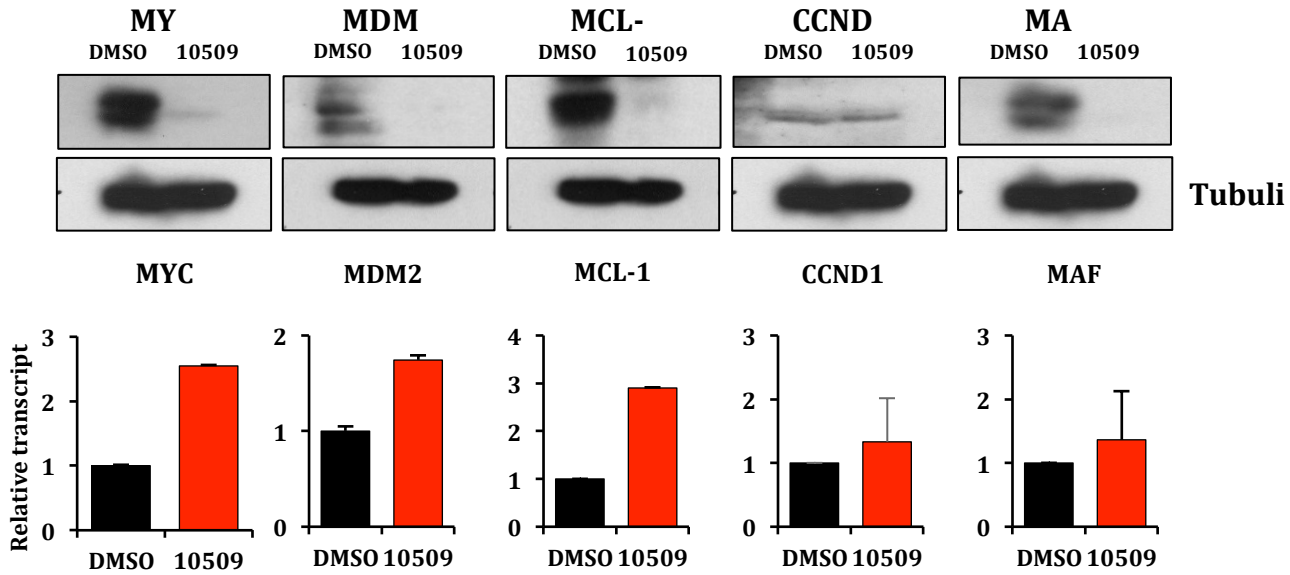

C. U266

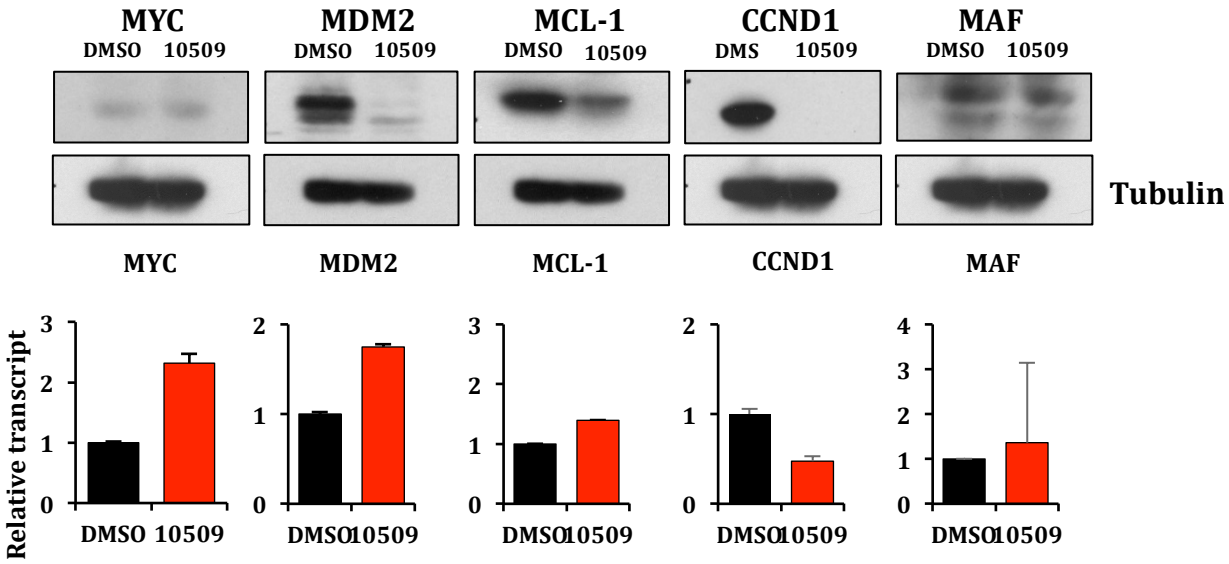
MYC
DMSO 10509
MDM2
DMSO 10509
MCL-1
DMSO 10509
CCND1
DMS 10509
MAF
DMSO 10509
Tubulin
MYC
MDM2
MCL-1
CCND1
MAF
Relative transcript
DMSO 10509
DMSO10509
DMSO10509
DMSO10509
DMSO10509

D. OPM2

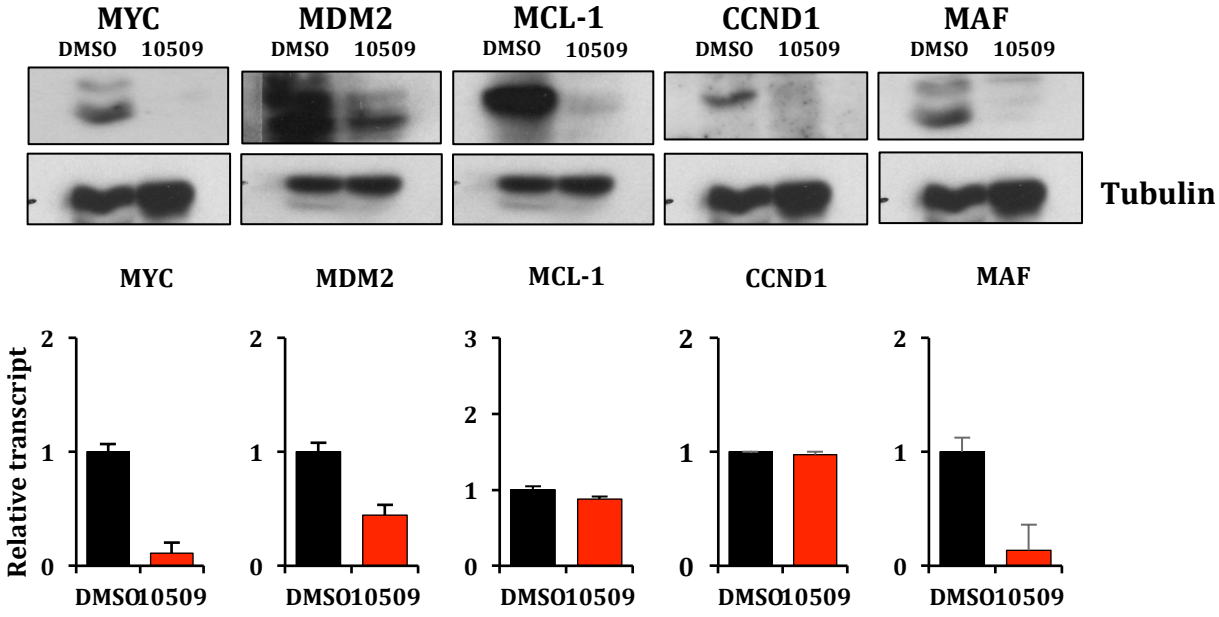
MYC
DMSO 10509
MDM2
DMSO 10509
MCL-1
DMSO 10509
CCND1
DMSO 10509
MAF
DMSO 10509
Tubulin
MYC
MDM2
MCL-1
CCND1
MAF
Relative transcript
DMSO10509
DMSO10509
DMSO10509
DMSO10509
DMSO10509

E. MM1R

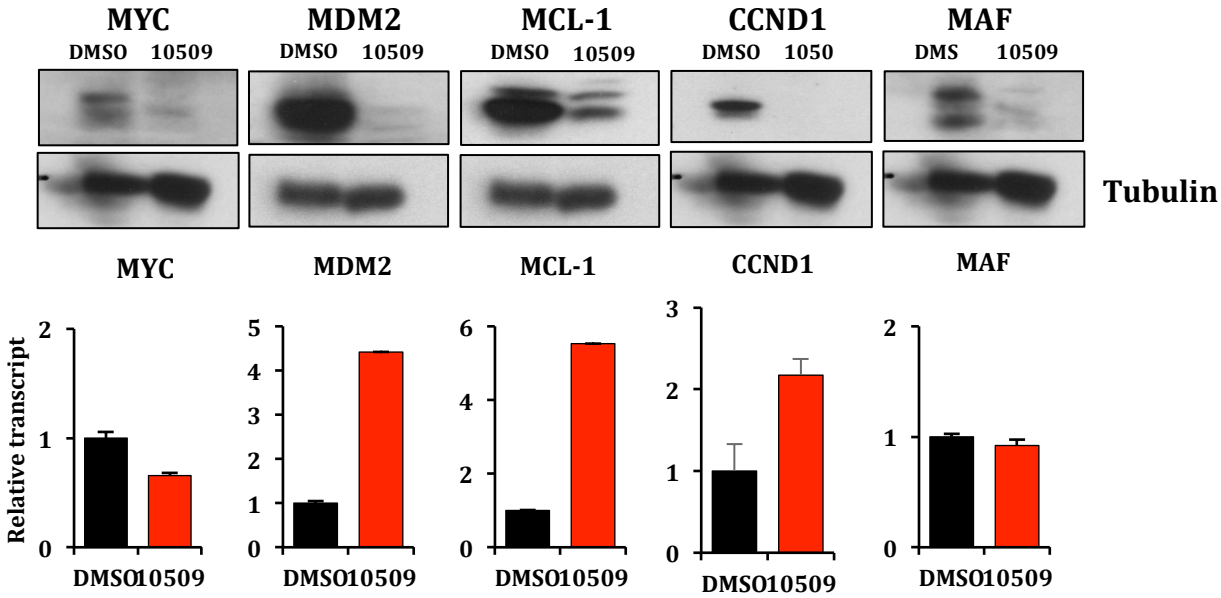
MYC
DMSO 10509
MDM2
DMSO 10509
MCL-1
DMSO 10509
CCND1
DMSO 1050
MAF
DMS 10509
Tubulin
MYC
MDM2
MCL-1
CCND1
MAF
Relative transcript
DMSO10509
DMSO10509
DMSO10509
DMSO10509
DMSO10509

F. KMM-1

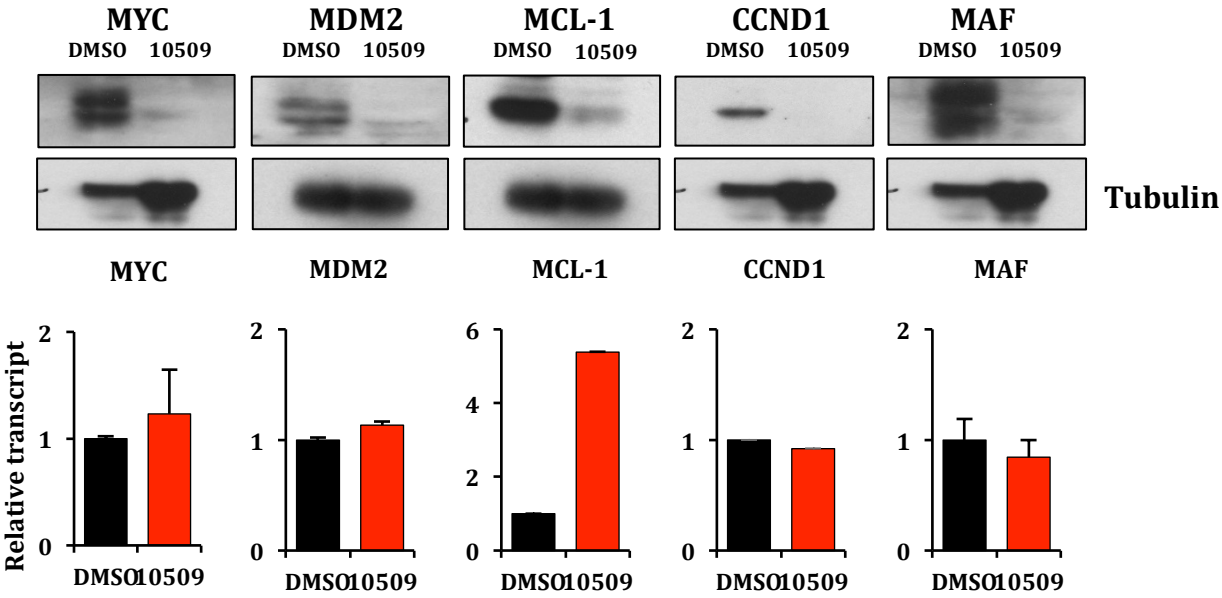
MYC
DMSO 10509
MDM2
DMSO 10509
MCL-1
DMSO 10509
CCND1
DMSO 10509
MAF
DMSO 10509
Tubulin
MYC
MDM2
MCL-1
CCND1
MAF
Relative transcript
DMSO10509
DMSO10509
DMSO10509
DMSO10509
DMSO10509

G. MM1S

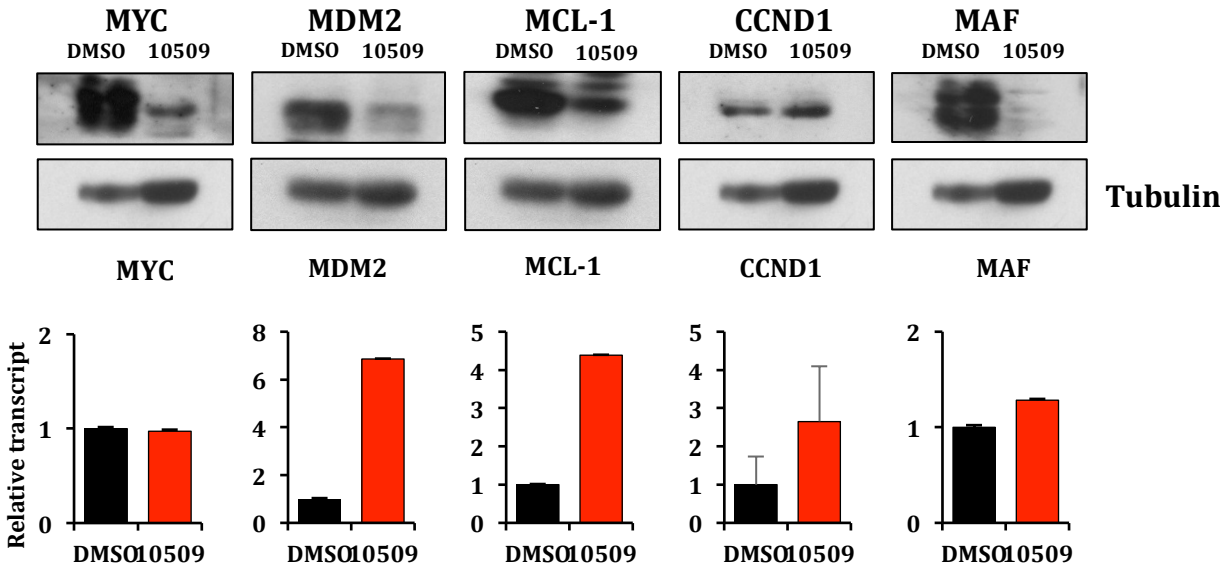

H.

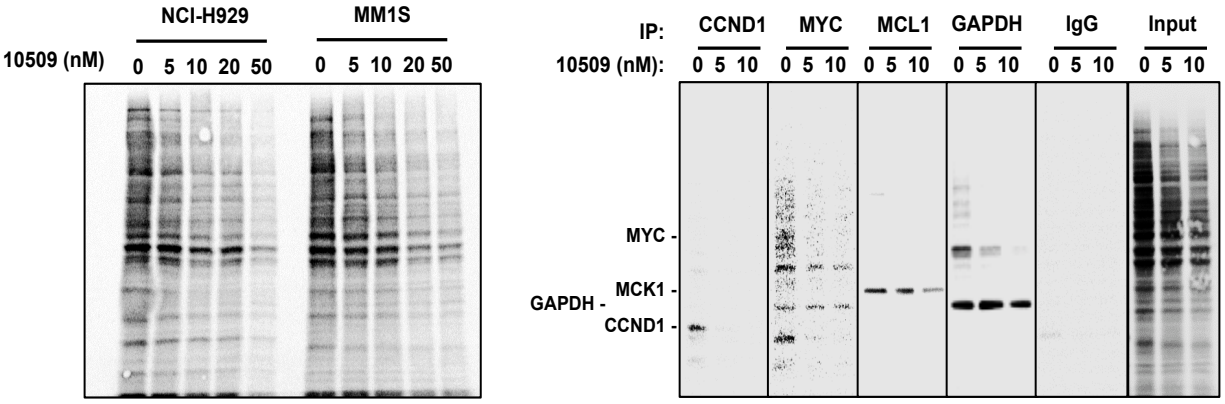

Fig. S4. RNA-seq and TMT proteomic data validations in several MM cell lines. Immunoblots (upper panels) and qRT-PCR analysis (lower panels) for MYC, MDM2, MCL-1, CCDN1, and MAF in 6 MM cell lines and NAMALWA after 3 hours of treatment with CMLD010509 or control vehicle. (**A**) NAMALWA, (**B**) KMS18, (**C**) U266, (**D**) OPM2, (**E**) MM1R, (**F**) KMM-1, and (**G**) MM1S. Error bars indicate mean +/- SD of triplicate experiments. **(H)** S35 pulse-chase labeling of MM1S and NCI-H929 cells treated with different concentrations of CMLD010509. Left panel: bulk of S35 labeled MM1S and NCI-H929 cells; right panel: immunoprecipitated CCND1, MYC, MCL1, GAPDH and IgG as a control.

Supplemental Figure 5

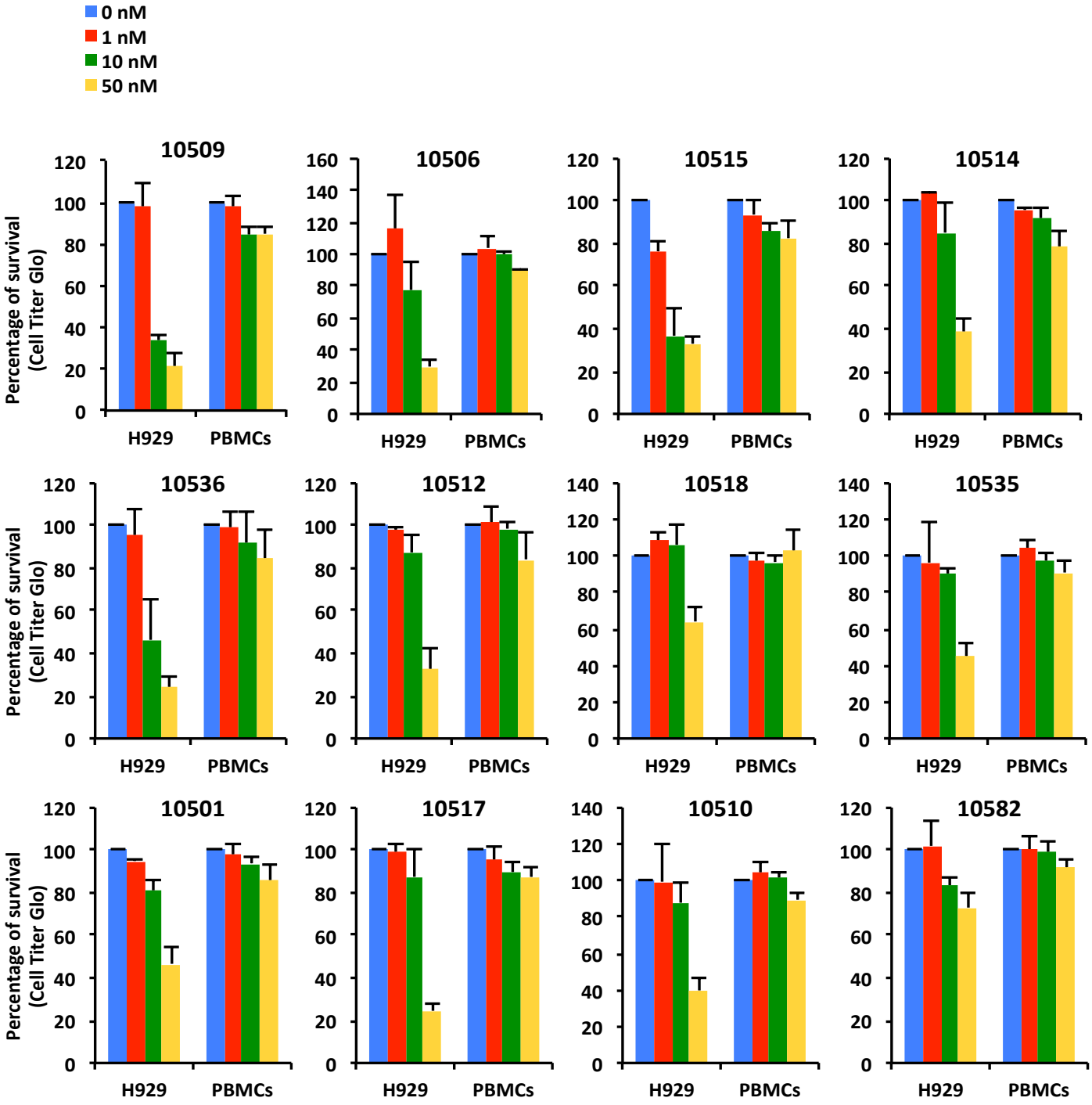

Fig. S5. Assessment of CMLD010509 toxicity on PBMCs. MM cell line, NCI-H929, and normal donor PBMCs were treated with 0, 1, 10, or 50 nM of 12 rocaglate derivatives for 72 hours. Percentage of survival was determined by Cell Titer Glo and normalized to untreated group for each different cell type. Error bars indicate mean+/-SD of triplicates.

Supplemental Figure 6

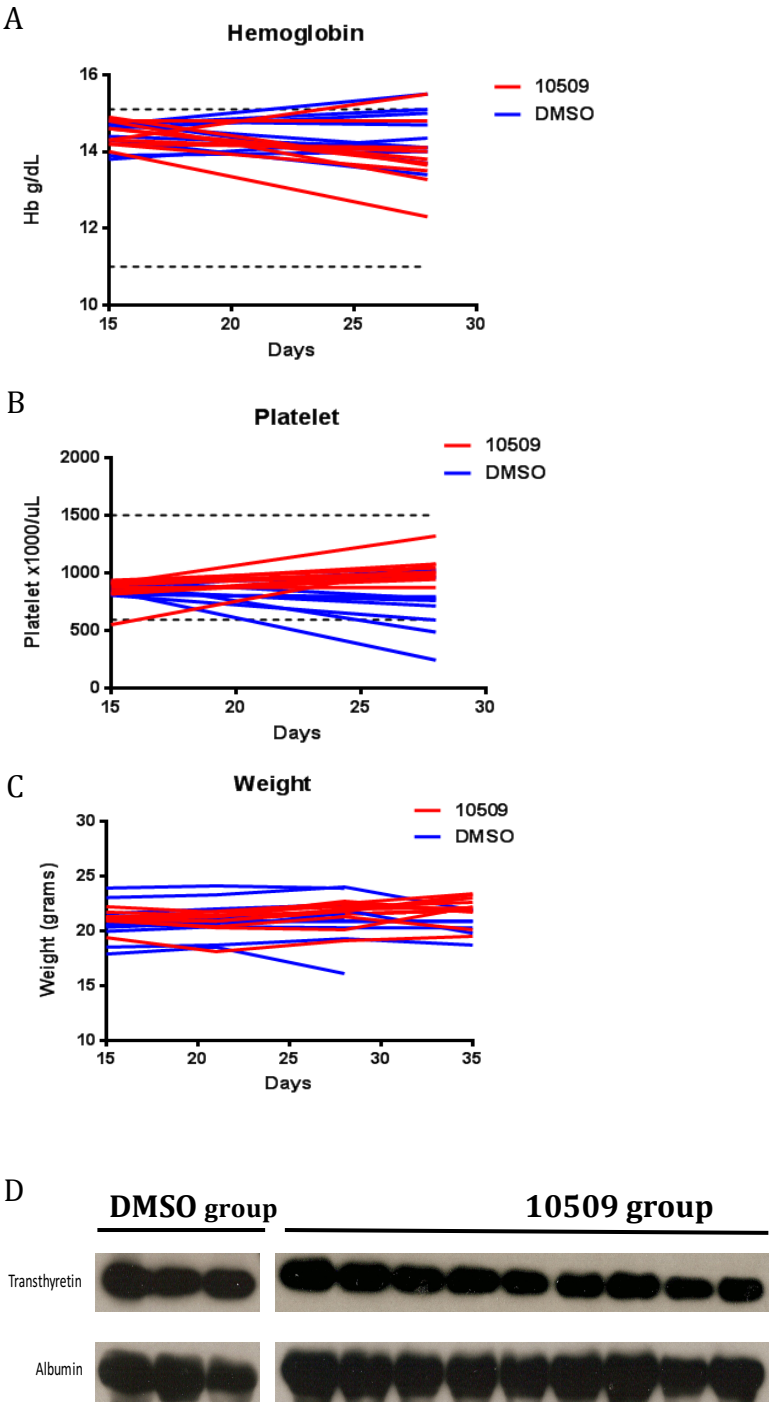

Fig. S6. Evaluation of CMLD010509 toxicity in vivo. Peripheral blood was collected from SCID mice receiving DMSO (n=10) or 10509 (n=10) every week and processed for blood (**A**) hemoglobin concentration and (**B**) platelet count. (**C**) Mice in both groups were weighed every week. (**D**) Immunoblotting for transthyretin and albumin. Serum samples were collected from the peripheral blood of BL-6 mice receiving DMSO (n=3) or 10509 (n=9) at 6 weeks after tumor cell injection. Transthyretin and albumin expression was similar in the two groups, as evaluated by western blot analysis for transthyretin and albumin.

DISCUSSION

Nos travaux explorent la possibilité de cibler MYC par interaction avec ses mécanismes de régulation et ses fonctions au sein des cellules myélomateuses. Dans notre premier travail, nous décrivons le rôle de l'axe LIN28B/let-7 et identifions let-7 comme une nouvelle approche thérapeutique potentielle pour cibler MYC. L'expression élevée de LIN28B dans MM est associée à la fois à un mauvais pronostic et à une surexpression MYC. LIN28B réprime l'expression de let-7 dans les cellules de MM, entraînant une dérégulation des ARNm de MYC et une prolifération cellulaire *in vitro* et *in vivo*. L'analyse des voies de signalisation dans les cellules KO pour LIN28B révèle l'importance de MYC et E2F dans l'axe LIN28B/let-7. En outre, l'altération de la prolifération tumorale *in vivo* par l'administration d'un LNA-GapmeR Let-7b fournit une preuve de principe d'une nouvelle option thérapeutique pour cibler MYC dans le MM.

Les miARN let-7 ont un rôle de suppresseurs de tumeurs dans plusieurs cancers [89]. La perte d'allèles [114-116] ou des facteurs épigénétiques [117] entrainant une sous-expression de let-7 ont été rapportés dans plusieurs cancers. Les membres de la famille let-7 sont situés dans des régions fréquemment délétées dans le MM, telles que let-7g en 3p21, let-7i en 12q14 ou let-7a-2 en 11q24. Ces aberrations du nombre de copies peuvent participer à la dérégulation de l'axe LIN28B/let-7 dans le MM. Dans ce travail, nous avons décrit un mécanisme de régulation des miARN let-7 impliquant LIN28B. Bien que l'oncogène LIN28B ait été décrit dans les cancers hépato-cellulaires comme pouvant agir de manière dépendante et indépendante de let-7 [104], nos résultats suggèrent la prédominance d'un mécanisme dépendant de let-7 dans le MM.

LIN28B est situé au niveau de 6q21, qui est amplifié dans certains cas de neuroblastomes, ce qui entraîne une surexpression LIN28B [105]. Dans MM, il n'a pas été retrouvé d'amplification du locus 6q21 [30]. L'expression accrue de LIN28B pourrait donc résulter de mécanismes épigénétiques, tels que les modifications de la méthylation et de l'acétylation des histones ou de mécanismes de régulation en amont de LIN28B. Le miARN miR-125b inhibe l'expression de LIN28B dans les cellules souches embryonnaires ainsi que dans certains cas de cancers [105,118,119]. Il est à noter que miR-125b est situé en 11q23, souvent siège de délétions dans le MM. Par ailleurs, les miARN let-7 régulent aussi l'expression LIN28B, réalisant une boucle de rétroaction [120]. Il a aussi été récemment montré que l'inactivation de DIS3 augmente l'expression LIN28B dans le MM [121]. DIS3 est une endoribonucléase impliquée dans le renouvellement et la dégradation des ARNm dans le cytoplasme. DIS3 est aussi l'un des gènes les plus fréquemment mutés dans le MM [122,123].

Nous avons ensuite cherché à établir le rôle pronostique des miARN présents au sein des exosomes circulants, dans le MM. Contrairement aux approches génomiques conventionnelles qui requièrent une biopsie de moelle osseuse, des miARN des exosomes peuvent être obtenues par une simple prise de sang, en faisant des biomarqueurs non-invasifs. Nos résultats montrent que l'expression de deux miARN, let-7b et miR-18a, au sein des exosomes circulants, peut prédire la SSP et la SG de patients atteints de MM, et améliore la valeur pronostique de l'ISS et du statut cytogénétique. Les exosomes sont activement sécrétés dans le sang périphérique par différents types de cellules, y compris les cellules cancéreuses. Ils favorisent aussi la prolifération tumorale dans certains cancers par transfert de miARN entre les cellules

tumorales et les cellules stromales, parfois à distance [133]. Des études récentes ont aussi montré que les exosomes possèdent la machinerie de biogenèse des miARN (DICER et DROSHA) et ont la capacité de maturer les miARN précurseurs en miARN matures, indépendamment de leurs cellules tumorales d'origine [129]. Cela indique que les miARN exosomaux peuvent représenter des biomarqueurs moléculaires spécifiques, indépendamment des cellules tumorales d'origines et des miARN circulants libres. Les exosomes périphériques ont démontré un intérêt diagnostique et pronostique dans plusieurs types de cancers. En effet, les patients atteints de mélanome de stade IV ont une concentration plus élevée d'exosomes circulants [127]. Plus spécifiquement, les marqueurs de mélanome, tels que TYRP2, VLA-4 et HSP70, sont significativement plus exprimés dans les exosomes circulants de patients atteints de mélanomes de stade IV. Une autre étude a permis d'identifier la présence de glypican-1 sur les exosomes circulants chez les patients atteints de cancer du pancréas, ce qui pourrait servir de marqueur de diagnostic et de dépistage pour cette maladie [148].

Notre étude, ainsi que l'ensemble de ces travaux, démontrent la faisabilité et l'intérêt de l'utilisation des exosomes circulants comme biomarqeurs dans le cancer.

Nous avons ensuite étudié les possibilités thérapeutiques pour cibler MYC dans le MM, à travers son rôle dans l'activation de la traduction. Le programme de traduction oncogénique des cellules cancéreuses est soutenu par une activation de la biogenèse du ribosome et de la machinerie d'initiation de la traduction [158-160]. Dans ce travail, nous rapportons la corrélation entre le niveau d'expression de MYC et l'activation de la traduction dans le MM. Nous avons identifié le dérivé de rocaglate CMLD010509

comme un inhibiteur spécifique du programme de traduction oncogénique dans le MM, comportant les oncoprotéines MYC, MDM2, CCND1, MAF et MCL1.

Bien que la biogénèse du ribosome et de l'initiation de la traduction soient perçus comme des processus passifs, plusieurs études récentes ont révélé qu'elles sont activement régulées pour soutenir des programmes de traduction spécifiques au sein des cellules tumorales [158,159]. Par une étude de protéomique, nous montrons que l'inhibition de l'initiation de la traduction dans MM affecte un sous-groupe spécifique de protéines. Ce processus sélectif peut s'expliquer notamment par la présence de structures secondaires complexes au niveau du 5'UTR, influençant la traduction des ARNm. Les transcrits ayant des structures secondaires 5'UTR complexes sont plus sensibles à l'inhibition de l'initiation de la traduction que des ARNm physiologiquement essentiels ayant des 5'UTR simples. Il est intéressant de noter que MYC, MDM2 et CCND1 possèdent en effet des structures 5'UTR complexes [160].

Les rocaglates sont des inhibiteurs de traduction [164,167] qui interagissent avec le facteur d'initiation de la traduction eucaryote 4A (eIF4A) - une sous-unité protéique du complexe d'initiation de la traduction [164,181]. Ils augmentent l'affinité entre eIF4A et l'ARNm empêchant ainsi les sous-unités ribosomiques d'initier la traduction [182].

Le blocage de la dégradation des protéines par utilisation d'inhibiteurs du protéasome est devenu central dans l'arsenal thérapeutique du MM, suggérant l'importance de l'homéostasie des protéines dans cette pathologie. Ici, nous suggérons qu'à l'inverse, l'inhibition d'un programme oncogénique de traduction permet de bloquer la prolifération des cellules de MM. Ce travail montre l'efficacité de CMLD010509 dans plusieurs modèles murins, ce qui supporte son développement préclinique à l'avenir.

REFERENCES

1. Palumbo A, Anderson K. Multiple myeloma. The New England journal of medicine 2011;364:1046-60.

2. International Myeloma Foundation. Multiple myeloma. Cancer of the bone marrow. 2008/2009 ed2008/2009.

3. Ludwig H, Bolejack V, Crowley J, et al. Survival and years of life lost in different age cohorts of patients with multiple myeloma. J Clin Oncol 2010;28:1599-605.

4. Greipp PR, San Miguel J, Durie BG, et al. International staging system for multiple myeloma. Journal of clinical oncology : official journal of the American Society of Clinical Oncology 2005;23:3412-20.

5. Palumbo A, Rajkumar SV, Dimopoulos MA, et al. Prevention of thalidomide- and lenalidomide-associated thrombosis in myeloma. Leukemia 2008;22:414-23.

6. Vital A. Paraproteinemic neuropathies. Brain Pathol 2001;11:399-407.

7. Rajkumar SV, Dimopoulos MA, Palumbo A, et al. International Myeloma Working Group updated criteria for the diagnosis of multiple myeloma. Lancet Oncol 2014;15:e538-48.

8. Kyle RA, Rajkumar SV. Criteria for diagnosis, staging, risk stratification and response assessment of multiple myeloma. Leukemia 2009;23:3-9.

9. Palumbo A, Avet-Loiseau H, Oliva S, et al. Revised International Staging System for Multiple Myeloma: A Report From International Myeloma Working Group. Journal of clinical oncology : official journal of the American Society of Clinical Oncology 2015;33:2863-9.

10. Kyle RA, Durie BG, Rajkumar SV, et al. Monoclonal gammopathy of undetermined significance (MGUS) and smoldering (asymptomatic) multiple myeloma:

IMWG consensus perspectives risk factors for progression and guidelines for monitoring and management. Leukemia 2010;24:1121-7.

11. Mateos MV, Hernandez MT, Giraldo P, et al. Lenalidomide plus dexamethasone for high-risk smoldering multiple myeloma. The New England journal of medicine 2013;369:438-47.

12. Stewart AK, Richardson PG, San-Miguel JF. How I treat multiple myeloma in younger patients. Blood 2009;114:5436-43.

13. Attal M, Harousseau JL, Stoppa AM, et al. A prospective, randomized trial of autologous bone marrow transplantation and chemotherapy in multiple myeloma. Intergroupe Francais du Myelome. N Engl J Med 1996;335:91-7.

14. Moreau P, Facon T, Attal M, et al. Comparison of 200 mg/m(2) melphalan and 8 Gy total body irradiation plus 140 mg/m(2) melphalan as conditioning regimens for peripheral blood stem cell transplantation in patients with newly diagnosed multiple myeloma: final analysis of the Intergroupe Francophone du Myelome 9502 randomized trial. Blood 2002;99:731-5.

15. Ladetto M, Pagliano G, Ferrero S, et al. Major tumor shrinking and persistent molecular remissions after consolidation with bortezomib, thalidomide, and dexamethasone in patients with autografted myeloma. J Clin Oncol 2010;28:2077-84.

16. Harousseau JL, Attal M, Avet-Loiseau H. The role of complete response in multiple myeloma. Blood 2009;114:3139-46.

17. Dimopoulos MA, Richardson PG, Schlag R, et al. VMP (Bortezomib, Melphalan, and Prednisone) is active and well tolerated in newly diagnosed patients with multiple myeloma with moderately impaired renal function, and results in reversal of renal impairment: cohort analysis of the phase III VISTA study. Journal of clinical oncology : official journal of the American Society of Clinical Oncology 2009;27:6086-93.

18. Benboubker L, Dimopoulos MA, Dispenzieri A, et al. Lenalidomide and dexamethasone in transplant-ineligible patients with myeloma. The New England journal of medicine 2014;371:906-17.

19. Dimopoulos MA, Oriol A, Nahi H, et al. Daratumumab, Lenalidomide, and Dexamethasone for Multiple Myeloma. The New England journal of medicine 2016;375:1319-31.

20. Lonial S, Vij R, Harousseau JL, et al. Elotuzumab in combination with lenalidomide and low-dose dexamethasone in relapsed or refractory multiple myeloma. Journal of clinical oncology : official journal of the American Society of Clinical Oncology 2012;30:1953-9.

21. Landgren O, Kyle RA, Pfeiffer RM, et al. Monoclonal gammopathy of undetermined significance (MGUS) consistently precedes multiple myeloma: a prospective study. Blood 2009;113:5412-7.

22. Weiss BM, Abadie J, Verma P, Howard RS, Kuehl WM. A monoclonal gammopathy precedes multiple myeloma in most patients. Blood 2009;113:5418-22.

23. Kyle RA, Therneau TM, Rajkumar SV, et al. A long-term study of prognosis in monoclonal gammopathy of undetermined significance. The New England journal of medicine 2002;346:564-9.

24. Chng WJ, Huang GF, Chung TH, et al. Clinical and biological implications of MYC activation: a common difference between MGUS and newly diagnosed multiple myeloma. Leukemia 2011;25:1026-35.

25. Chesi M, Robbiani DF, Sebag M, et al. AID-dependent activation of a MYC transgene induces multiple myeloma in a conditional mouse model of post-germinal center malignancies. Cancer cell 2008;13:167-80.

26. Walker BA, Wardell CP, Murison A, et al. APOBEC family mutational signatures are associated with poor prognosis translocations in multiple myeloma. Nat Commun 2015;6:6997.

27. Avet-Loiseau H, Gerson F, Magrangeas F, et al. Rearrangements of the c-myc oncogene are present in 15% of primary human multiple myeloma tumors. Blood 2001;98:3082-6.

28. Shou Y, Martelli ML, Gabrea A, et al. Diverse karyotypic abnormalities of the c-myc locus associated with c-myc dysregulation and tumor progression in multiple myeloma. Proceedings of the National Academy of Sciences of the United States of America 2000;97:228-33.

29. Affer M, Chesi M, Chen WD, et al. Promiscuous MYC locus rearrangements hijack enhancers but mostly super-enhancers to dysregulate MYC expression in multiple myeloma. Leukemia 2014;28:1725-35.

30. Carrasco DR, Tonon G, Huang Y, et al. High-resolution genomic profiles define distinct clinico-pathogenetic subgroups of multiple myeloma patients. Cancer cell 2006;9:313-25.

31. Avet-Loiseau H, Li C, Magrangeas F, et al. Prognostic significance of copy-number alterations in multiple myeloma. Journal of clinical oncology : official journal of the American Society of Clinical Oncology 2009;27:4585-90.

32. Lopez-Corral L, Sarasquete ME, Bea S, et al. SNP-based mapping arrays reveal high genomic complexity in monoclonal gammopathies, from MGUS to myeloma status. Leukemia 2012;26:2521-9.

33. Manier S, Salem KZ, Park J, Landau DA, Getz G, Ghobrial IM. Genomic complexity of multiple myeloma and its clinical implications. Nature reviews Clinical oncology 2016.

34. Chng WJ, Gonzalez-Paz N, Price-Troska T, et al. Clinical and biological significance of RAS mutations in multiple myeloma. Leukemia 2008;22:2280-4.

35. Sears R, Leone G, DeGregori J, Nevins JR. Ras enhances Myc protein stability. Mol Cell 1999;3:169-79.

36. Sears R, Nuckolls F, Haura E, Taya Y, Tamai K, Nevins JR. Multiple Ras-dependent phosphorylation pathways regulate Myc protein stability. Genes Dev 2000;14:2501-14.

37. Mittrucker HW, Matsuyama T, Grossman A, et al. Requirement for the transcription factor LSIRF/IRF4 for mature B and T lymphocyte function. Science 1997;275:540-3.

38. Shaffer AL, Emre NC, Lamy L, et al. IRF4 addiction in multiple myeloma. Nature 2008;454:226-31.

39. Dominguez-Sola D, Ying CY, Grandori C, et al. Non-transcriptional control of DNA replication by c-Myc. Nature 2007;448:445-51.

40. Felsher DW, Bishop JM. Transient excess of MYC activity can elicit genomic instability and tumorigenesis. Proc Natl Acad Sci U S A 1999;96:3940-4.

41. Zeller KI, Zhao X, Lee CW, et al. Global mapping of c-Myc binding sites and target gene networks in human B cells. Proceedings of the National Academy of Sciences of the United States of America 2006;103:17834-9.

42. Kress TR, Sabo A, Amati B. MYC: connecting selective transcriptional control to global RNA production. Nature reviews Cancer 2015;15:593-607.

43. Lin CY, Loven J, Rahl PB, et al. Transcriptional amplification in tumor cells with elevated c-Myc. Cell 2012;151:56-67.

44. Nie Z, Hu G, Wei G, et al. c-Myc is a universal amplifier of expressed genes in lymphocytes and embryonic stem cells. Cell 2012;151:68-79.

45. Sabo A, Kress TR, Pelizzola M, et al. Selective transcriptional regulation by Myc in cellular growth control and lymphomagenesis. Nature 2014;511:488-92.

46. Christofk HR, Vander Heiden MG, Harris MH, et al. The M2 splice isoform of pyruvate kinase is important for cancer metabolism and tumour growth. Nature 2008;452:230-3.

47. David CJ, Chen M, Assanah M, Canoll P, Manley JL. HnRNP proteins controlled by c-Myc deregulate pyruvate kinase mRNA splicing in cancer. Nature 2010;463:364-8.

48. Koh CM, Bezzi M, Low DH, et al. MYC regulates the core pre-mRNA splicing machinery as an essential step in lymphomagenesis. Nature 2015;523:96-100.

49. Arabi A, Wu S, Ridderstrale K, et al. c-Myc associates with ribosomal DNA and activates RNA polymerase I transcription. Nat Cell Biol 2005;7:303-10.

50. Grandori C, Gomez-Roman N, Felton-Edkins ZA, et al. c-Myc binds to human ribosomal DNA and stimulates transcription of rRNA genes by RNA polymerase I. Nat Cell Biol 2005;7:311-8.

51. Pourdehnad M, Truitt ML, Siddiqi IN, Ducker GS, Shokat KM, Ruggero D. Myc and mTOR converge on a common node in protein synthesis control that confers synthetic lethality in Myc-driven cancers. Proc Natl Acad Sci U S A 2013;110:11988-93.

52. Gingras AC, Raught B, Gygi SP, et al. Hierarchical phosphorylation of the translation inhibitor 4E-BP1. Genes Dev 2001;15:2852-64.

53. de Alboran IM, O'Hagan RC, Gartner F, et al. Analysis of C-MYC function in normal cells via conditional gene-targeted mutation. Immunity 2001;14:45-55.

54. Prathapam T, Tegen S, Oskarsson T, Trumpp A, Martin GS. Activated Src abrogates the Myc requirement for the G0/G1 transition but not for the G1/S transition. Proc Natl Acad Sci U S A 2006;103:2695-700.

55. Mateyak MK, Obaya AJ, Sedivy JM. c-Myc regulates cyclin D-Cdk4 and -Cdk6 activity but affects cell cycle progression at multiple independent points. Mol Cell Biol 1999;19:4672-83.

56. Santoni-Rugiu E, Falck J, Mailand N, Bartek J, Lukas J. Involvement of Myc activity in a G(1)/S-promoting mechanism parallel to the pRb/E2F pathway. Mol Cell Biol 2000;20:3497-509.

57. Leone G, Sears R, Huang E, et al. Myc requires distinct E2F activities to induce S phase and apoptosis. Mol Cell 2001;8:105-13.

58. Vlach J, Hennecke S, Alevizopoulos K, Conti D, Amati B. Growth arrest by the cyclin-dependent kinase inhibitor p27Kip1 is abrogated by c-Myc. EMBO J 1996;15:6595-604.

59. Martins CP, Berns A. Loss of p27(Kip1) but not p21(Cip1) decreases survival and synergizes with MYC in murine lymphomagenesis. EMBO J 2002;21:3739-48.

60. Carrano AC, Eytan E, Hershko A, Pagano M. SKP2 is required for ubiquitin-mediated degradation of the CDK inhibitor p27. Nat Cell Biol 1999;1:193-9.

61. O'Hagan RC, Ohh M, David G, et al. Myc-enhanced expression of Cul1 promotes ubiquitin-dependent proteolysis and cell cycle progression. Genes Dev 2000;14:2185-91.

62. Gao P, Tchernyshyov I, Chang TC, et al. c-Myc suppression of miR-23a/b enhances mitochondrial glutaminase expression and glutamine metabolism. Nature 2009;458:762-5.

63. Wise DR, DeBerardinis RJ, Mancuso A, et al. Myc regulates a transcriptional program that stimulates mitochondrial glutaminolysis and leads to glutamine addiction. Proc Natl Acad Sci U S A 2008;105:18782-7.

64. Stine ZE, Walton ZE, Altman BJ, Hsieh AL, Dang CV. MYC, Metabolism, and Cancer. Cancer Discov 2015;5:1024-39.

65. Lowe SW, Cepero E, Evan G. Intrinsic tumour suppression. Nature 2004;432:307-15.

66. Martin-Subero JI, Odero MD, Hernandez R, et al. Amplification of IGH/MYC fusion in clinically aggressive IGH/BCL2-positive germinal center B-cell lymphomas. Genes Chromosomes Cancer 2005;43:414-23.

67. Knezevich S, Ludkovski O, Salski C, et al. Concurrent translocation of BCL2 and MYC with a single immunoglobulin locus in high-grade B-cell lymphomas. Leukemia 2005;19:659-63.

68. Adams JM, Harris AW, Pinkert CA, et al. The c-myc oncogene driven by immunoglobulin enhancers induces lymphoid malignancy in transgenic mice. Nature 1985;318:533-8.

69. Strasser A, Harris AW, Bath ML, Cory S. Novel primitive lymphoid tumours induced in transgenic mice by cooperation between myc and bcl-2. Nature 1990;348:331-3.

70. Letai A, Sorcinelli MD, Beard C, Korsmeyer SJ. Antiapoptotic BCL-2 is required for maintenance of a model leukemia. Cancer Cell 2004;6:241-9.

71. Casey SC, Tong L, Li Y, et al. MYC regulates the antitumor immune response through CD47 and PD-L1. Science 2016;352:227-31.

72. Holien T, Vatsveen TK, Hella H, Waage A, Sundan A. Addiction to c-MYC in multiple myeloma. Blood 2012;120:2450-3.

73. Snead NM, Wu X, Li A, et al. Molecular basis for improved gene silencing by Dicer substrate interfering RNA compared with other siRNA variants. Nucleic Acids Res 2013;41:6209-21.

74. Hart JR, Roberts TC, Weinberg MS, Morris KV, Vogt PK. MYC regulates the non-coding transcriptome. Oncotarget 2014;5:12543-54.

75. Stellas D, Szabolcs M, Koul S, et al. Therapeutic effects of an anti-Myc drug on mouse pancreatic cancer. J Natl Cancer Inst 2014;106.

76. Delmore JE, Issa GC, Lemieux ME, et al. BET bromodomain inhibition as a therapeutic strategy to target c-Myc. Cell 2011;146:904-17.

77. Amorim S, Stathis A, Gleeson M, et al. Bromodomain inhibitor OTX015 in patients with lymphoma or multiple myeloma: a dose-escalation, open-label, pharmacokinetic, phase 1 study. Lancet Haematol 2016;3:e196-204.

78. Albrecht BK, Gehling VS, Hewitt MC, et al. Identification of a Benzoisoxazoloazepine Inhibitor (CPI-0610) of the Bromodomain and Extra-Terminal (BET) Family as a Candidate for Human Clinical Trials. J Med Chem 2016;59:1330-9.

79. Siu KT, Ramachandran J, Yee AJ, et al. Preclinical activity of CPI-0610, a novel small-molecule bromodomain and extra-terminal protein inhibitor in the therapy of multiple myeloma. Leukemia 2017.

80. McCarthy PL, Owzar K, Hofmeister CC, et al. Lenalidomide after stem-cell transplantation for multiple myeloma. N Engl J Med 2012;366:1770-81.

81. Palumbo A, Hajek R, Delforge M, et al. Continuous lenalidomide treatment for newly diagnosed multiple myeloma. N Engl J Med 2012;366:1759-69.

82. Kronke J, Udeshi ND, Narla A, et al. Lenalidomide causes selective degradation of IKZF1 and IKZF3 in multiple myeloma cells. Science 2014;343:301-5.

83. Lu G, Middleton RE, Sun H, et al. The myeloma drug lenalidomide promotes the cereblon-dependent destruction of Ikaros proteins. Science 2014;343:305-9.

84. Hsu TY, Simon LM, Neill NJ, et al. The spliceosome is a therapeutic vulnerability in MYC-driven cancer. Nature 2015;525:384-8.

85. Howlader N, Noone AM, Yu M, Cronin KA. Use of imputed population-based cancer registry data as a method of accounting for missing information: application to estrogen receptor status for breast cancer. Am J Epidemiol 2012;176:347-56.

86. Morgan GJ, Walker BA, Davies FE. The genetic architecture of multiple myeloma. Nature reviews Cancer 2012;12:335-48.

87. Mertz JA, Conery AR, Bryant BM, et al. Targeting MYC dependence in cancer by inhibiting BET bromodomains. Proceedings of the National Academy of Sciences of the United States of America 2011;108:16669-74.

88. Reinhart BJ, Slack FJ, Basson M, et al. The 21-nucleotide let-7 RNA regulates developmental timing in Caenorhabditis elegans. Nature 2000;403:901-6.

89. Roush S, Slack FJ. The let-7 family of microRNAs. Trends Cell Biol 2008;18:505-16.

90. Lu J, Getz G, Miska EA, et al. MicroRNA expression profiles classify human cancers. Nature 2005;435:834-8.

91. Sampson VB, Rong NH, Han J, et al. MicroRNA let-7a down-regulates MYC and reverts MYC-induced growth in Burkitt lymphoma cells. Cancer Res 2007;67:9762-70.

92. Johnson SM, Grosshans H, Shingara J, et al. RAS is regulated by the let-7 microRNA family. Cell 2005;120:635-47.

93. Takamizawa J, Konishi H, Yanagisawa K, et al. Reduced expression of the let-7 microRNAs in human lung cancers in association with shortened postoperative survival. Cancer Res 2004;64:3753-6.

94. Shell S, Park SM, Radjabi AR, et al. Let-7 expression defines two differentiation stages of cancer. Proceedings of the National Academy of Sciences of the United States of America 2007;104:11400-5.

95. Emmrich S, Rasche M, Schoning J, et al. miR-99a/100~125b tricistrons regulate hematopoietic stem and progenitor cell homeostasis by shifting the balance between TGFbeta and Wnt signaling. Genes Dev 2014;28:858-74.

96. Gerrits A, Walasek MA, Olthof S, et al. Genetic screen identifies microRNA cluster 99b/let-7e/125a as a regulator of primitive hematopoietic cells. Blood 2012;119:377-87.

97. Schulman BR, Esquela-Kerscher A, Slack FJ. Reciprocal expression of lin-41 and the microRNAs let-7 and mir-125 during mouse embryogenesis. Dev Dyn 2005;234:1046-54.

98. Wulczyn FG, Smirnova L, Rybak A, et al. Post-transcriptional regulation of the let-7 microRNA during neural cell specification. FASEB J 2007;21:415-26.

99. Viswanathan SR, Daley GQ, Gregory RI. Selective blockade of microRNA processing by Lin28. Science 2008;320:97-100.

100. Viswanathan SR, Powers JT, Einhorn W, et al. Lin28 promotes transformation and is associated with advanced human malignancies. Nature genetics 2009;41:843-8.

101. Feng C, Neumeister V, Ma W, et al. Lin28 regulates HER2 and promotes malignancy through multiple mechanisms. Cell cycle 2012;11:2486-94.

102. King CE, Cuatrecasas M, Castells A, Sepulveda AR, Lee JS, Rustgi AK. LIN28B promotes colon cancer progression and metastasis. Cancer Res 2011;71:4260-8.

103. Guo Y, Chen Y, Ito H, et al. Identification and characterization of lin-28 homolog B (LIN28B) in human hepatocellular carcinoma. Gene 2006;384:51-61.

104. Nguyen LH, Robinton DA, Seligson MT, et al. Lin28b is sufficient to drive liver cancer and necessary for its maintenance in murine models. Cancer cell 2014;26:248-61.

105. Molenaar JJ, Domingo-Fernandez R, Ebus ME, et al. LIN28B induces neuroblastoma and enhances MYCN levels via let-7 suppression. Nature genetics 2012;44:1199-206.

106. Diskin SJ, Capasso M, Schnepp RW, et al. Common variation at 6q16 within HACE1 and LIN28B influences susceptibility to neuroblastoma. Nature genetics 2012;44:1126-30.

107. Urbach A, Yermalovich A, Zhang J, et al. Lin28 sustains early renal progenitors and induces Wilms tumor. Genes Dev 2014;28:971-82.

108. Tu HC, Schwitalla S, Qian Z, et al. LIN28 cooperates with WNT signaling to drive invasive intestinal and colorectal adenocarcinoma in mice and humans. Genes Dev 2015;29:1074-86.

109. International Myeloma Working G. Criteria for the classification of monoclonal gammopathies, multiple myeloma and related disorders: a report of the International Myeloma Working Group. Br J Haematol 2003;121:749-57.

110. Shalem O, Sanjana NE, Hartenian E, et al. Genome-scale CRISPR-Cas9 knockout screening in human cells. Science 2014;343:84-7.

111. Leleu X, Jia X, Runnels J, et al. The Akt pathway regulates survival and homing in Waldenstrom macroglobulinemia. Blood 2007;110:4417-26.

112. Tomayko MM, Reynolds CP. Determination of subcutaneous tumor size in athymic (nude) mice. Cancer chemotherapy and pharmacology 1989;24:148-54.

113. Shyh-Chang N, Daley GQ. Lin28: primal regulator of growth and metabolism in stem cells. Cell Stem Cell 2013;12:395-406.

114. Zhang L, Volinia S, Bonome T, et al. Genomic and epigenetic alterations deregulate microRNA expression in human epithelial ovarian cancer. Proceedings of the National Academy of Sciences of the United States of America 2008;105:7004-9.

115. Nagayama K, Kohno T, Sato M, Arai Y, Minna JD, Yokota J. Homozygous deletion scanning of the lung cancer genome at a 100-kb resolution. Genes Chromosomes Cancer 2007;46:1000-10.

116. Yamada H, Yanagisawa K, Tokumaru S, et al. Detailed characterization of a homozygously deleted region corresponding to a candidate tumor suppressor locus at 21q11-21 in human lung cancer. Genes Chromosomes Cancer 2008;47:810-8.

117. Lu L, Katsaros D, de la Longrais IA, Sochirca O, Yu H. Hypermethylation of let-7a-3 in epithelial ovarian cancer is associated with low insulin-like growth factor-II expression and favorable prognosis. Cancer Res 2007;67:10117-22.

118. Liang L, Wong CM, Ying Q, et al. MicroRNA-125b suppressesd human liver cancer cell proliferation and metastasis by directly targeting oncogene LIN28B2. Hepatology 2010;52:1731-40.

119. Wang J, Cao N, Yuan M, et al. MicroRNA-125b/Lin28 pathway contributes to the mesendodermal fate decision of embryonic stem cells. Stem Cells Dev 2012;21:1524-37.

120. Rybak A, Fuchs H, Smirnova L, et al. A feedback loop comprising lin-28 and let-7 controls pre-let-7 maturation during neural stem-cell commitment. Nat Cell Biol 2008;10:987-93.

121. Segalla S, Pivetti S, Todoerti K, et al. The ribonuclease DIS3 promotes let-7 miRNA maturation by degrading the pluripotency factor LIN28B mRNA. Nucleic Acids Res 2015;43:5182-93.

122. Lohr JG, Stojanov P, Carter SL, et al. Widespread genetic heterogeneity in multiple myeloma: implications for targeted therapy. Cancer cell 2014;25:91-101.

123. Bolli N, Avet-Loiseau H, Wedge DC, et al. Heterogeneity of genomic evolution and mutational profiles in multiple myeloma. Nat Commun 2014;5:2997.

124. Chng WJ, Dispenzieri A, Chim CS, et al. IMWG consensus on risk stratification in multiple myeloma. Leukemia 2014;28:269-77.

125. Avet-Loiseau H, Durie BG, Cavo M, et al. Combining fluorescent in situ hybridization data with ISS staging improves risk assessment in myeloma: an International Myeloma Working Group collaborative project. Leukemia 2013;27:711-7.

126. Thery C, Zitvogel L, Amigorena S. Exosomes: composition, biogenesis and function. Nat Rev Immunol 2002;2:569-79.

127. Peinado H, Aleckovic M, Lavotshkin S, et al. Melanoma exosomes educate bone marrow progenitor cells toward a pro-metastatic phenotype through MET. Nat Med 2012;18:883-91.

128. Roccaro AM, Sacco A, Maiso P, et al. BM mesenchymal stromal cell-derived exosomes facilitate multiple myeloma progression. The Journal of clinical investigation 2013;123:1542-55.

129. Melo SA, Sugimoto H, O'Connell JT, et al. Cancer exosomes perform cell-independent microRNA biogenesis and promote tumorigenesis. Cancer cell 2014;26:707-21.

130. Krol J, Loedige I, Filipowicz W. The widespread regulation of microRNA biogenesis, function and decay. Nat Rev Genet 2010;11:597-610.

131. Pichiorri F, Suh SS, Ladetto M, et al. MicroRNAs regulate critical genes associated with multiple myeloma pathogenesis. Proceedings of the National Academy of Sciences of the United States of America 2008;105:12885-90.

132. Gutierrez NC, Sarasquete ME, Misiewicz-Krzeminska I, et al. Deregulation of microRNA expression in the different genetic subtypes of multiple myeloma and correlation with gene expression profiling. Leukemia 2010;24:629-37.

133. Calin GA, Ferracin M, Cimmino A, et al. A MicroRNA signature associated with prognosis and progression in chronic lymphocytic leukemia. The New England journal of medicine 2005;353:1793-801.

134. Yanaihara N, Caplen N, Bowman E, et al. Unique microRNA molecular profiles in lung cancer diagnosis and prognosis. Cancer Cell 2006;9:189-98.

135. Yu SL, Chen HY, Chang GC, et al. MicroRNA signature predicts survival and relapse in lung cancer. Cancer cell 2008;13:48-57.

136. Ueda T, Volinia S, Okumura H, et al. Relation between microRNA expression and progression and prognosis of gastric cancer: a microRNA expression analysis. Lancet Oncol 2010;11:136-46.

137. Liu N, Chen NY, Cui RX, et al. Prognostic value of a microRNA signature in nasopharyngeal carcinoma: a microRNA expression analysis. Lancet Oncol 2012;13:633-41.

138. Cortez MA, Bueso-Ramos C, Ferdin J, Lopez-Berestein G, Sood AK, Calin GA. MicroRNAs in body fluids--the mix of hormones and biomarkers. Nat Rev Clin Oncol 2011;8:467-77.

139. Durie BG, Harousseau JL, Miguel JS, et al. International uniform response criteria for multiple myeloma. Leukemia 2006;20:1467-73.

140. Taylor DD, Zacharias W, Gercel-Taylor C. Exosome isolation for proteomic analyses and RNA profiling. Methods Mol Biol 2011;728:235-46.

141. Kodani M, Yang G, Conklin LM, et al. Application of TaqMan low-density arrays for simultaneous detection of multiple respiratory pathogens. Journal of clinical microbiology 2011;49:2175-82.

142. D'Haene B, Mestdagh P, Hellemans J, Vandesompele J. miRNA expression profiling: from reference genes to global mean normalization. Methods Mol Biol 2012;822:261-72.

143. Schwarzenbach H, Nishida N, Calin GA, Pantel K. Clinical relevance of circulating cell-free microRNAs in cancer. Nat Rev Clin Oncol 2014;11:145-56.

144. Kubiczkova L, Kryukov F, Slaby O, et al. Circulating serum microRNAs as novel diagnostic and prognostic biomarkers for multiple myeloma and monoclonal gammopathy of undetermined significance. Haematologica 2014;99:511-8.

145. Hao M, Zang M, Wendlandt E, et al. Low serum miR-19a expression as a novel poor prognostic indicator in multiple myeloma. Int J Cancer 2015;136:1835-44.

146. Rocci A, Hofmeister CC, Geyer S, et al. Circulating miRNA markers show promise as new prognosticators for multiple myeloma. Leukemia 2014;28:1922-6.

147. Huang X, Yuan T, Liang M, et al. Exosomal miR-1290 and miR-375 as prognostic markers in castration-resistant prostate cancer. Eur Urol 2015;67:33-41.

148. Melo SA, Luecke LB, Kahlert C, et al. Glypican-1 identifies cancer exosomes and detects early pancreatic cancer. Nature 2015;523:177-82.

149. Xiang M, Zeng Y, Yang R, et al. U6 is not a suitable endogenous control for the quantification of circulating microRNAs. Biochemical and biophysical research communications 2014;454:210-4.

150. Mestdagh P, Van Vlierberghe P, De Weer A, et al. A novel and universal method for microRNA RT-qPCR data normalization. Genome biology 2009;10:R64.

151. Cui W, Ma J, Wang Y, Biswal S. Plasma miRNA as biomarkers for assessment of total-body radiation exposure dosimetry. PloS one 2011;6:e22988.

152. Manier S, Powers JT, Sacco A, et al. The LIN28B/let-7 axis is a novel therapeutic pathway in multiple myeloma. Leukemia 2016.

153. Jacobsen A, Silber J, Harinath G, Huse JT, Schultz N, Sander C. Analysis of microRNA-target interactions across diverse cancer types. Nature structural & molecular biology 2013;20:1325-32.

154. Spizzo R, Nicoloso MS, Croce CM, Calin GA. SnapShot: MicroRNAs in Cancer. Cell 2009;137:586- e1.

155. Mendell JT. miRiad roles for the miR-17-92 cluster in development and disease. Cell 2008;133:217-22.

156. Krutilina R, Sun W, Sethuraman A, et al. MicroRNA-18a inhibits hypoxia-inducible factor 1alpha activity and lung metastasis in basal breast cancers. Breast cancer research : BCR 2014;16:R78.

157. Teng Y, Mu J, Hu X, et al. Grapefruit-derived nanovectors deliver miR-18a for treatment of liver metastasis of colon cancer by induction of M1 macrophages. Oncotarget 2016;7:25683-97.

158. Truitt ML, Ruggero D. New frontiers in translational control of the cancer genome. Nature reviews Cancer 2016;16:288-304.

159. Truitt ML, Conn CS, Shi Z, et al. Differential Requirements for eIF4E Dose in Normal Development and Cancer. Cell 2015;162:59-71.

160. Bhat M, Robichaud N, Hulea L, Sonenberg N, Pelletier J, Topisirovic I. Targeting the translation machinery in cancer. Nat Rev Drug Discov 2015;14:261-78.

161. Vogel C, Marcotte EM. Insights into the regulation of protein abundance from proteomic and transcriptomic analyses. Nat Rev Genet 2012;13:227-32.

162. Brown LE, Chih-Chien Cheng K, Wei WG, et al. Discovery of new antimalarial chemotypes through chemical methodology and library development. Proceedings of the National Academy of Sciences of the United States of America 2011;108:6775-80.

163. Rodrigo CM, Cencic R, Roche SP, Pelletier J, Porco JA. Synthesis of rocaglamide hydroxamates and related compounds as eukaryotic translation inhibitors: synthetic and biological studies. J Med Chem 2012;55:558-62.

164. Bordeleau ME, Robert F, Gerard B, et al. Therapeutic suppression of translation initiation modulates chemosensitivity in a mouse lymphoma model. The Journal of clinical investigation 2008;118:2651-60.

165. Chu J, Cencic R, Wang W, Porco JA, Jr., Pelletier J. Translation Inhibition by Rocaglates Is Independent of eIF4E Phosphorylation Status. Mol Cancer Ther 2016;15:136-41.

166. Subramanian A, Tamayo P, Mootha VK, et al. Gene set enrichment analysis: a knowledge-based approach for interpreting genome-wide expression profiles. Proc Natl Acad Sci U S A 2005;102:15545-50.

167. Santagata S, Mendillo ML, Tang YC, et al. Tight coordination of protein translation and HSF1 activation supports the anabolic malignant state. Science 2013;341:1238303.

168. Mendillo ML, Santagata S, Koeva M, et al. HSF1 drives a transcriptional program distinct from heat shock to support highly malignant human cancers. Cell 2012;150:549-62.

169. Agnelli L, Bicciato S, Mattioli M, et al. Molecular classification of multiple myeloma: a distinct transcriptional profile characterizes patients expressing CCND1 and negative for 14q32 translocations. Journal of clinical oncology : official journal of the American Society of Clinical Oncology 2005;23:7296-306.

170. Zhan F, Huang Y, Colla S, et al. The molecular classification of multiple myeloma. Blood 2006;108:2020-8.

171. Mulligan G, Mitsiades C, Bryant B, et al. Gene expression profiling and correlation with outcome in clinical trials of the proteasome inhibitor bortezomib. Blood 2007;109:3177-88.

172. Huttlin EL, Jedrychowski MP, Elias JE, et al. A tissue-specific atlas of mouse protein phosphorylation and expression. Cell 2010;143:1174-89.

173. Wade M, Li YC, Wahl GM. MDM2, MDMX and p53 in oncogenesis and cancer therapy. Nature reviews Cancer 2013;13:83-96.

174. Beroukhim R, Mermel CH, Porter D, et al. The landscape of somatic copy-number alteration across human cancers. Nature 2010;463:899-905.

175. Hurt EM, Wiestner A, Rosenwald A, et al. Overexpression of c-maf is a frequent oncogenic event in multiple myeloma that promotes proliferation and pathological interactions with bone marrow stroma. Cancer Cell 2004;5:191-9.

176. Sonenberg N, Hinnebusch AG. Regulation of translation initiation in eukaryotes: mechanisms and biological targets. Cell 2009;136:731-45.

177. Kozak M. Influences of mRNA secondary structure on initiation by eukaryotic ribosomes. Proceedings of the National Academy of Sciences of the United States of America 1986;83:2850-4.

178. Pelletier J, Sonenberg N. Insertion mutagenesis to increase secondary structure within the 5' noncoding region of a eukaryotic mRNA reduces translational efficiency. Cell 1985;40:515-26.

179. Koromilas AE, Lazaris-Karatzas A, Sonenberg N. mRNAs containing extensive secondary structure in their 5' non-coding region translate efficiently in cells overexpressing initiation factor eIF-4E. EMBO J 1992;11:4153-8.

180. Feoktistova K, Tuvshintogs E, Do A, Fraser CS. Human eIF4E promotes mRNA restructuring by stimulating eIF4A helicase activity. Proceedings of the National Academy of Sciences of the United States of America 2013;110:13339-44.

181. Wolfe AL, Singh K, Zhong Y, et al. RNA G-quadruplexes cause eIF4A-dependent oncogene translation in cancer. Nature 2014;513:65-70.

182. Iwasaki S, Floor SN, Ingolia NT. Rocaglates convert DEAD-box protein eIF4A into a sequence-selective translational repressor. Nature 2016;534:558-61.

183. Lajkiewicz NJ, Roche SP, Gerard B, Porco JA, Jr. Enantioselective photocycloaddition of 3-hydroxyflavones: total syntheses and absolute configuration

assignments of (+)-ponapensin and (+)-elliptifoline. J Am Chem Soc 2012;134:13108-13.

184. Akbay EA, Moslehi J, Christensen CL, et al. D-2-hydroxyglutarate produced by mutant IDH2 causes cardiomyopathy and neurodegeneration in mice. Genes & development 2014;28:479-90.

185. Lane AA, Chapuy B, Lin CY, et al. Triplication of a 21q22 region contributes to B cell transformation through HMGN1 overexpression and loss of histone H3 Lys27 trimethylation. Nature genetics 2014;46:618-23.